Targeted cytokine-induced killer cells in non-small cell lung cancer

Doctoral thesis

to obtain a doctorate (Med.Doc/Doc. of Philosophy)

from the Faculty of Medicine

of the University of Bonn

Yutao Li

from Hebei, China

2024

Written with authorization of

the Faculty of Medicine of the University of Bonn

First reviewer: Prof. Dr. med Ingo G.H. Schmidt-Wolf

Second reviewer: Prof. Dr. Hans Weiher

Day of oral examination: 23.02.2024

From the Department of Integrated Oncology, CIO Bonn, University Hospital Bonn
Director: Prof. Dr.med Ingo G.H. Schmidt-Wolf

Table of Contents

List of Abbreviations

A

ADCC	antibody-dependent cell-mediated cytotoxicity

C

CAF	cancer-associated fibroblasts
CAR-T cells	chimeric antigen receptor T-cells
CBD	cannabidiol
CCK-8	cell counting kit-8
CIK cells	cytokine-induced killer cells
CM	central memory T cells
CTLA-4	Cytotoxic T lymphocyte-associated antigen-4
CRP	reactive protein
CSC	cancer stem cell

D

DC	dendritic cell

E

ECM	extracellular matrix
EM	effector memory T cells
EMRA	terminal effector memory T cells
ETS	environmental tobacco smoke

F

FADD	Fas-associated protein with DD
FasL	Fas ligand
FBS	fetal bovine serum
FDA	US Food and Drug Administration

G

GM-CSF granulocyte-macrophage colony-stimulating factor

I

ICI immune checkpoint inhibitors

ICAM-1 Intercellular Adhesion Molecule 1

IFN-γ interferon-γ

IgG immunoglobulin gamma

IgV Ig variable-type

IL-1β interleukin-1β

IL-2 interleukin-2

IRAE immune-related adverse event

ITIMs immunoreceptor tyrosine-based inhibitory motifs

ITSMs immunoreceptor tyrosine-based switch motifs

L

LC lung cancer

LDH lactate dehydrogenase

LINE-1 Long Interspersed Nuclear Element-1

LUAD lung adenocarcinoma

LUSC lung squamous cell carcinoma

M

MARK mitogen-activated protein kinase

MFI mean fluorescence intensity

MSCs marijuana smoke condensates

mTOR mechanistic target of rapamycin

N

NSCLC Non-small cell lung cancer

nsSNPs non-synonymous single nucleotide polymorphisms

P

PBMC	peripheral blood mononuclear cell
PD-1	programmed cell death protein 1
PD-L1	programmed cell death protein 1 ligand 1
p-ERK	phosphor-Extracellular signal-Regulated Kinase
PFA	paraformaldehyde
PFS	progression-free survival
PPI	protein-protein interaction
PNE	Pulmonary neuroendocrine

R

ROS	reactive oxygen species

S

SCLC	small cell lung cancer
SHP-1/2	Src homology 2-containing tyrosine phosphatase 1/2
SIRPα	signal‐regulated protein

T

TAMs	tumor-associated macrophages
TGF-β	transforming growth factor β
TILs	tumor-infiltrating lymphocytes
TKI	tyrosine kinase inhibitor
TLS	TRPV2 antagonist tranilast
TMB	tumor mutation burden
Treg	regulatory T cells
TRPV2	Transient Receptor Potential Cation Channel Subfamily V Member 2

V

VEGF	vascular endothelial growth factor

7-AAD 7-aminoactinomycin D

STUDY I

A Combination of Cytokine-Induced Killer Cells With PD-1 Blockade and ALK Inhibitor Showed Substantial Intrinsic Variability Across Non-Small Cell Lung Cancer Cell Lines

Published as: Li Y, Sharma A, Wu X, Weiher H, Skowasch D, Essler M and Schmidt-Wolf IGH (2022) A Combination of Cytokine-Induced Killer Cells With PD-1 Blockade and ALK Inhibitor Showed Substantial Intrinsic Variability Across Non-Small Cell Lung Cancer Cell Lines. Front. Oncol. 12:713476. doi: 10.3389/fonc.2022.713476

1.1. Introduction

1.1.1. Epidemiology of Lung cancer

Lung cancer remains the second most commonly diagnosed cancer worldwide (Sung H., et al., 2021), being categorized into two main types: non-small cell lung cancer (NSCLC) and small cell lung cancer (SCLC). Approximately 85% of patients exhibit a group of histological subtypes referred as NSCLC, of which lung adenocarcinoma (LUAD) and lung squamous cell carcinoma (LUSC) represent the most common subtypes (Herbst RS., et al., 2018). In the United States, 5-year survival between 2008 and 2014 was 24% for all patients with NSCLC and 5.5% for those with distant metastases (Noone AM., et al., 2018). Likewise, the median overall survival of German advanced NSCLC patients was equally as low as that of other countries as shown in a German retrospective data analysis (Hardtstock F., et al., 2020). Unlike NSCLC, the SCLC accounts for approximately 13%-15% of all lung cancers with a 5-

year survival rate of less than 7%, a rapid doubling time and a high propensity to metastasize. SCLC is considered a "recalcitrant" cancer as no significant improvements in survival and therapeutic approaches have been achieved for more than 30 years (Kahnert K., et al., 2016; Karachaliou N., et al., 2016).

1.1.2. Landscape of PD-1/PD-L1 axis in NSCLC

1.1.2.1 The role of PD-1/PD-L1 in the tumor immune microenvironment of NSCLC

Cancer stem cell (CSC)

Human lungs are composed of two distinct areas: the conducting airway, including the trachea, bronchi, and bronchioles, and the gas exchange regions, alveolar spaces. The division of these stem cells is thought to be sufficient to renew the lung's structure of the lung during normal adult life. In the trachea and main bronchi, the tracheal epithelium consists mainly of columnar and mucus secreting goblet cells. In addition, airway basal cells are considered as a stem cell population, which can maintain the balance between their proliferation and differentiation. The imbalance can contribute to squamous cell metaplasia or dysplasia, which are precursors of squamous cell lung carcinoma (Rock J.R., et al., 2010; George P.J., et al., 2007). Meanwhile, in bronchioles and alveoli, non-ciliated club cells (Clara cells) are located in the bronchiolar and alveolar epithelium and could differentiate into ciliated cells after exposure to oxidant induced damage (Stevens T.P., et al., 1997; Reynolds S.D., et al., 2000). Pulmonary neuroendocrine (PNE) cells are thought to serve as a precursor for the progress of small cell lung carcinoma. Clara cells are not necessary for PNE cell hyperplasia since proliferation and hyperplasia of PNE cells occurred in the conditional Clara

cell ablation (Reynolds S.D., et al., 2000). It is also believed that adenocarcinomas can originate from broncho alveolar stem cells or pneumocytes of type I and type II (Hardavella G., et al., 2016). (Figure 1).

Fig 1. The putative origin of lung cancer stem cells in lung anatomical sites.

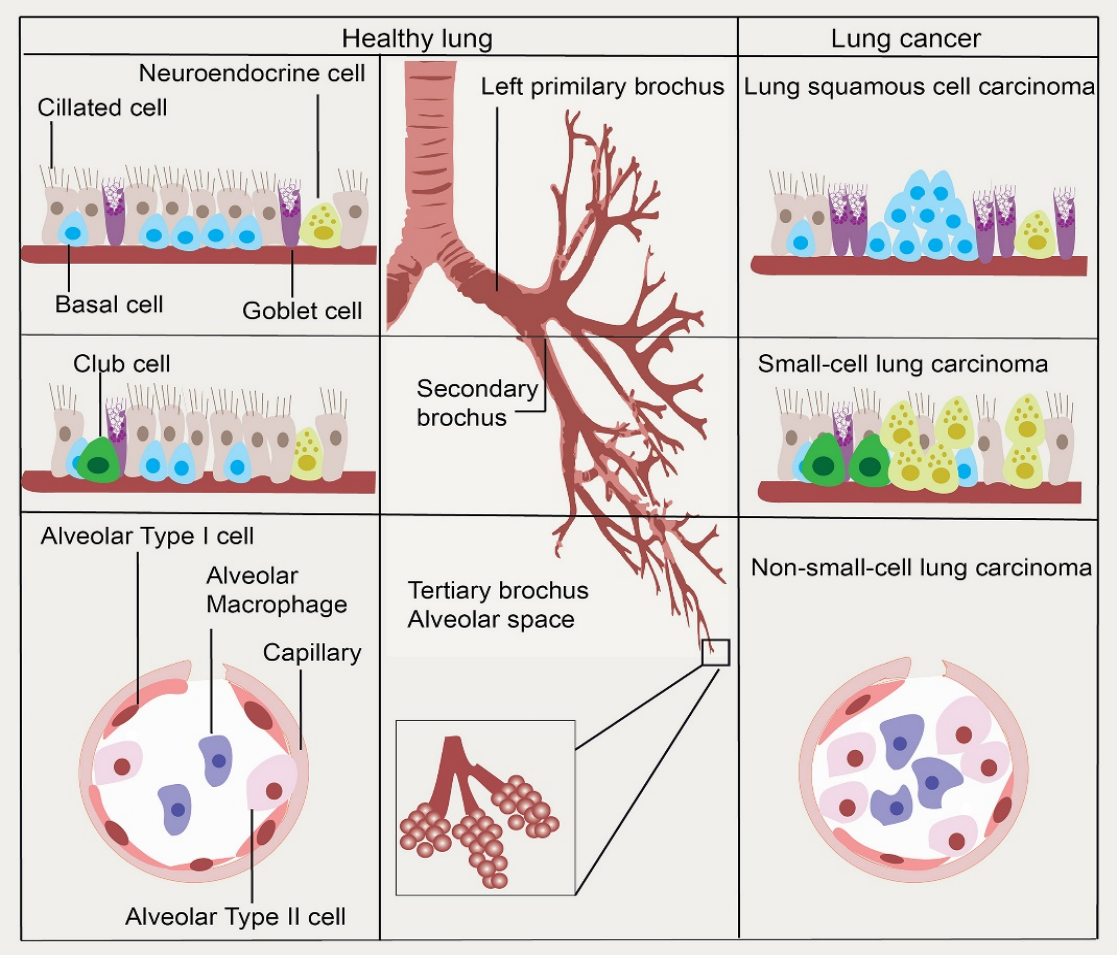

Accepted by *Molecular Cancer*

Figure 1. The putative origin of lung cancer stem cells in lung anatomical sites. In the trachea and main bronchi, airway basal cells are considered as a stem cell population, precursors of squamous cell lung carcinoma. Pulmonary neuroendocrine (PNE) cells are thought to serve as a precursor for

the progress of small cell lung carcinoma. It is also believed that adenocarcinomas can originate from broncho alveolar stem cells or pneumocytes of type I and type II.

CSCs are thought to be responsible for cancer initiation, progression, metastasis, recurrence, and drug resistance. The presence of CSCs with PD-L1 expression in the metastatic lymph nodes (LNs) in lung cancer patients might correlate with immunotherapy (Raniszewska A., et al., 2019). Additional data showed that PD-L1^{+} lung cancer stem cells modified the metastatic lymph-node immune microenvironment in NSCLC patients, positively correlated with the percentage of Tregs, PD-1^{+} CD4^{+} T cells and Tim3^{+} CD4^{+} T cells, while negatively correlated with that of CD4^{+} T cells and CD28^{+} CD4^{+} T cells (Raniszewska A., et al., 2021). Indeed, this suppressive immunophenotype correlated with tumor PD-L1 can be evaluated by endobronchial ultrasound-guided transbronchial needle aspiration before immune therapy (Murthy V., et al., 2019) (Figure 2).

Tumor-associated macrophages (TAMs)

Tumor-associated macrophages (TAMs) play an important role on the tumorigenesis of lung cancer. TAMs conduct pro-angiogenic effects and polarization of TAMs can affect the proliferation, migration, invasion. TGF-β and IL-10 secreted from TAMs are important factors that form the microenvironment of immunosuppressive tumours (Zhu S., et al., 2021). TAMs are known to be instrumental in the immunosuppressive effects of the PD-1/PD-L1 pathway in the cancer microenvironment. Our previous study demonstrated that PD-L1 is highly expressed in multiple NSCLC cell lines (Li Y., et al., 2022). PD-L1 was significantly higher in macrophages in both tumor and stromal compartment compared with other immune cells in

NSCLC patients, which was correlated with better overall survival was also found to be significantly higher in macrophages across tumor and stromal compartments when compared to other immune cells in NSCLC patients, correlating with better overall survival (Liu Y., et al., 2020). This self-protective immune escape could aid cells to evade being eliminated by neighbouring cells, which might also benefit from PD-1/PD-L1 inhibitors. PD-L1 overexpression on macrophages induced via STAT3 activation by cancer cell-derived GM-CSF was suggested to promote cancer progression in lung adenocarcinoma in vitro and vivo animal models (Shinchi Y, et al., 2022). Furthermore, data from lung adenocarcinoma patients has confirmed that high PD-L1 expression on macrophages was correlated with the presence of EGFR mutation, a lower cancer grade, and a shorter cancer-specific overall survival (Watanabe H., et al., 2019). Another study revealed that in patients with early-stage lung adenocarcinoma, expression of PD-L1 on the cell surface of tumor cells was observed, which was accompanied by an increase in TAMs, cytotoxic $CD8^+$ T cells, and regulatory $FoxP3^+$ T cells (Shima T., et al., 2020). Additional in vitro investigations revealed that PD-L1 expression in lung cancer cell lines was significantly upregulated by co-culture with M2-differentiated macrophages, whereas it was downregulated by a transforming growth factor-β inhibitor. It is known that the interaction of CD47 on tumor cells and signal-regulated protein (SIRPα) expressed on the surface of macrophages can protect cells from being "eaten" by macrophages, as has been reported in NSCLC patients. And that dual targeting of CD47/PD-L1 innate and adaptive checkpoints may serve as new combined dual-targeting immunotherapy to enhances macrophage phagocytosis (Yang Z., et al., 2021). Taken

together, tumor‐infiltrating TAM are extrinsic regulators of tumor PD‐L1 expression, indicating that combination therapy targeting both tumor PD‐L1 and stromal TAM molecular might be a possible strategy for effective treatment of lung cancer (Figure 2). Recently, Carfilzomib modulates tumor microenvironment via driving M2 macrophages to express M1 cytokines to potentiate PD-1 antibody immune therapy for lung cancer (Zhou Q., et al., 2022). Liu M et al. suggested that the transcription factor c-Maf critically regulates human M2 macrophages/monocytes infiltrating the tumor and circulating monocytes from patients with NSCLC, as inhibition of c-Maf partially overcomes resistance to anti-PD-1 therapy in a subcutaneous LLC tumor model (Liu M., et al., 2020). How c-Maf promotes immunoregulation of PD-1-expressed TAMs or $CD8^+$ T cells in NSCLC patients is still unknown, while it has already been demonstrated in multiple sclerosis and relapsed/refractory classic Hodgkin lymphoma (Koto S., et al., 2022; Gusak A., et al., 2021).

Cancer-associated fibroblasts (CAF)

Some clinical studies on immunotherapy via immune check emphasized the role of TGF-β. For instance, albumin-to-globulin ratio was identified as a predictive biomarker in patients with NSCLC (Nakanishi Y., et al., 2020). In metastatic urothelial cancer (mUC), TGF-β attenuates tumor response to PD-L1 blockade (atezolizumab) by contributing to exclusion of T cells. The lack of response was associated with a transforming growth factor β (TGF-β) signature in fibroblasts, particularly in patients with $CD8^+$ T cells excluded from the tumor parenchyma and instead found in the fibroblast and collagen-rich peritumoral stroma. In an animal model, these immune exclusion properties were also recapitulated, and a TGF-β-

blocking antibody together with anti-PD-L1 reduced TGF-β signalling in stromal cells, facilitated T cell entry into the centre of the tumor, and elicited potent anti-tumor immunity (Mariathasan S., et al., 2018). TGF-β signalling primarily mediates extracellular matrix (ECM) remodelling in the human NSCLC cell line A549. Ln-γ2, a member of the laminin family of ECM, was transcriptionally activated by TGF-β1 secreted from cancer-associated fibroblasts via JNK/AP1 signalling, and the mediated cell exclusion attenuates the response to anti-PD-1 therapy (Li L., et al., 2021) (Figure 2).

TCR-αβ T cells exhaustion

T cell repertoire analysis has revealed that in early-stage NSCLC patients, there is greater homology of the T-cell repertoire between the tumor and the uninvolved tumor-adjacent lung, suggesting a less tumor-focused T-cell response as well as an association with inferior survival. Furthermore, the accumulation of regulatory $CD4^+$ T cells in the tumor centre may impair the ability of $CD8^+$ T cells to proliferate in response to antigens (Reuben A., et al., 2020), although the increased proliferation of PD-1^+ $CD8^+$ T cells in peripheral blood after PD-1-targeting therapy in lung cancer patients may overcome it (Kamphorst AO., et al., 2017). Conversely, PD-$L1^+$ $CD8^+$ T cells exerted regulatory functions that inhibit $CD8^+$ T cell proliferation and cytotoxic capabilities via the PD-L1/PD-1 axis. Moreover, tumor-derived IL-27 promotes PD-$L1^+$ $CD8^+$ T cell development through STAT1/STAT3 signalling (Zheng Y., et al., 2022). Therefore, it is plausible that adoptive T-cell therapy combined with PD-1/PD-L1 inhibitors might increase clinical benefits and reduce toxicity with immunotherapy (Figure 2).

Soluble PD-1/PD-L1

Soluble PD-1/PD-L1 forms are generated by proteolytic shedding or alternative splicing of pre-mRNA, presenting an active circulating protein, with immune-modulatory functions (Bailly C., et al., 2021). In the recent study, PD-L1–vInt4, a splicing variant of PD-L1, was reported to be detectable in clinical samples of lung squamous cell carcinoma (LUSC) and its secretion resisted anti–PD-L1 antibody treatment via alternative polyadenylation. It is noteworthy that several LUSC samples presented a lack of capability of antigen presentation due to the loss of HLA expression overexpression in vitro experiment of PD-L1–vInt4 in vitro experiment (Sagawa R., et al., 2022). Besides, sPD-L1expression in plasma of small cell lung cancer is associated with disease progression (Lu F., et al., 2022). In contrast, some animal outcomes have been documented the anti-tumor effect of sPD-1 (Yuan Y., et al., 2004; He L., et al., 2005). An increased or stable sPD-1 level independently correlated with longer PFS in two cycles of nivolumab-treated metastatic NSCLC patients, suggesting sPD-1 as a predictive biomarker of response to ICI treatment in patients with lung cancer (Meyo M.T., et al., 2020; Ohkuma R., et al., 2021). Considering the analysis of sPD-L1 with immune-assays (ELISA) method may not distinguish between vesicular and soluble forms in circulation of cancer patients in some studies, dynamic blood PD-L1 expression for immune checkpoint inhibitors in advanced NSCLC patients might be more reliable as a biomarker (Yang Q., et al., 2021). Nevertheless, further work is required to better understand the functions of soluble PD-1/PD-L1 variants in lung cancer (Figure 2).

TCR-γδ T cells tumor-infiltrating lymphocytes (TILs)

γ/δ T lymphocytes localize in different epithelial tissues and are phenotypically distinct from peripheral γ/δ T cell-population. In about one-fourth of human lung cancers, γ/δ T cells represented a significant proportion of freshly isolated tumor-infiltrating lymphocytes (Ferrarini M., et al.,1994). M. Ferrarini et al. found that half of the Vδ1$^+$ (as well as Vδ1-Vδ2-) γ/δ-lymphocytes that could be selectively expanded from human lung cancers also co-expressed the CD8α/α homodimer (Ferrarini M., et al., 1994). Furthermore, it has been reported that TCS1$^+$ γ/δ$^+$ tumor-infiltrating lymphocytes from human lung carcinomas lysed only autologous tumor cells and K-562 (Zocchi M.R., et al., 1990). Human normal lung tissues and NSCLCs harbour resident populations of γδ T cells, particularly enriched in the Vδ1 subtype. Intratumoral Vδ1 T cells exhibited stemness characteristics and were skewed toward cytolysis and helper T cell type 1 function, similar to intratumoral natural killer and CD8$^+$ T cells, which are considered beneficial to the patients (Wu Y., et al., 2022). Based on deconvolution of human cancers microarrays, TCRVγ9Vδ2$^+$γδ TIL abundance in lung carcinoma was also reassessed by a study in ~10,000 cancer biopsies. However, TCRVγ9Vδ2$^+$ γδ TIL was not positively correlated with cytolytic activity and favourable outcome like αβ TIL (Tosolini M., et al., 2017). In contrast, Cazzetta V, et al. revealed that NKG2A expression identifies a subset of human Vδ2 T cells exerting the highest antitumor effector functions (Cazzetta V. et al., 2021). This apparent discrepancy illustrates the complexity of the relationship between TCRVγ9Vδ2$^+$ γδ TIL and lung cancer and also depends on differences in measurement methodologies (whole-tissue transcriptomic analysis, phenotypic analysis or immunohistochemistry analysis).

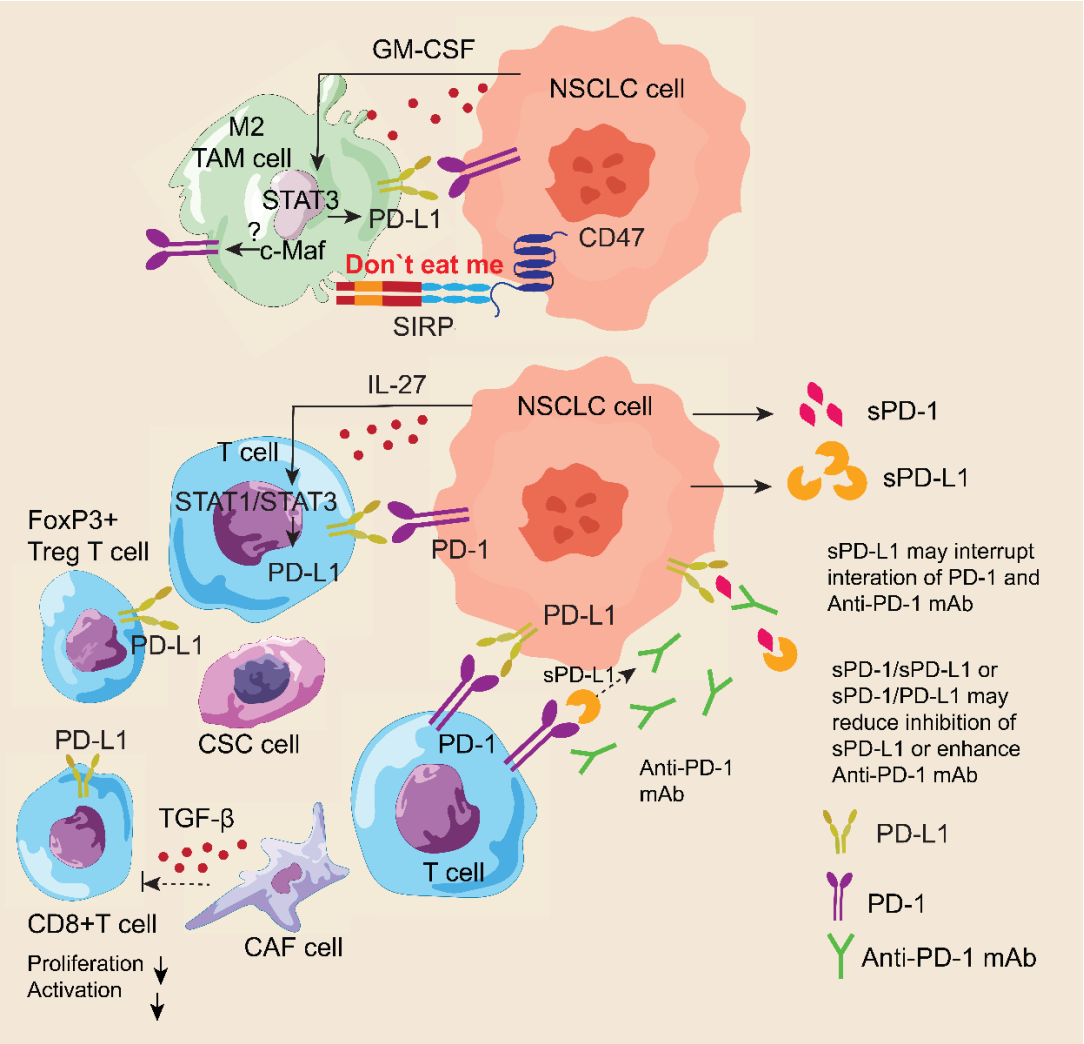

Accepted by *Molecular Cancer*

Figure 2. Schematic representation of the negative regulation of anti-tumor immune responses of PD-1/PD-L1 in NSCLC. PD-L1 expression in lung cancer cell lines was significantly upregulated by co-culture with M2-differentiated tumor-associated macrophages (TAMs). PD-L1 overexpression on macrophages might be induced via STAT3 activation by cancer cell-derived GM-CSF. The interaction of CD47 on tumor cells and signal-regulated protein (SIRPα) expressed on the surface of macrophages can protect cells from being “eaten” by macrophages in NSCLC patients. TGF-β secreted from cancer-associated fibroblasts (CAF cells) also reduced the proliferation and activation of $CD8^+$ T cells. In addition, $PD\text{-}L1^+$ lung cancer stem (CSC) cells as well as $FoxP3^+$ Treg T cells may

modify the metastatic lymph-node immune microenvironment in NSCLC patients. Besides, soluble PD-L1 (sPD-L1) might interrupt PD-1 and Anti-PD-1 mAb whereas interaction of sPD-1/sPD-L1 or sPD-1/PD-L1 may reduce inhibition of sPD-L1 or enhance Anti-PD-1 mAb. The interaction of PD-1/PD-L1 between TCRVγ9Vδ2^{+}γδ tumor-infiltrating lymphocytes (TILs) and αβ T cells could restrain the activation of T cells. Intratumoral Vδ1 T cells demonstrated natural killer and CD8^{+} T cell function.

1.1.1.2. The possible mechanism of PD-1/PD-L1 in NSCLC cells

Several extrinsic factors (e.g., release of interferon-γ by immune cells that upregulate PD-L1 expression) and intrinsic factors regulate PD-L1 expression in NSCLC. As one of extrinsic factors, environmental tobacco smoke (ETS), contributes to a distinct PI3K (phosphatidylinositol 3-kinase)–Akt pathway that leads to cell survival in adenocarcinoma (Sun S., et al., 2007). Genomic alterations that activate KRAS, EGFR, and ALK, as well as the loss of PTEN, have been associated with increased PD-L1 expression. Several tumorigenic intrinsic factors such as activation of the mechanistic target of rapamycin (mTOR), mitogen-activated protein kinase (MAPK) and Myc pathways can increase PD-L1. Alternatively, methylation, allelic loss and gene silencing expression might be considered (Lamberti G., et al., 2020). Also, the molecular involvement of PD-L1 single nucleotide polymorphisms and non-synonymous single nucleotide polymorphisms (nsSNPs) with oncogenic potential in NSCLC, cannot be excluded (Re M.D., et al., 2021; Dhakar R., et al., 2022).

PD-1, is a type I transmembrane protein encoded by the PDCD1 gene of the CD28 immunoglobulin superfamily, comprised of a single Ig variable-type (IgV) extracellular domain, a transmembrane domain and a cytoplasmic domain. N-terminal and C-terminal tyrosine

residues in the cytoplasmic domain are involved in the formation of immunoreceptor tyrosine-based inhibitory motifs (ITIMs) and immunoreceptor tyrosine-based switch motifs (ITSMs) (Shinohara T., et al., 1994). The engagement of PD-1 in T cells and PD-1 ligands leads to the recruitment of SHP-1/2 (Src homology 2-containing tyrosine phosphatase 1/2) to the C-terminal of the ITSM. SHP-2 then dephosphorylates TCR-associated CD-3ζ and ZAP70, resulting in the inhibition of downstream signalling (Jiang X., et al., 2019). The advent of human T cell non-Hodgkin lymphomas and relative animal models has revealed that the activity of PD-1 enhances levels of the tumor suppressor PTEN and attenuates signalling by the kinases PI3K/AKT and PKCθ/NF-κB pathways in oncogenic T cells (Wartewig T., et al., 2019). PD-1 on $CD4^+$ T regulates cell cycle and inhibits T cell proliferation via Akt and Ras pathways (Patsoukis N, et al., 2012). Moreover, Lck signalling has been shown to contribute to PD-1^+ T cell exhaustion via CD28 co-stimulation in a humanized mouse model (Gulati P., et al., 2018) (Figure 3A, 3B).

In recent years, the role of intrinsic PD-1 in NSCLC cells raises consideration. Wang X, et al. proposed that PD-1 and PD-L1 reduces tumor growth by suppressing AKT and ERK1/2. In the absence of an adaptive immune system, tumor cell-intrinsic PD-1/PD-L1 mediates the resistance to anti-PD-1/PD-L1 antibodies by activating AKT and ERK1/2, which induces tumor growth (Wang X., et al., 2020) (Figure 3C, 3D).

Fig 3. Interaction of PD-1/PD-L1 between T cells and NSCLC cells.

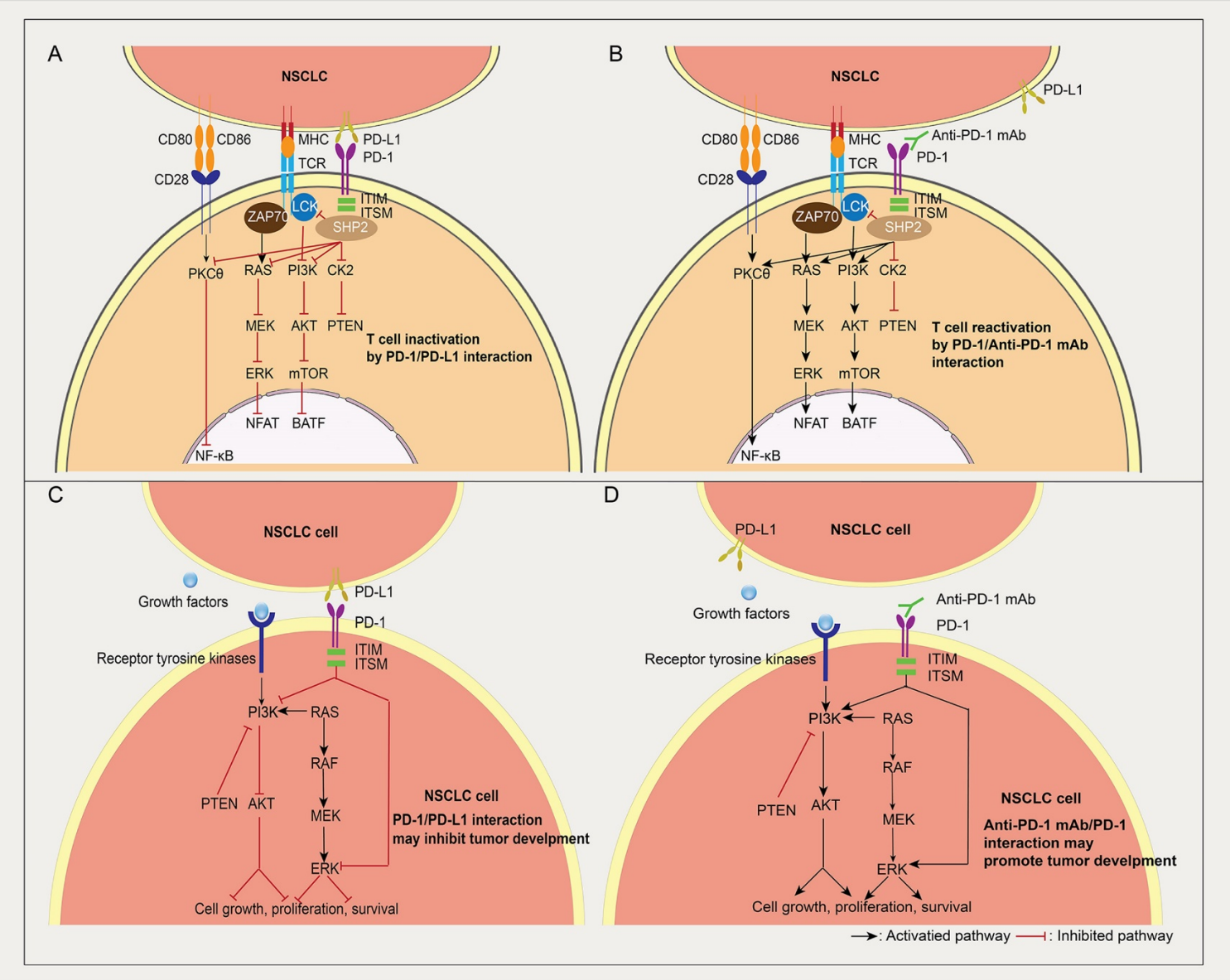

Accepted by *Molecular Cancer*

Figure 3. Interaction of PD-1/PD-L1 between T cells and NSCLC cells. (A-B) The engagement of PD-1 in T cells and PD-1 ligands leads to the recruitment of SHP-1/2 (Src homology 2-containing tyrosine phosphatase 1/2) to the C-terminal of the ITSM. SHP-2 then dephosphorylates TCR-associated CD-3ζ and ZAP70, resulting in the inhibition of downstream signalling and T cell inactivation (A). In the

presence of Anti-PD-1 mAb, T cells might be reactivated via PD-1/PD-L1 axis (B). (C-D) The effect of tumor cell-intrinsic PD-1 on NSCLC cells. PD-L1 expressed by NSCLC cells or other cells acts on PD-1^+ tumor cells to mediate PD-1 signalling in tumor cells via ITIM and ITSM. The AKT and ERK1/2 pathways can suppress tumor growth by dampening AKT and ERK signalling (C). Anti-PD 1 mAb blocks PD-1/PD-L1-mediated tumor suppression, leading to hyper progression in NSCLC cells (D).

1.1.3. Current clinical trials of CIK/DC-CIK cells combined with PD-1/PD-L1 blockades in lung cancer

1.1.3.1. PD-1/PD-L1 inhibitors by FDA

Since cancer cells have several mechanisms to evade immune surveillance, including the PD-1/PD-L1 axis, this axis has also been focused on for LC. Thus, the programmed cell death protein 1 (PD-1 [also known as CD279]) and its ligand, programmed death ligand 1 (PD-L1 [also known as CD274]), have been utilized in several standard first-line LC treatments. PD-L1, also known as Cluster of Differentiation (CD274) or B7 homolog 1 (B7-H1), belongs to the growing B7 family of immune molecules and is involved in the regulation of cellular and humoral immune responses. B7-H1 belongs to the cell surface immunoglobulin superfamily with two Ig-like domains in the extracellular region and a short cytoplasmic domain within the extracellular region and a short cytoplasmic domain. Subsequent to nivolumab (Horn L., et al., 2017; Lu S., et al., 2021), there have been additional PD-1 (pembrolizumab and cemiplimab) and PD-L1 (atezolizumab and durvalumab) inhibitors approved by the FDA. Unlike NSCLC cells, the efficacy of a combination of nivolumab and ipilimumab was enhanced in patients with high tumor mutation burden (TMB) in the nonrandomized or randomized cohorts of CheckMate 032 (Hellmann M.D., et al., 2018), possibly due to the

nearly universal association of SCLC with smoking (Alexandrov L.B., et al., 2013; Byers L.A., et al., 2015). However, in addition to improving survival, PD-1/PD-L1 inhibitors were associated with a wide range of unfavourable effects, for instance, immune-related adverse events (irAEs), including rash, colitis, hepatitis, endocrinopathies, and pneumonitis (Friedman C.F., et al., 2016). Thus, it is imperative to explore new therapeutic strategies to alleviate irAEs and improve the efficacy of immune effector cells.

1.1.3.2. Blockade of PD-1 immunosuppression boosts CIK/DC-CIK therapy

Shortly after injection of CIK cells, a bioluminescent signal was detected in the lung followed by the liver and spleen in the animal model (Edinger M., et al., 2003). CIK cells are heterogenous T cells, composed of $CD3^+CD8^+$, $CD3^+CD4^+$, $CD3^+CD56^+$ subpopulations and the main dominant of CIK cells is TCR αβ T cells (Pievani A., et al., 2011). Mechanistically, cell signaling not only through TCR/CD3 but also through NKG2D, DNAM-1, and NKp30 leads to CIK cell activation resulting in granule exocytosis, cytokine secretion, and cytotoxicity (Pievani A., et al., 2011; Wu X., et al., 2021). FasL is another major effector mechanism used by CIK cells to induce the apoptosis of tumor cells (Verneis M.R., et al., 2004). Alternatively, it has been reported that TCR αβ $CD3^+CD56^+$CIK cells can be retargeted to exert ADCC function by antigen-specific mAbs (Cappuzzelloa E., et al., 2016). Although CIK/DC-CIK therapy has improved anti-tumor responses in a total of 12 clinical trials targeting lung cancer in recent years (Zhang Y., et al., 2020), the dynamic phenotype profiles of checkpoint molecules on CIK cells derived from patients with NSCLC patients has revealed that CIK cells may partly be exhausted before the clinical transfusion. This has been also characterized by the elevated expression of PD-L1, LAG-3, TIM-3 and the reduced

expression of PD-1 and CTLA-4. Based on these findings, blocking PD-1/PD-L1 improve the efficiency of CIK therapy for NSCLC patients (Zhang L., et al., 2016). Furthermore, a clinical report on the enhancement of autologous CIK cells after treatment with PD-1 blocking antibodies in patients with advanced NSCLC provided additional evidence for this combination strategy (Han Y., et al., 2021).

Alternatively, in a phase I clinical trial in patients with advanced solid tumors including NSCLC, pembrolizumab-activated DC-CIK cells demonstrated superior antitumor properties with increased IFN-γ secretion in ex vivo and an overall disease control rate of 64.5% (Chen C.L., et al., 2018). A case report of a 63-year-old man with squamous cell carcinoma has provided further clinical evidence. The patient received a diagnosis of squamous cell carcinoma after biopsy of the right lower lobe lung mass and had developed multiple metastases on CT scans. After first-line and second-line chemotherapy, the disease was processed. After receiving pembrolizumab in combination with seven cycles of CIK cell transfer, the patient continued to be in remission 185 days posttreatment and had no adverse events. The tumor cells from pretreatment biopsies showed strongly expression of PD-L1 instead of PD-1, and large number of tumor-infiltrating $CD3^+$ T cells were observed (Wang Z., et al., 2018). Taken together, this study suggested that a combination of CIK cells and pembrolizumab could synergistically enhance therapeutic efficacy in metastatic NSCLC patients, especially when PD-L1 expression in tumor biopsies was high. Ying Han, et al. also documented that autologous CIK cells improved the clinical response to PD-1 blocking antibodies in patients with advanced NSCLC (Han Y. et al., 2021). Recently, a Phase IB Trial of autologous CIK

cells in combination with Sintilimab, (mAb PD-1), plus chemotherapy in patients with advanced NSCLC also showed encouraging efficacy (NCT03987867) (Zhou L., et al., 2022). Additionally, Joanne M Mankor et al. observed that the efficacy of nivolumab and ipilimumab in patients with malignant pleural mesothelioma was related to a subtype of cytotoxic T cells effector memory (Mankor J.M., et al., 2022). Therefore, it is important to stratify patients using accessible markers of T-cell status or tumor genomic detection to design therapeutic trials.

1.1.3.3. A combination of blockade of PD-1 and ALK inhibitors in immune therapy

It is also worth mentioning that the effective use of combined cancer therapies remains a challenge, especially when optimization is concerned. This can be evident from a recent clinical trial involving crizotinib (ALK inhibitor) and nivolumab (PD-1 inhibitor) in NSCLC that was discontinued due to the safety concerns (CheckMate 370) (Spigel D.R., et al., 2018). However, the clinical trials based on a similar combination strategy such as TKI/ALK inhibitor with ICI are still in progress. Primarily, the concern about short-term gastrointestinal toxicity also emerged in the above-mentioned clinical trial, however, it was resolved with the standard medical care. Notably, the treatment sequence also appeared to be pivotal, as evidenced by the fact that treatment in reverse sequence (osimertinib followed by nivolumab) did not result in higher levels of toxicity compared to treatment with nivolumab followed by osimertinib (Yamaguchi O., et al., 2020). To mention, the second generation ALK inhibitor ceritinib showed a synergistic effect with PD-1/PD-L1 blockade to provide an improved anti-tumor response along with favorable side effect tolerability in vivo NSCLC xenograft model (Du P., 2020) and clinical trial (Felip E., et al., 2020). Despite T cells dominated the immune cell

composition in NSCLC tumours (Stankovic B., et al., 2019), the function of $CD4^+$ and $CD8^+$ T lymphocytes was dysregulated with decreasing of IFN-γ production (Sheng S.Y., et al., 2017). In this particular scenario, the inclusion of alternative adjuvant treatments, for instance, cytokine-induced killer (CIK) cells, may help to reshape the therapeutic paradigm in NSCLC patients. CIK cells are heterogeneous in vitro expanded T lymphocytes with a natural killer (NK)/T phenotype generated primarily by ex vivo incubation of human peripheral blood mononuclear cells (PBMC) or cord blood mononuclear cells. The transfusion of CIK cells after ex-vivo expansion in cancer patients has already been tested in more than 80 reported clinical trials (Zhang Y., et al., 2020). Moreover, recent studies provide functional details on the function and optimization of CIK cells to maximize their functional potential (Li Y., et al. 2021; Wu X., et al., 2021; Zhang Y., et al., 2021). Of note, there have been autologous and allogeneic clinical trials showing that CIKs immunotherapy has potential benefits in the safety and efficacy of patients with advanced NSCLC (Li D.P. et al., 2015; Luo H., et al., 2016; Wu C., et al., 2008; Li R., et al., 2012; Gu Y., et al., 2017), given that clinical trials of DC-CIK (dendritic cells cytokine-induced killer cells) in combination with chemotherapy for advanced lung cancer have shown very limited success. To improve the efficiency of such therapies, several paradigms have been discussed, including inhibition of inflammatory mediators released by tumor cells in combination with vaccination to reduce recruitment of tumorigenic immune cells to the tumor microenvironment in pre/postoperative advanced lung cancer (Mohsenzadegan M., et al., 2020). Certainly, the DCs loaded with tumor antigens along with CIK cells may have a lower risk compared to CAR-T cells alone. To mention, the combination of CIK cells with PD-1 blockade before transfusion might improve the efficiency of CIK therapy

for NSCLC patients in vitro (Chen J., et al., 2018). Alternatively, autologous cytokine-induced killer (CIK) cells enhance the clinical response to PD-1 blocking antibodies in patients with advanced non-small-cell lung cancer (Han Y., et al., 2021). Recently, the benefits of combining anti-PD-1 antibody with antiangiogenic drugs anlotinib in NSCLC patients have been reported (Wang P., et al., 2021). Although there is some previous evidence of ICIs combinations, there has been no report on the combination of CIK with ALK inhibitors and PD-1 inhibitors neither in vitro nor vivo.

1.4. Purpose of this study

We aim to understand whether pretreated-nivolumab CIK cells before transfusion can enhance the antitumor immune response to NSCLC cell lines at different concentrations of crizotinib in vitro. To achieve this, we used three NSCLC cell lines: NCI-H2228 (EML4-ALK), A549 (KRAS mutation), and HCC-78 (ROS1 rearrangement) having different genetic alterations and employing multiple techniques (flow cytometry, intracellular staining for granzyme B, cell viability assays, ELISA, RT-PCR, Western blot).

1.2. Materials and methods

1.2.1. Regents and Antibodies

Anti-PD-1 mAb nivolumab (purity 99.50%) and ALK inhibitor crizotinib (purity ⩾98% (HPLC) were purchased from Selleckchem Co., Ltd. (Houston, TX). Crizotinib was dissolved in dimethyl sulfoxide (DMSO). DMSO was used as a control for crizotinib and 20 μg/mL IgG4 isotype (Biolegend, San Diego, CA) as a control for nivolumab. Concerning antibodies (Abs):

The fluorochrome-conjugated FITC anti-human CD3 antibody (Clone OKT3), brilliant violet 421 anti-human CD8 antibody (RPA-T8), APC anti-human CD4 antibody (Clone OKT4), PE-CD56 (Clone 5.1 H11), APC anti-human PD1 (Clone NAT105), PE anti-human PD-L1(Clone 29E-2A3), APC anti-human CTLA-4 antibody (Clone L3D10), PE anti-human GITR antibody (Clone 621), brilliant violet 421 anti-human CD134 (OX40) antibody (Clone Ber-ACT35), and FITC anti-human/mouse granzyme B antibody (GB11) were purchased from Biolegend (San Diego, CA). For APC-anti-human PD-1 detection, its isotype control is mouse IgG1k, which is not compatible to nivolumab as an IgG4 antibody. Anti-Human Foxp3 Staining Set FITC kit (eBioscience, San Diego, CA) was used to identify $Foxp3^{+}CD4^{+}CD25^{+}$/$CD4^{+}CD25^{-}$ cells according to the manufacturer's instructions. For Western blot: Anti-FasL (Biolegend, San Diego, CA) and beta Tubulin Loading Control Monoclonal Antibody (BT7R) (Thermo Fisher Scientific, San Diego, CA) were used.

1.2.2. Cell Culture

CIK cells were generated, as previously described (Schmidt-Wolf I.G., et al., 1991; Wu X., et al., 2020). PBMCs required for the experiments were isolated from the blood of healthy donors registered at the blood bank of University Hospital Bonn. Three epithelial lung cancer cell lines: A549 cells (KRAS mutation), HCC-78 (ROS1 rearrangement, SLC34A2-ROS1), and NCI-H2228 (EML4-ALK variant 3) were primarily used in this study. All cell lines were mycoplasma negative and cultured in RPMI medium supplemented with 10% heat-inactivated FBS (Sigma-Aldrich GmbH, Munich, Germany) and 1% penicillin/streptomycin (P/S) (Gibco, Germany) at 37°C (5% CO_2). As mentioned above, to avoid the excessive

toxicity of simultaneous treatment of nivolumab and crizotinib, CIK cells were pre-treated with 20 μg/mL anti-PD-1 mAb nivolumab or IgG4 isotype control for 24 h and then co-cultured with the tumor cells along with different concentrations of ALK inhibitor crizotinib.

1.2.3. Cell Viability Assessment by CCK-8 Assay and Cell Death Analysis by Flow Cytometry

CCK-8 cell viability assay was performed, as described by the manufacturer (Dojindo Laboratories, Kumamoto, Japan). NSCLC cells were seeded into 96-well plates ($1x10^4$ cells/well) and treated with various concentrations of crizotinib or DMSO for 24 h in the presence or absence of nivolumab. Similarly, the flow cytometry-based cytotoxicity was performed, as described protocol. Briefly, the target cells were labeled with CFSE (1×10^6 cells in 1 ml PBS with 0.5 u M CFSE, 20 min, 37˚C in the dark) and washed twice with warm culture medium. CFSE-labeled 5×10^4 tumor cells were incubated at various concentrations of crizotinib for 24 h with CIK cells pre-incubated with 20 μg/mL nivolumab or IgG 4 isotype (24 h) to perform redirected cytolysis assay at an E/T ratio of 10:1. Following 24 h of culturing, the cells were stained with Hoechst 33258 (Cayman Chemical, Hamburg, Germany) and were quantified using BD FACS Canto II. The absolute number of 3000 beads (Biolegend, San Diego, CA) was acquired by a BD Canto II cytometer. Then the absolute numbers of cells per uL were analyzed by FlowJo V10 software (Tree Star, Ashland, Oregon). The absolute number of cells were calculated according to Precision Count protocol provided by Biolegend Company as follows:

Absolute Cell Count (Cells/uL)=(Cell Count)/(Precision Count Beads^{TM}) x Precision Count BeadsTM Concentration

1.2.4. Intracellular Staining for Granzyme B by Flow Cytometry

A fixable Viability Zombie Aqua™ Dye (Biolegend, San Diego, CA) was used to exclude dead cells from the analysis. Mainly, after staining the surface receptors with PE anti-human CD3 antibody and APC anti-human CD56, the cells were fixed with 100 µL fix solution (eBioscience, San Diego, CA) for 30 min at room temperature (in the dark). Cells were then washed and resuspended in 100 µL 1x permeabilization buffer and stained with FITC anti-human granzyme B antibody for 30 min at room temperature. Subsequently, the cells were washed twice with 2 mL 1x permeabilization buffer, resuspended in DPBS, and recorded with a BD Canto II cytometer.

1.2.5. Enzyme-Linked Immunosorbent Assay (ELISA)

The ELISA assay was performed using the standard protocol. Briefly, 1 x 10^6 CIK cells incubated with 20 µg/mL nivolumab or IgG4 isotype control for 24 h. After that, CIK cells were co-cultured with 5 x 10^4 tumor cells in the presence of various concentrations of crizotinib for 24 h. Thereafter, the cell-free supernatant was collected to perform sandwich ELISA assay (IFN Gamma Kit, Invitrogen, Camarillo, CA), according to the manufacturer's instructions.

1.2.6. Reverse Transcription and Quantifying PCR (RT-qPCR)

CIK cells were incubated with 20 ug/mL nivolumab or IgG4 isotype control for 48 h. Afterward, CIK cells were washed twice with cold DPBS. RNA was extracted using RNeasy® Plus Mini

Kit (QIAGEN, Hilden, Germany) and cDNA synthesis was performed by SuperScript™ III First-Strand Synthesis Super Mix Kit (Invitrogen, CA), according to the manufacturer's instructions. Quantitative real-time PCR analysis was performed using QuantStadio 6 Flex Sequence Detection System (384-well, Applied Biosystems, CA) using SYBR® Select Master Mix (Applied Biosystems, CA). For q-PCR, the following primers were used to amplify PD-1 [as described (Mariotti F.R., et al., 2019)]: forward primer 5#-CAGGGTGACAGAGAAGGG-3#, reverse primer 5#-CCTGGCTCCTATTGTCCCTC-3#, β-actin: 5#-ACCGCGAGAAGATGACCCAGA3# (forward) and 5#-GGATAGCACAGCCTGGATAGCAA3# (reverse) (obtained by Eurofins Genomics Germany GmbH, Ebersberg, Germany). The relative expression of PD-1 was normalized to β-actin expression by ΔΔCt method. To determine C - reactive protein (CRP) transcription level, the following primers were used to amplify (as described (Chen Y., et al., 2018)): forward primer 5´- CAGACAGACATGTCGAGGAAGG-3#, reverse primer 5´-AGGCTTTGAGAGGCTTCGTT-3´, HPRT: 5´-TCAGGCAGTATAATCCAAAGATGGT-3´, (forward) and 5´-AGTCTGGCTTATATCCAACACTTCG-3´ (reverse) (obtained by Eurofins Genomics Germany GmbH, Ebersberg, Germany). The relative expression of c-reaction protein (CRP) was normalized to HPRT expression by the ΔΔCt method.

1.2.7. Western Blot Assay

CIK cells incubated with 20 ug/mL nivolumab and various concentrations of crizotinib for 48 h were washed twice with cold DPBS. Cell pellets were lysed using NuPAGE LDS buffer, lysates were separated on 4-12% Tris-glycine gels and transferred to PVDF membranes.

Anti-FasL antibody (Biolegend, San Diego, CA) were used for primary antibody. Beta Tubulin Loading Control Monoclonal Antibody (BT7R) (Thermo Fisher Scientific, Inc. San Diego, CA) was used as a loading control.

1.2.8. LDH Assay for the Assessment Hepatoxicity

The cytotoxicity of a combined nivolumab and crizotinib simultaneously in the absence or presence of CIK cells on hepatocyte-like cell line CCL-13, which exhibits the liver function of primary human hepatocytes, was detected by CyQUANT™ LDH Cytotoxicity Assay Kit (Invitrogen, Inc. San Diego, CA.). Briefly, we co-cultured CIK with $1x10^4$ CCL-13 cell line at an E:T ratio 1:1 in the presence of crizotinib/nivolumab triplicate in 96-well flat plates for 16 h. We calculated the percentage of hepatoxicity with the following formula:

$$\%\,\text{hepatoxicity} = \frac{experimental\ LDH\ activity\ -\ spontaneous\ CCL\ -\ 13\ LDH\ activity - spontaneous\ CIK\ LDH\ activity}{Maximum\ LDH\ activity\ -\ spontenous\ CCL\ -13\ LDH\ activity}$$

1.2.9. Statistical Analysis

All data were presented as the mean ± SD from at least three independent experiments. FACS data sets were analyzed using FlowJo V10.6 software (FlowJo, LLC, Ashland, Oregon). The statistical analysis was performed using SPSS Statistics 23. The data groups were compared using one-way analysis of variance with Turkey post hoc test and Student's t-test. P-values < 0.05 were considered significant differences and are marked: * < 0.05; ** < 0.01; *** < 0.001.

1.3. Results

1.3.1. Elevated PD-1/PD-L1 Expression in CIK Subsets After 14 Days of In Vitro Expansion

We have previously shown that CIK cells are heterogeneous and are composed of $CD3^+$ $CD8^+$, $CD3^+$ $CD4^+$ and $CD3^+$ $CD56^+$ specifically on Day 14 (Dehno M.N.,et al., 2020). Therefore, we first determined the phenotypes of PD-1 and PD-L1 CIK cells primarily on Day 0 and Day 14 for these three CIK subsets. The analysis showed that the percentage of PD-1^+ $CD3^+$ $CD4^+$ CIK cells increased significantly after 14 days of expansion compared to Day 0 (Figures 4A, B, 20.6 ± 2.0 vs. 4.7 ± 1.0%, $P < 0.001$). However, no significant difference in the $CD3^+$ $CD56^+$ and $CD3^+$ $CD8^+$ CIK cell subsets was observed (6.2 ± 0.7 vs. 7.7 ± 0.7%, P= 0.177; 10.2 ± 2.1 vs. 7.7 ± 0.8%, P= 0.630, respectively). Similarly, the proportion of PD-L1+ CIK cells was also increased among the $CD3^+$ $CD56^+$, $CD3^+$ $CD8^+$ and $CD3^+$ $CD4^+$ subsets of CIK cells on Day 14 compared to Day 0 (Figure 1B, 39. 5 ± 4.6% vs. 21.4 ± 5.9%, P= 0.025; 35.2 ± 4.5% vs. 12.1 ± 3.3%, $P < 0.001$; 51.6 ± 8.1% vs. 19.7 ± 4.2%, P= 0.008). To mention, we confirmed that all cell lines expressed PD-L1, but at different levels (Figure 1C, NCI-H2228 > HCC-78 > A549, 69.2 ± 8.0% on NCI-H2228, 61.8 ± 4.6% on HCC-78 and 6.0 ± 2.0% on A549).

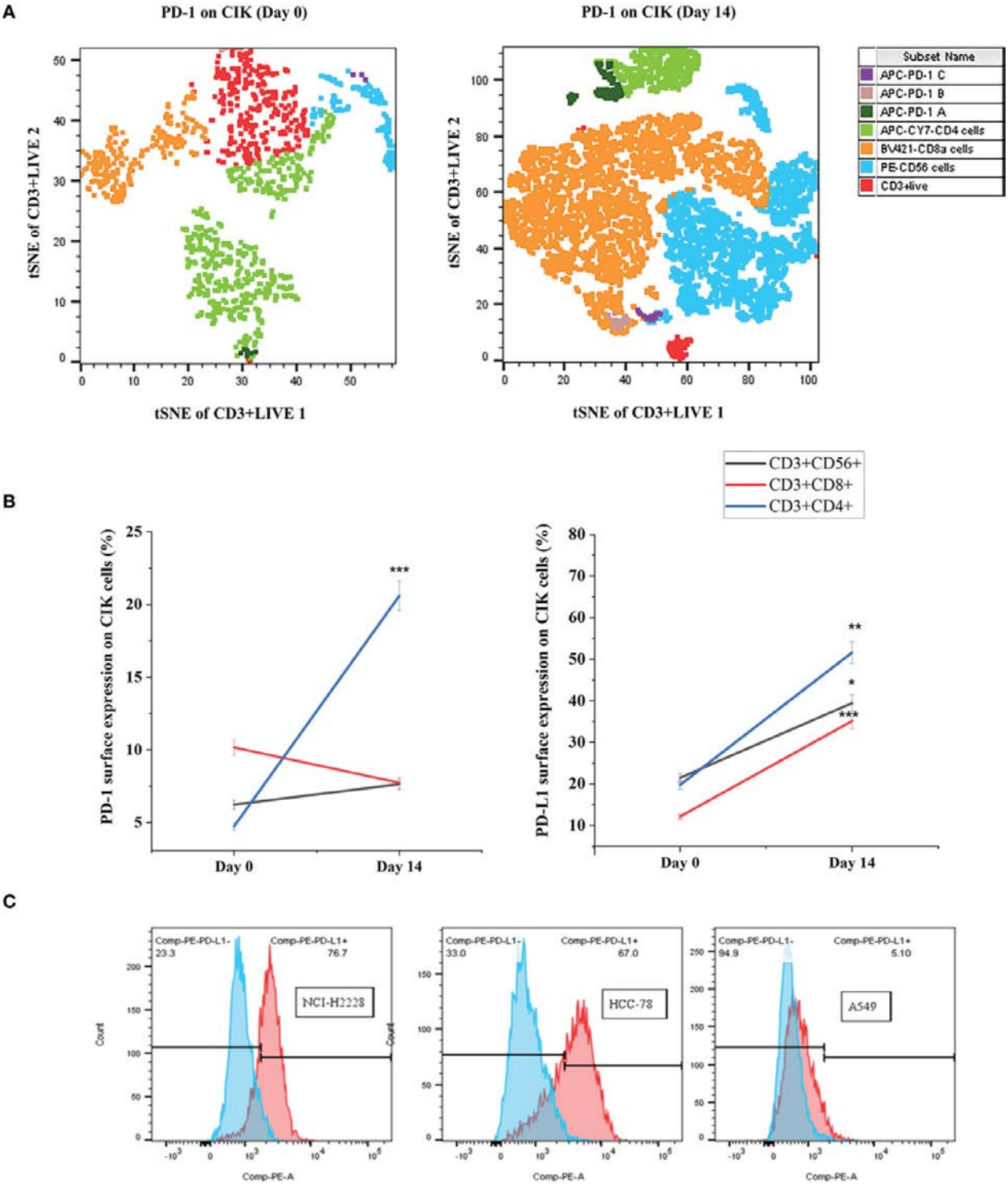
A
PD-1 on CIK (Day 0)
PD-1 on CIK (Day 14)
tSNE of CD3+LIVE 2
tSNE of CD3+LIVE 1
Subset Name
APC-PD-1 C
APC-PD-1 B
APC-PD-1 A
APC-CY7-CD4 cells
BV421-CD8a cells
PE-CD56 cells
CD3+live
B
CD3+CD56+
CD3+CD8+
CD3+CD4+
PD-1 surface expression on CIK cells (%)
PD-L1 surface expression on CIK cells (%)
Day 0
Day 14
***
**
*
C
Comp-PE-PD-L1-
Comp-PE-PD-L1+
23.3
76.7
NCI-H2228
33.0
67.0
HCC-78
94.9
5.10
A549
Count
Comp-PE-A

Figure 4. PD-1$^+$/PD-L1$^+$ surface expression on Day 0 and Day 14 of CIK cells. The differential expression of PD-1/PD-L1 phenotypic subsets of CIK cells over in vitro culture is shown by flow cytometric analysis. PBMC were isolated from healthy donors and cultured in the presence of IFN- γ on Day 0, anti-human CD3 antibody, IL-1 β and IL-2 on Day 1. After 14 days of expansion with IL-2 induction, CIK cells were investigated by flow cytometric method by staining with FITC-CD3, PE-CD56, APC-Cy7-CD4, Bv421-CD8, and APC-PD-1. Dead CIK cells were gated excluding by 7-AAD. (A) The percentage of PD-1 on Day 0 and Day 14 CIK cells represented by tSNE plots using Flowjo V10 software. APC-PD-1 A represented APC-PD-1$^+$ APC-CY7-CD4$^+$ cells; APC-PD-1 B represented APC-PD-1$^+$BV421-CD8a$^+$ cells; APC-PD-1 C represented APC-PD-1$^+$PE-CD56$^+$ cells. (B) Summary data of the frequency of PD-1$^+$/PD-L1$^+$ CIK subsets in healthy subjects. (C) Variation of PD-L1 surface expression on the 3 NSCLC cell lines, measured by flow cytometry. All data are shown as the mean ± SD. * representative of three independent experiments. *P < 0.05, **P < 0.01, ***P < 0.001 vs. Day 0 CIK cells calculated by Student's t-test. CIK cells derived from three healthy donors.

1.3.2. Nivolumab Harbours the Potential to Block Surface Expression of PD-1 on CIK Cells

Next, we examined the association between CIK cell activation and PD-1 surface expression in the presence of nivolumab and found that PD-1 expression on the surface of CD3$^+$ CIK cells decreased significantly from 6.7 ± 2.7% to 0.4 ± 0.04% after 48 h of treatment with nivolumab compared to the IgG4 isotype control (Figure 5A). Also, the assessment of the mean fluorescence intensity (MFI) of surface expression of potential immune-associated markers, including PD-L1, PD-L2, CD28, CTLA-4, GITR, and CD134 on CD3$^+$ CIK cells, showed no alterations (Figure 5B). When counting the absolute number of PD-1$^+$ CIK cells, there was also a notable decrease in both PD-1$^+$ CD3$^+$ CIK cells and/or PD-1$^+$ CD3$^+$ CD56$^+$ CIK cells after the nivolumab treatment (Figure 5C, 0.01 ± 0.01 vs. 0.57 ± 0.18 cells/μL, P= 0.045; 0.01 ± 0.01 vs. 0.38 ± 0.13 cells/μL, P= 0.036, respectively). Besides, PD-1 mRNA

levels were not altered by nivolumab (Figure 2D, P= 0.408). These findings suggest that nivolumab blocks PD-1 on the surface of CIK cells. Interestingly, nivolumab caused a significant increase in the levels of $CD4^+$ $CD25^+$ CIK cells expressing Foxp3 (Figure 2E, P= 0.044).

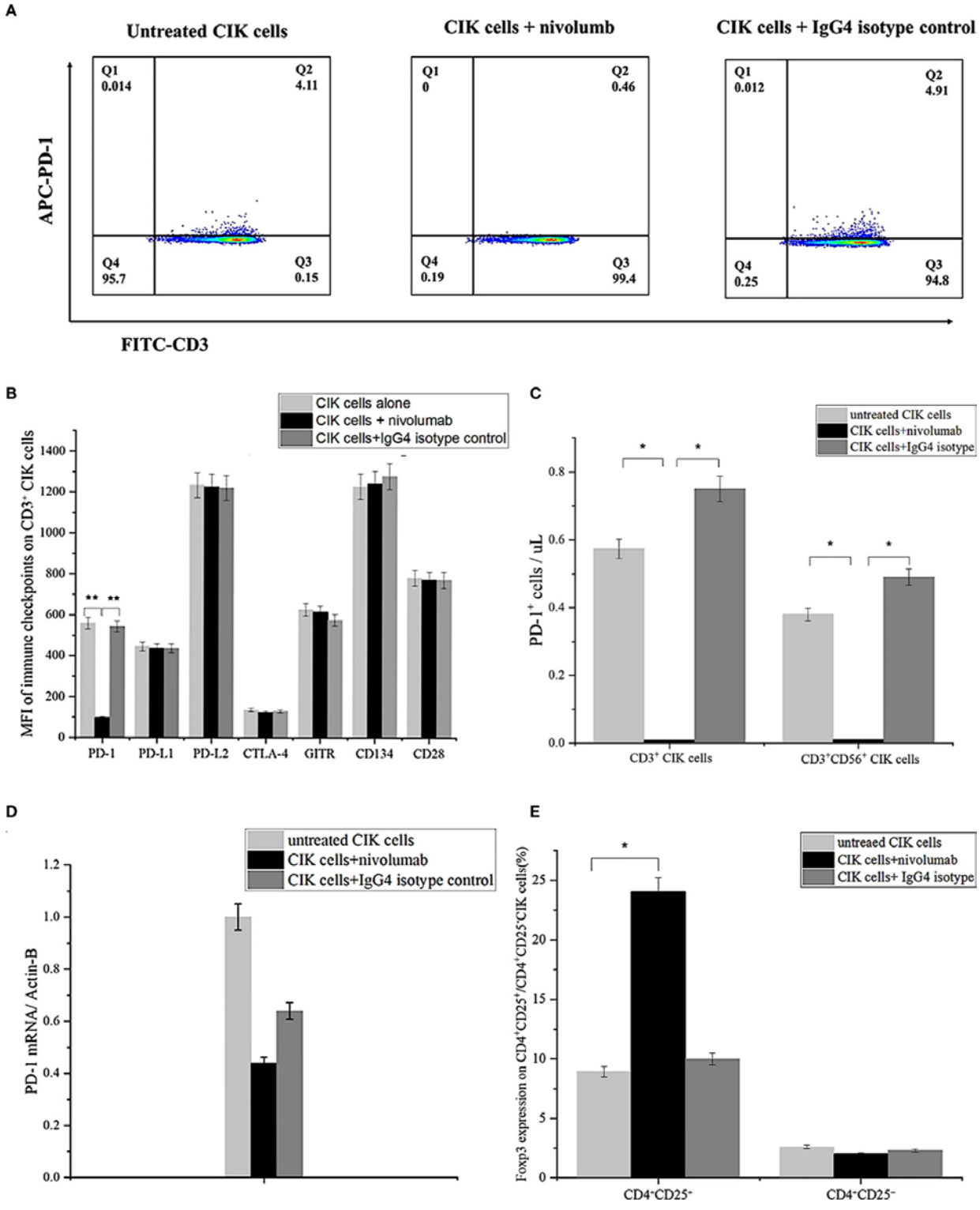
A
Untreated CIK cells
CIK cells + nivolumb
CIK cells + IgG4 isotype control
Q1 0.014
Q2 4.11
Q4 95.7
Q3 0.15
Q1 0
Q2 0.46
Q4 0.19
Q3 99.4
Q1 0.012
Q2 4.91
Q4 0.25
Q3 94.8
APC-PD-1
FITC-CD3
B
CIK cells alone
CIK cells + nivolumab
CIK cells+IgG4 isotype control
MFI of immune checkpoints on CD3+ CIK cells
PD-1
PD-L1
PD-L2
CTLA-4
GITR
CD134
CD28
C
untreated CIK cells
CIK cells+nivolumab
CIK cells+IgG4 isotype
PD-1+ cells / uL
CD3+ CIK cells
CD3+CD56+ CIK cells
D
untreated CIK cells
CIK cells+nivolumab
CIK cells+IgG4 isotype control
PD-1 mRNA/ Actin-B
E
untreaed CIK cells
CIK cells+nivolumab
CIK cells+ IgG4 isotype
Foxp3 expression on CD4+CD25+/CD4+CD25+CIK cells(%)
CD4+CD25+
CD4+CD25-

Figure 5. PD-1 expression on CIK cells after treatment with nivolumab for 48 (h) (A) PD-1 surface expression on CIK cells in the presence of nivolumab 20 μg/mL for 48 h compared to untreated CIK cells or IgG4 isotype control 20 μg/mL measured by flow cytometry. Dead CIK cells were gated and excluded by 7-AAD. Numbers represent the percentage of the gated population. (B) The mean fluorescent intensity (MFI) level of PD-1, PD/L1, PD-L2, CTLA-4, GITR, and CD134 (OX40) on the $CD3^+$ CIK cells was observed after 48 h of treatment with nivolumab by flow cytometry. (C) Numbers represent the percentage of the gated population. Quantification of the absolute $PD\text{-}1^+$ CIK cells by count beads. (D) Analysis of q-RCR mRNA expression in CIK cells after incubation with nivolumab for 48 (h) PD-1 expression is normalized over β-actin expression. (E) Foxp3 expression on $CD4^+$ $CD25^+/CD4^+CD25^-$ CIK cells after 48 h nivolumab treatment. Data from three independent experiments were shown as mean ± SD. Statistical analysis was performed using one-way ANOVA followed by the Tukey–Kramer post hoc test. *$p < 0.05$, **$p < 0.01$ vs. untreated CIK cells or CIK cells treated with IgG4 isotype control. CIK cells derived from three healthy donors.

1.3.3. Nivolumab Affected the Cell Viability of Crizotinib-Treated NCI-H2228

Considering that nivolumab may reduce the tumor cell viability, we performed the CCK-8 assay and found that the combined treatment of nivolumab with crizotinib significantly impaired the viability of NCI-H2228 cells (Figure 6A). Primarily, a significant change was observed when 20 μg/mL nivolumab and 100 nM crizotinib/1000 nM crizotinib were administered in NCI-H2228 cells compared to DMSO control (Figure 6A, 65.0% ± 3.9% vs. 97.2% ± 3.0%, $p < 0.001$; 58.3% ± 3.1% vs. 97.2% ± 3.0%, $p < 0.001$, respectively). However, no such change was observed in the HCC-78 and A549 cell lines as well as CIK cells, suggesting that this effect is cell line (or EML4-ALK variant 3) specific (Figures 6B–D).

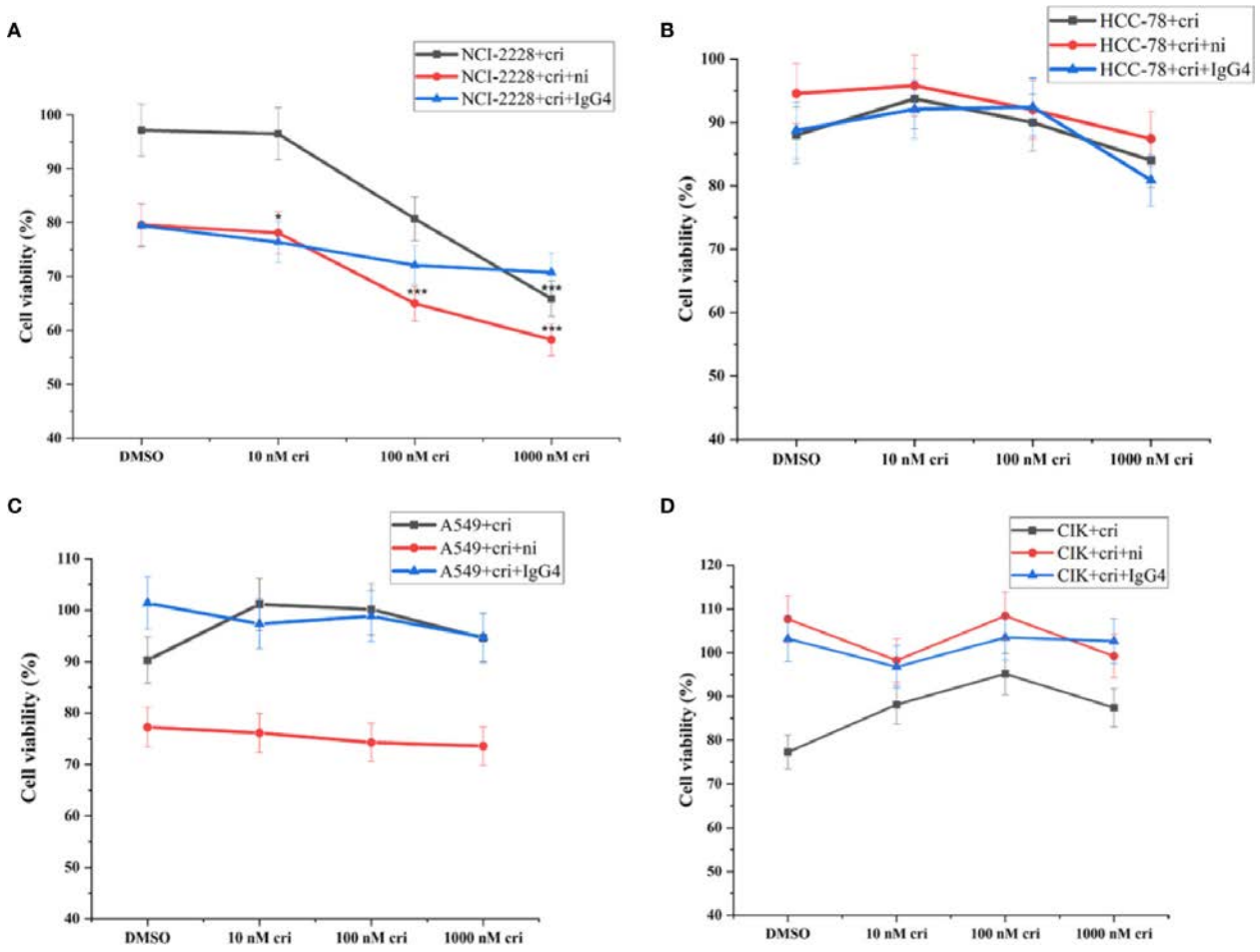

Figure 6. The tumor cell viability after the combination of nivolumab and crizotinib in the absence of CIK cells and CIK cells viability after the combination of nivolumab and crizotinib in the absence of tumor cells. (A–C) Tumor cells were pretreated with 20 ug/mL nivolumab for 24 h prior to incubation with crizotinib for 24 h. (D) CIK cells were pretreated with 20 ug/mL nivolumab for 24 h prior to incubation with crizotinib for 24 h. Each experiment repeated 3 times and CIK cells derived from four donors. All data are shown as the mean ± SD. *representative of three independent experiments. *P < 0.05, ***P < 0.001 vs. NCI-H2228 treatedwith DMSO control. One-way ANOVA followed by the Tukey–Kramer post hoc test was performed. CIK cells derived from three healthy donors.

1.3.4. Nivolumab and Crizotinib Displayed an Additive Effect on the Cytotoxicity

To assess the absolute quantification of dead tumor cells (that may directly reflect the cytotoxic activity of CIK cells), we pre-labelled the NSCLC cells with carboxyfluorescein

diacetate succinimidyl ester (CFSE) and co-cultured with nivolumab-pretreated CIK cells at an effector-target ratio of 10:1 in the presence of crizotinib. The absolute number of dead NCI-H2228 cells was found to be significantly elevated after combining 10 nM crizotinib/100 nM crizotinb/1000 nM crizotinb with nivolumab compared to the NCI-H2228 control (32.2 ± 3. 9 cells/μL vs. 3.3 ± 0.9 cells/μL, P< 0.001; 30.6 ± 3.8 cells/μL vs. 3.3 ± 0.9 cells/μL, P< 0.001; 24.9 ± 2.7 cells/μL vs. 3.3 ± 0.9 cells/μL, P = 0.004, respectively) (Figure 7A). Here again, two other cell lines (HCC-78 and A549) showed weaker sensitivity to CIK cytotoxicity when combined with crizotinib and nivolumab (Figures 7B, C). Meanwhile, this combination strategy did not influence the dead cell number in CIK cells (Figure 7D).

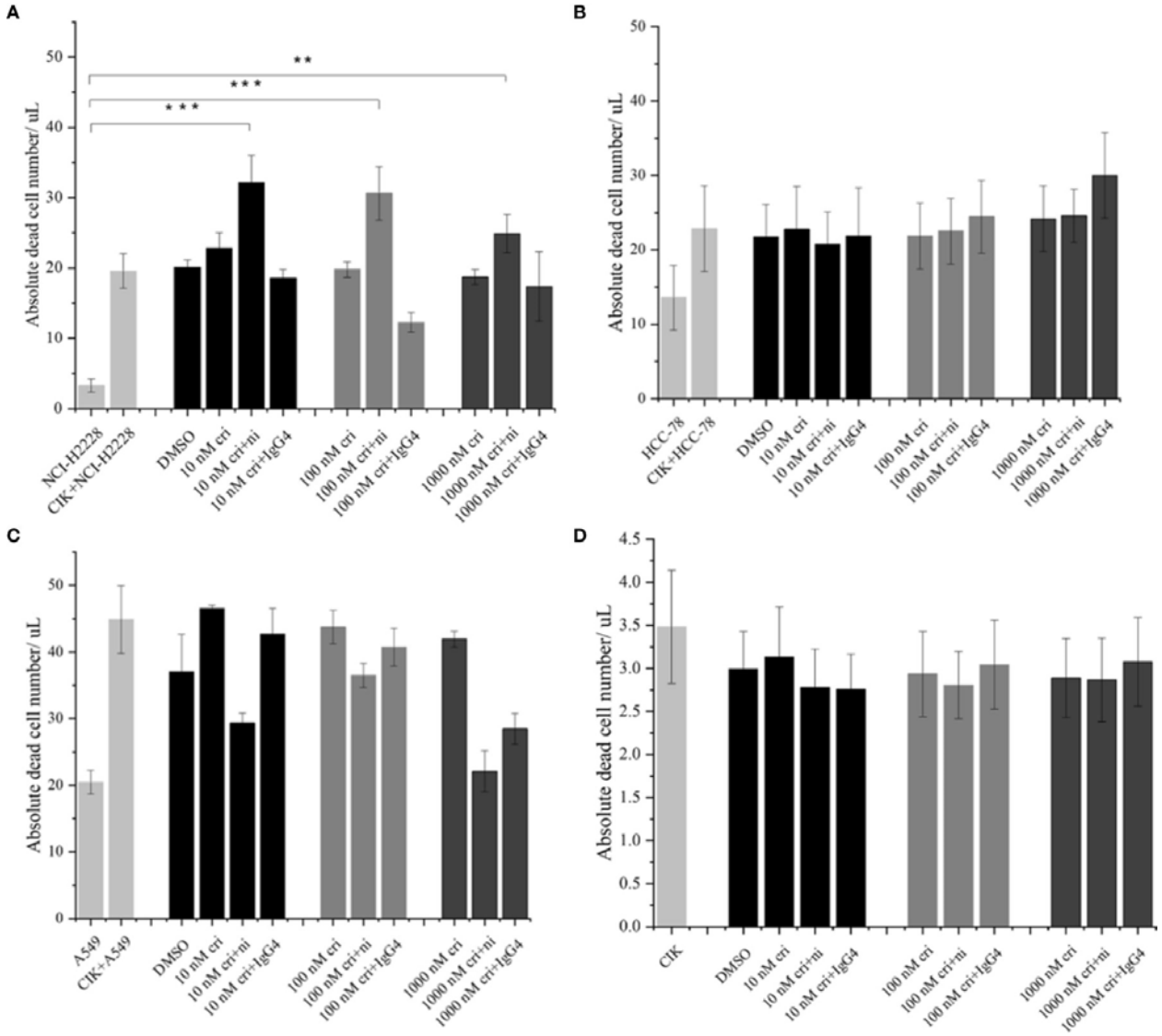

Figure 7. The absolute dead cell concentration after the combination of nivolumab and crizotinib. (A–C) The absolute number of dead cells in NSCLC cell lines after the co-culture with 24 h nivolumab-pretreated CIK, and in the presence of crizotinib (for 24 h) were detected by flow cytometry. NSCLC cells were labelled with CFSE and stained with dead cell Dye Hoechst 33258 before data was recorded in the flow cytometer. Dead $CFSE^{+}$ tumor cells were analyzed by count beads and recorded by absolute cells/μL. (D) Similarly, 24 h nivolumab-pretreated CIK incubated with crizotinib (for 24 h) in the absence of tumor cells were stained with dead cell Dye Hoechst 33258 and detected by flow cytometry. Each experiment repeated 3 times and CIK cells derived from three donors. Data from

three independent experiments were shown as mean ± SD. Statistical analysis was performed using one-way ANOVA followed by the Tukey–Kramer post hoc test. **p < 0.01, ***p < 0.001 vs. untreated NCI-H2228.

1.3.5. Cumulative Effect of PD-1 Inhibitor With Crizotinib Influenced Interferon-γ and Intracellular Granzyme B

To investigate the potential variations in immune markers and cytokines primarily associated with the cytotoxicity of CIK cells, we subsequently examined IFN-γ expression (by ELISA) and intracellular expression of granzyme B by flow cytometry (Figures 8A, B) and IFN-γ expression by ELISA (Figure 8C). CIK cells responded to a combination of PD-1 blockade and crizotinib against NCI-H2228 with a strong secretion of IFN-γ and a significant increase in granzyme B in the $CD3^+$ $CD56^+$ subpopulation of CIK cells. Specifically, in combination with CIK cells, anti-PD-1 and 10 nM crizotinib showed a significant increase compared to either crizotinib or isotype control and/or crizotinib alone (320.3 ± 48.2 vs. 232.8 ± 41.6 pg/mL, P= 0.004; 320.3 ± 48.2 vs. 251.1 ± 40.1 pg/mL, P= 0.022). However, no significant change was observed in the HCC-78 and A549 cell lines (Figure 9).

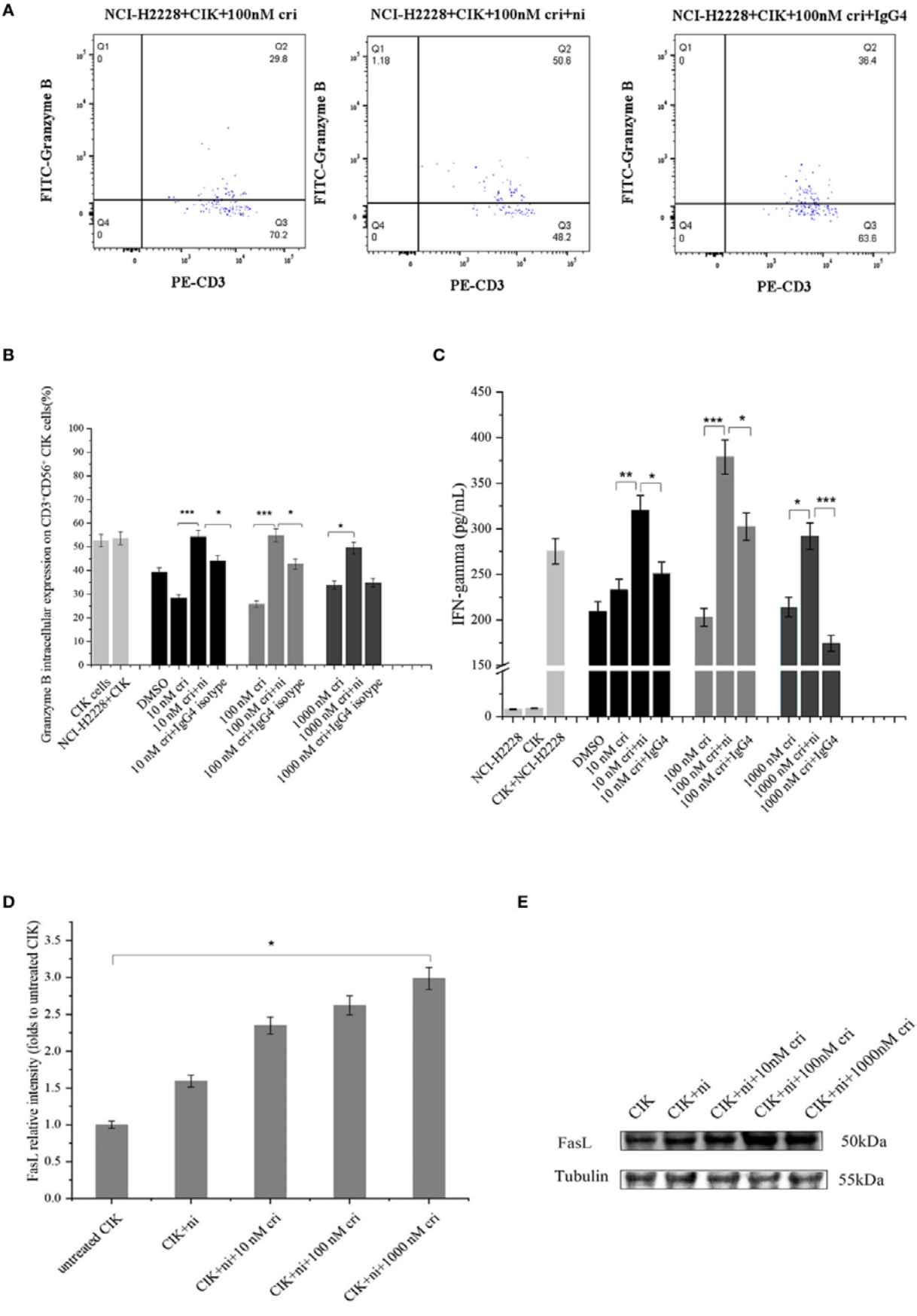
A
NCI-H2228+CIK+100nM cri
NCI-H2228+CIK+100nM cri+ni
NCI-H2228+CIK+100nM cri+IgG4
FITC-Granzyme B
PE-CD3
Q1 0
Q2 29.8
Q4 0
Q3 70.2
Q1 1.18
Q2 50.6
Q4 0
Q3 48.2
Q1 0
Q2 36.4
Q4 0
Q3 63.6
B
Granzyme B intracellular expression on CD3+CD56+ CIK cells(%)
CIK cells
NCI-H2228+CIK
DMSO
10 nM cri
10 nM cri+ni
10 nM cri+IgG4 isotype
100 nM cri
100 nM cri+ni
100 nM cri+IgG4 isotype
1000 nM cri
1000 nM cri+ni
1000 nM cri+IgG4 isotype
C
IFN-gamma (pg/mL)
NCI-H2228
CIK
CIK+NCI-H2228
DMSO
10 nM cri
10 nM cri+ni
10 nM cri+IgG4
100 nM cri
100 nM cri+ni
100 nM cri+IgG4
1000 nM cri
1000 nM cri+ni
1000 nM cri+IgG4
D
FasL relative intensity (folds to untreated CIK)
untreated CIK
CIK+ni
CIK+ni+10 nM cri
CIK+ni+100 nM cri
CIK+ni+1000 nM cri
E
CIK
CIK+ni
CIK+ni+10nM cri
CIK+ni+100nM cri
CIK+ni+1000nM cri
FasL
50kDa
Tubulin
55kDa

Figure 8. Effects of a combination of blocking PD-1 immune checkpoint and crizotinib on CIK-derived IFN-γ, granzyme B in $CD3^+$ $CD56^+$ CIK cells. CIK cells were pretreated in the presence or absence of 20 ug/ml nivolumab. At 24 h post mAb treatment in CIK cells, CIK cells were co-cultured with NCI-H2228. (A) Intracellular granzyme B expression in $CD3^+$ $CD56^+$ CIK cells in the presence of PD-1 blockade against NCI-H2228 cells is shown in a dot plot, measured by flow cytometry at different levels of crizotinib. (B) Bar plots depict the percentage of intracellular granzyme B expression on CIK cells and (C) IFN-γ levels from CIK cells after treatment with a combination of PD-1 blockade and crizotinib on NCI-H2228 target cells. *$p < 0.05$, **$p < 0.01$, ***$p < 0.001$ vs. crizotinib monotherapy or IgG4 isotype control. (D) FasL expression was observed by Western blots. CIK cells were treated with nivolumab for 24 h prior to the addition of different concentrations of crizotinib. (E) The relative intensities of FasL expression normalized to each Tubulin control without treatment were defined as 1.0. Then, the other relative intensity (folds) was presented. Data were presented as means ± SD of the results from three independent experiments. *$p < 0.05$ vs. CIK control without any treatment. Each experiment repeated 3 times and CIK cells derived from three donors and the data were shown as mean ± SD. Statistical analysis was performed using one-way ANOVA followed by the Tukey–Kramer post hoc test.

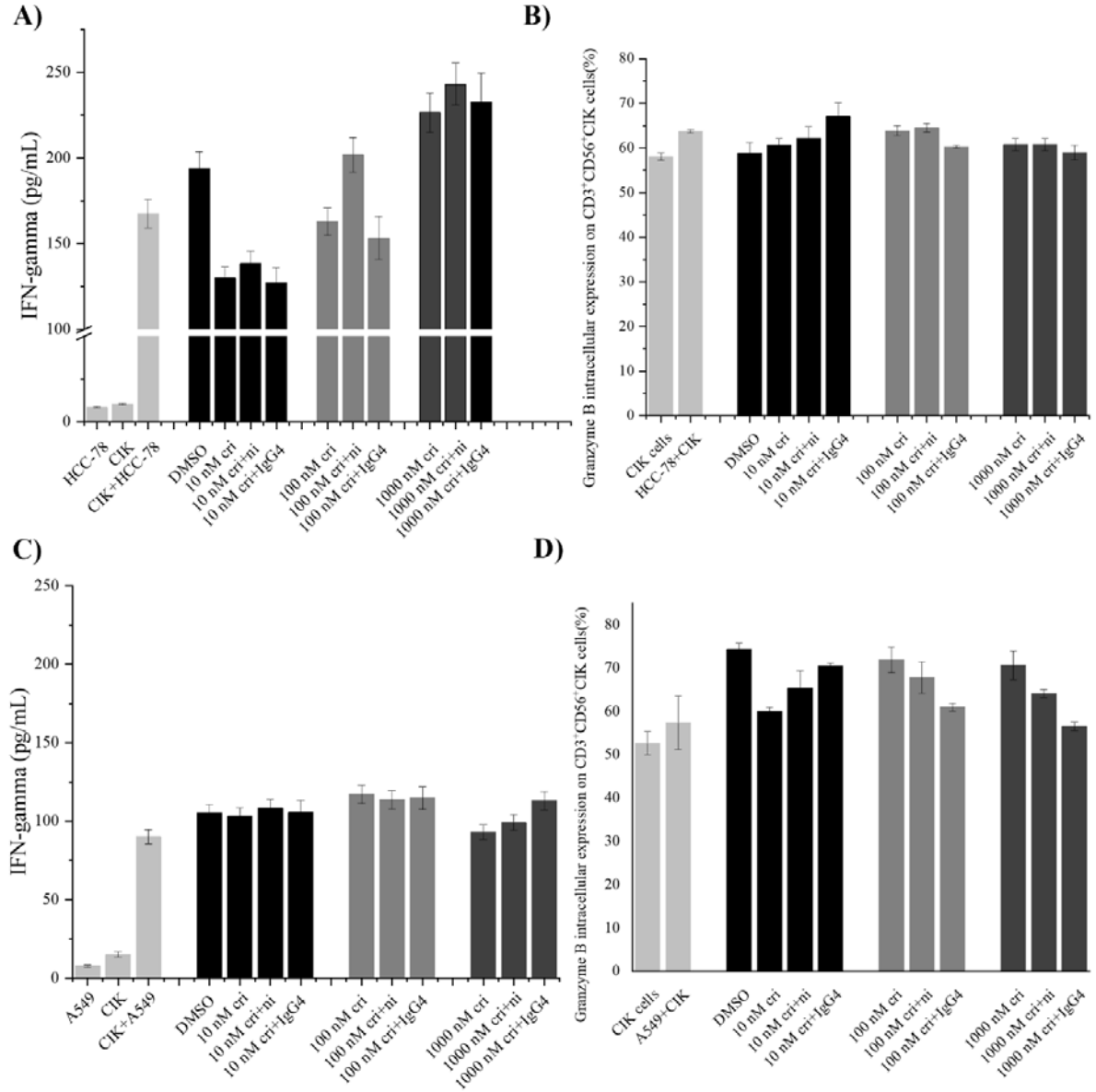

Figure 9. Effects of a combination of blocking PD-1 immune checkpoint and crizotinib on CIK-derived IFN-γ, granzyme B in $CD3^+$ $CD56^+$ CIK cells. a) The level of IFN-γ from CIK cells co-culturing with HCC-78 cells, b) granzyme B expression in CIK cells co-culturing with HCC-78 cells, c) the level of IFN- γ from CIK cells co-culturing with A549 cells, d) granzyme B expression in CIK cells co-culturing with A549 cells.

1.3.6. Nivolumab Combined Crizotinib Upregulated the Intrinsic FasL Expression in CIK Cells

Considering that cell surface FasL expression is specific to the immune system, we investigated FasL surface expression on the CIK cells. The analysis showed a low level of surface FasL (less than 5%), which was further verified using an additional methodological approach (Western blot) (Figures 8D, E). Importantly, nivolumab combined with 1000 nM crizotinib resulted in significant upregulation of intrinsic FasL expression compared to the untreated CIK control (the band intensity 3.0 ± 0.7 vs. 1.0 ± 0.0, P= 0.028).

1.3.7. CIK Cells Ameliorated the Hepatoxicity in CCL-13 Cell Line Concurrent Incubation With Nivolumab Combined With Crizotinib

To assess the hepatoxicity, LDH release assay was performed. After incubation with CIK cells, cytotoxicity of the simultaneous combination of 1000 nM crizotinib and nivolumab was significantly reduced compared to cytotoxicity without CIK (Figure 10A, $P<0.001$). Furthermore, the combination of CIK cells with crizotinib and nivolumab significantly decreased the mRNA expression of C - reactive protein (CRP), which is known to be associated with reactive oxygen species (ROS) (Figure 10B, P=0.047).

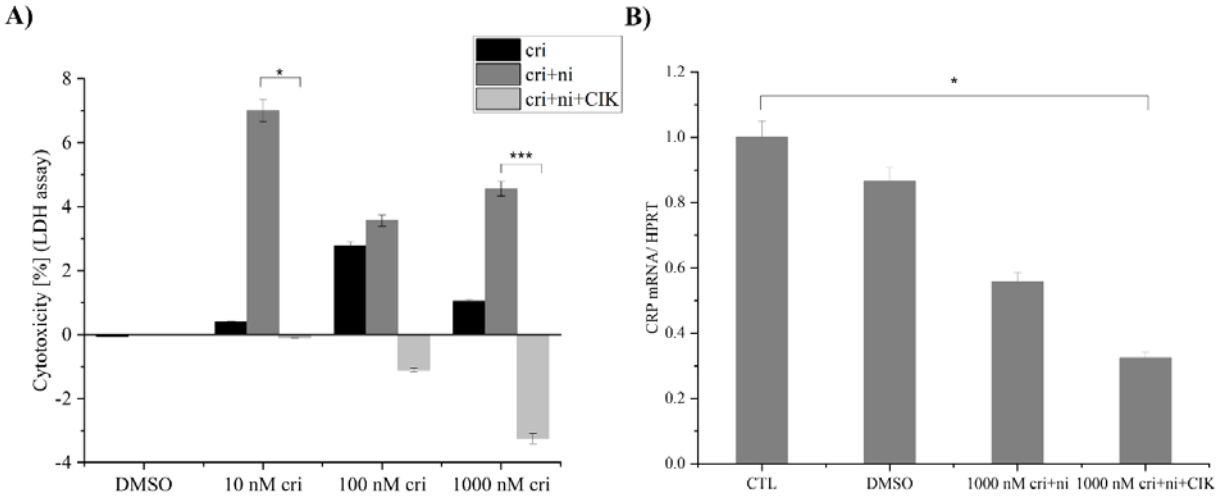

Figure 10. The hepatoxicity of a combination of blocking PD-1 immune checkpoint and crizotinib on hepatocyte-like cell line CCL-13 in the presence of CIK cells simultaneously. a) The percentage of the cytotoxicity detected by lactate dehydrogenase (LDH) release for 16 hours co-culture with CIK cells and CCL-13 in the presence of crizotinib and nivolumab simultaneously, b) the mRNA expression of C-Reactive Protein (CRP) in CCL-13 co-culture with CIK cells in the presence of crizotinib and nivolumab simultaneously for 24 hours. Each experiment was repeated 3 times, CIK cells were derived from three donors and the E:T ratio is 1:1. The data are shown as mean ± SD. Statistical analysis was performed using one-way ANOVA followed by the Tukey–Kramer post hoc test. * $p < 0.05$, *** $p < 0.001$.

1.4. Discussion

Given cancer is quite a complex disease and monotherapies pose a serious challenge regarding patient survival rate, the development of new combination therapies has partially improved patient outcomes. The combined use of therapeutic agents within combination therapy has proven to be advantageous (over monotherapy) in several ways, such as enhanced efficacy, reduced side effects, and minimal drug resistance. Of clinical importance, several cancers have been reported to optimize this therapeutic approach, such as renal cell

carcinoma, melanoma, Hodgkin's lymphoma, and breast cancer to name a few (Zhang L., et al.,2021; Sanchez J.N., et al., 2021; Pezeshki P.S., et al., 2021; Ma H., et al., 2021). In particular, non-small cell lung cancer (NSCLC) is one of the prominent cancers where a number of studies documenting the clinical outcomes of mono and/or combination therapies have been reported (www.cancer.gov). However, there are serious concerns when the combination of compounds showed a synergistic effect in the preclinical models while failing in the clinical application. As mentioned above, the clinical trial with the combination of crizotinib (ALK inhibitor) and nivolumab (PD-1 inhibitor) was terminated due to safety concerns in NSCLC, while the same combination of compounds showed an improved antitumor response with favourable side-effect tolerability in the in vivo model.

In this current study, we investigated whether the inclusion of alternative treatments (for instance, cytokine-induced killer cells) and variable genetic backgrounds (NCI-H2228: EML4-ALK, A549: KRAS mutation, HCC-78: ROS1 rearrangement) within the same cancer type can help to provide an advantageous therapeutic paradigm in NSCLC. In the context of genetic variations, mutations in a few genes (KRAS, EGFR, ALK, ROS1, BRAF, RET, MET, NTRK) have been shown to be clinically relevant and proven to be pivotal to identify patient subgroups with early/advanced-stage patients. Moreover, accumulating data from different ethnic groups has confirmed these previous findings on the NSCLC-associated mutational paradigm and highlighted the potential genetic differences across different racial groups (Wu X., et al., 2013; Arauz R.F., et al., 2020; Aye P.S., et al., 2021), given that CIK cells have previously shown positive outcome in NSCLC treatment, and nivolumab has been shown to be highly promising in NSCLC (Sundar R., et al., 2015). As a proof of concept, we first

confirmed that all cell lines expressed PD-L1, but at different levels. Next, we demonstrated that a combination of nivolumab and crizotinib improved the immune function of CIK cells compared to monotherapy with crizotinib, especially in the NSCLC-specific cell line NCI-H2228. We further first verified that PD-1 surface expression on CIK cells decreased dramatically after the treatment with nivolumab and it had no effect on PD-1 mRNA expression in CIK cells. Our findings revealed that PD-1 inhibitors only conjugate on the surface of CIK cells without PD-1 mRNA alternation. Nevertheless, nivolumab was found to bind to T lymphocytes for more than 20 weeks in NSCLC patients, even after stopping treatment, suggesting a sustained therapeutic effect (Osa A., et al., 2018). Although one clinical trial reported that treatment of NSCLC patients with anti-PD-1 antibodies nivolumab expanded the levels of effector T cells expressing the costimulatory molecules CD28, CD27, and ICOS (Xiong Y., et al., 2020), we did not observe the similar immuno-logical events (Figure 5B). Importantly, our study showed that nivolumab caused an increase in the proportion of $Foxp3^+$ $CD4^+$ $CD25^+$ CIK cells (Figure 5E), which is consistent with the previous reports (He Y., et al., 2018). This suggests compensatory expression of immune molecules after PD-1 blockade. Second, we observed that the blocking of the PD-1/PD-L1 pathway by nivolumab increased the cytotoxicity of CIK cells targeted to NCI-H2228 rather than HCC-78 and A549 cells. Additionally, the evidence obtained from multiple markers in our study, such as increased production of IFN-γ from CIK cells, activation of FASL in CIK cells, and increased intracellular expression of granzyme B on $CD3^+$ $CD56^+$ NKT CIK cells, suggest that the combination of nivolumab and crizotinib accelerates the release of immune-related effector molecules. Previously, CIK cells were reported to express a high percentage of

granzyme B, a serine protease that together with another protein perforin mediates apoptosis in target cells (Niu C., et al., 2015). Similarly, an addition of anti-PD-1 inhibitor has been shown to enhance the granzyme B expression in DC-CIK cells (Zhang W., et al., 2019). Considering this, we assessed and found an increased level of intracellular granzyme B in PD-1 activated CIK cells after being combined with an ALK inhibitor. FasL, expressed on activated T cells and natural killer (NK) cells, poses another way to kill cancer cells by recruiting Fas-associated protein with DD (FADD) and activating caspase pathways. Notably, Verneris et al. found that CIK cells are resistant to apoptosis by expressing anti-apoptotic genes and can synthesize FasL to induce Fas-dependent apoptosis of sensitive tumor cells (Verneris M.R., et al., 2000). In our current study, we are reporting for the first time that a combination of dose-dependent crizotinib and nivolumab can also promote FASL expression in CIK cells, overall suggesting that CIK cells use a different apoptosis pathway to eliminate NSCLC cells in vitro. Thus, our findings about the elevated granzyme B levels (along with activation of FASL) in a similar experimental setup suggest a yet unknown mechanism that may be of interest for future NSCLC immunotherapy.

Since our analysis showed predominance in NCI-H2228 compared to HCC-78 and A549 cells, we can assume three possibilities: (1) heterogeneity across cancer cell lines may lead to major discrepancies in the experimental data, as previously discussed by Sharma et al. (Sharma A., et al., 2020), (2) origin of cell lines, A549 is a lung adenocarcinoma cell line with a mesenchymal signature and is known to be more resistant to the drugs targeting PI3K-AKT pathway (Byers L.A., et al., 2013), and (3) the presence of intrinsic PD-1 protein expression

in NSCLC cells that may inhibit tumor cell proliferation and might exert resistance to PD-1/PD-L1 blockades (Wang X., et al., 2020). Nevertheless, our study supports the idea that combination therapies have enormous potential if they are optimized on a patient-by-patient basis. Like other cancers, the clonal heterogeneity and the existence of cancer stem cells (CSCs) in lung cancer also continue to be subjects of discussion (Testa U., et al., 2018). In an interesting study, six small cell lung cancer (SCLC) cell lines were used to investigate whether CD133 or CD87 could be a potential marker for CSCs (Kubo T., et al., 2013). The authors showed that both CD133 and CD87 are expressed in the SBC-7 cell line as inadequate markers of CSCs and might be beneficial for predicting chemotherapy resistance. Recently, a study confirmed the identification of CSCs and showed that PD-L1^{+} CSCs are strongly associated with altered T cell phenotypes and, in particular, the frequency of regulatory molecule-expressing T cells in metastatic lymph nodes of NSCLC patients (Raniszewska A., et al., 2021). Of note, our current study mainly concerns enhancing the cytotoxicity and did not emphasize CSCs; however, we cannot exclude the contribution of lung cancer associated CSCs. Certainly, future studies utilizing CIK/ALK/PD inhibitors axis in context with the tumor microenvironment of NSCLCs will be of interest. Here, it is also important to mention CheckMate 370, which was discontinued due to severe hepatotoxicity in 2018. In this context, we also performed analysis to determine whether CIK cells can alleviate the hepatoxicity after incubation with ALK inhibitor and PD-1 inhibitor simultaneously. To achieve this, we used the hepatocyte-like cell line CCL-13, which exhibits the liver function of primary human hepatocytes, and found that: (1) after incubation with CIK cells, the cytotoxicity of the simultaneous combination of crizotinib and nivolumab was significantly

reduced as detected by LDH assay. (2) The combination of CIK cells with crizotinib and nivolumab significantly decreased the mRNA expression of C-reactive protein (CRP), which is known to associate with reactive oxygen species (ROS). Therefore, it is reasonable to conclude that CIK cells may have mitigated with hepatotoxicity. In broader terms, the limitations of our study are also worth mentioning, such as (A) we did not investigate the combination of DC-CIK and ALK inhibitor with PD-1 inhibitor, which may exert more potent cytotoxic effects than CIK cells as shown in previous studies (Zhang W., et al., 2019). (B) The data from a few additional cell lines (e.g., with KRAS, EGFR, and p53 mutation status) would be valuable in this analysis. (C) Our findings require in vivo validation. Despite these facts, our data as preclinical model provide an insight about the antitumor immune response by CIK cells in combination with crizotinib and nivolumab.

Based on our results and the existing literature, a few perspectives can be considered for NSCLC, for example, (a) given that response to therapies and improved survival varies significantly in NSCLC subtype, a clear emphasis on precision medicine/therapy should be considered. (b) With the development of second- and third-generation ALK inhibitors, their synergistic effects in preclinical studies, mainly on experimental models associated with NSCLC mutations, may improve their efficacy and resistance problem. (c) As recently proposed, the combinatorial aspect of CIK cell therapy combined with other contemporary anti-cancer therapies in a complementary (rather than competitive) manner may be the key to combat cancer (Sharma A., et al., 2021), also applies in NSCLC. (d) Identifying a subpopulation of NSCLC patients (with ALK rearrangement) who may benefit from the

combination of an ALK inhibitor and PD-1 inhibitor must be stratified according to known risk factors (Hill H., et al., 2021) and potential biomarkers (e.g., C-reactive protein levels) (Ried J.M., et al., 2020). In a broader prospective, though different cancers are represented with their unique mutational/epigenomic profiles, they still share few common/overlapping signalling pathways (Liu H., et al., 2020) and, therefore, it is important to stratify the uniqueness of each cancer type already in the preclinical models.

1.5. Conclusions

CIK cells in combination with crizotinib and nivolumab can enhance the antitumor immune response through FasL activation, leading to increased IFN-γ and granzyme B, but only in NCI-H2228 cells with EML4-ALK rearrangement. Hence, our study suggests that genetic background plays a significant role, and the combination therapies should be optimized by considering underlying factors (genetic background and immune response) on a patient-by-patient basis.

1.6. Abstract

Background: Cancer heterogeneity poses a serious challenge concerning the toxicity and adverse effects of therapeutic inhibitors, especially when it comes to combinatorial therapies that involve more than one targeted inhibitor. In particular, in non-small cell lung cancer (NSCLC), a number of studies have reported synergistic effects of drug combinations in the preclinical models, while they were only partially successful in the clinical setup, suggesting those alternative clinical strategies (with genetic background and immune response) should be considered. Herein, we investigated the antitumor effect of cytokine-induced killer (CIK)

cells in combination with nivolumab and crizotinib in vitro on NSCLC cell lines.

Methods: We co-cultured the three genetically different NSCLC cell lines NCI-H2228 (EML4-ALK), A549 (KRAS mutation), and HCC-78 (ROS1 rearrangement) in the presence or absence of nivolumab and crizotinib. We profiled the variablity of surface expression multiple immune checkpoints, the concentration of absolute dead cell numbers, intracellular granzyme B on CIK cells by flow cytometry as well as mRNA by RT-qPCR. ELISA and western blot were applied to verify the activation of CIK cells.

Results: Our analysis showed that, a) nivolumab significantly weakened PD-1 surface expression on CIK cells without impacting other immune checkpoints or PD-1 mRNA expression. b) this combination strategy showed an effective response on cell viability, IFN-γ production and intracellular release of granzyme B in $CD3^+$ $CD56^+$ CIK cells, but solely in NCI-H2228, c) the intrinsic expression of Fas ligand (FasL) as a T-cell activation marker in CIK cells was upregulated by this additive effect. d) nivolumab induced Foxp3 expression in $CD4^+CD25^+$ subpopulation of CIK cells significantly increased. Taken together, we could show that CIK cells in combination with crizotinib and nivolumab can enhance the anti-tumor immune response through FasL activation, leading to increased IFN-γ and granzyme B, but only in NCI-H2228 cells with EML4-ALK rearrangement. Therefore, we hypothesize that CIK therapy may be a potential alternative in NSCLC patients harboring EML4-ALK rearrangement, in addition, we support the idea that combination therapies offer significant potential when they are optimized on a patient-by-patient basis (Published in *Front Oncol*. 2022;12: 713476).

1.7. References

Sung H, Ferlay J, Siegel RL, et al. Global Cancer Statistics 2020: GLOBOCAN Estimates of incidence and Mortality Worldwide for 36 Cancers in 185 Countries. CA Cancer J Clin. 2021;71:209-249. doi: 10.3322/caac.21660.

Herbst RS, Morgensztern D and Boshoff C. The biology and management of non-small cell lung cancer. Nature, 2018; 553, 446–454.

Noone AM, Howlader N, Krapcho M, et al. SEER Cancer Statistics Review, 1975-2015. Bethesda, MD: National Cancer Institute; 2018. http://seer.cancer.gov/archive/csr/1975_2012/

Hardtstock F, Myers D, Li T, et al. Real-world treatment and survival of patients with advanced non-small cell lung Cancer: a German retrospective data analysis. BMC Cancer. 2020; 20: 260. doi: 10.1186/s12885-020-06738-z.

Kahnert K, Kauffmann-Guerrero D, and Huber RM. SCLC-state of the art and what does the future have in store? Clin. Lung Cancer, 2016; 17:325–333. doi: 10.1016/j.cllc.2016.05.014.

Karachaliou N, Pilotto S, Lazzari C, et al. Cellular and molecular biology of small cell lung cancer: an overview. Transl. Lung Cancer Res. 2016; 5: 2-15. doi: 10.3978/j.issn.2218-6751.2016.01.02.

Rock JR, Randell SH, Hogan BL. Airway basal stem cells: a perspective on their roles in epithelial homeostasis and remodeling. Dis Model Mech. 2010; 3: 545-56. doi: 10.1242/dmm.006031.

George PJ, Banerjee AK, Read CA, et al. Surveillance for the detection of early lung cancer in patients with bronchial dysplasia. Thorax. 2007; 62: 43-50. doi: 10.1136/thx.2005.052191.

Stevens TP, McBride JT, Peake JL, et al. Cell proliferation contributes to PNEC hyperplasia after acute airway injury. Am J Physiol. 1997; 272: L486-93. doi: 10.1152/ajplung.1997.272.3.L486.

Reynolds SD, Hong KU, Giangreco A, et al. Conditional clara cell ablation reveals a self-renewing progenitor function of pulmonary neuroendocrine cells. Am J Physiol Lung Cell Mol Physiol. 2000; 278: L1256-63. doi: 10.1152/ajplung.2000.278.6.L1256.

Hardavella G., George R., Sethi T. Lung Cancer Stem Cells-Characteristics, Phenotype. Transl. Lung Cancer Res. 2016; 5: 272–279. 10.21037/tlcr.2016.02.01.

Raniszewska A, Polubiec-Kownacka M, Rutkowska E, et al. PD-L1 Expression on Lung Cancer Stem Cells in Metastatic Lymph Nodes Aspirates. Stem Cell Rev Rep. 2019; 15: 324-330. doi: 10.1007/s12015-018-9860-7.

Raniszewska A, Vroman H, Dumoulin D, et al. PD-L1^{+} lung cancer stem cells modify the metastatic lymph-node immunomicroenvironment in nsclc patients. Cancer Immunol Immunother. 2021, 70: 453-461. doi: 10.1007/s00262-020-02648-y.

Murthy V, Katzman DP, Tsay JJ, et al. Tumor-draining lymph nodes demonstrate a suppressive immunophenotype in patients with non-small cell lung cancer assessed by endobronchial ultrasound-guided transbronchial needle aspiration: A pilot study. Lung Cancer. 2019; 137: 94-99. doi: 10.1016/j.lungcan.2019.08.008.

Zhu S, Luo Z, Li X, Han X, Shi S, and Zhang T. Tumor-associated macrophages: role in tumorigenesis and immunotherapy implications. J Cancer. 2021; 12: 54-64. doi: 10.7150/jca.49692.

Li Y, Sharma A, Wu X, et al. A Combination of Cytokine-Induced Killer Cells With PD-1

Blockade and ALK Inhibitor Showed Substantial Intrinsic Variability Across Non-Small Cell Lung Cancer Cell Lines. Front Oncol. 2022; 12: 713476. doi: 10.3389/fonc.2022.713476.

Liu Y, Zugazagoitia J, Ahmed FS, et al. Immune Cell PD-L1 Colocalizes with Macrophages and Is Associated with Outcome in PD-1 Pathway Blockade Therapy. Clin Cancer Res. 2020; 26: 970-977. doi: 10.1158/1078-0432.CCR-19-1040.

Shinchi Y, Ishizuka S, Komohara Y, et al. The expression of PD-1 ligand 1 on macrophages and its clinical impacts and mechanisms in lung adenocarcinoma. Cancer Immunol Immunother. 2022: 1-17. doi: 10.1007/s00262-022-03187-4.

Watanabe H, Ohashi K, Nishii K, et al. A Long-term Response to Nivolumab in a Case of PD-L1-negative Lung Adenocarcinoma with an EGFR Mutation and Surrounding PD-L1-positive Tumor-associated Macrophages. Intern Med. 2019; 58(20):3033-3037. doi: 10.2169/internalmedicine.2875-19.

Shima T, Shimoda M, Shigenobu T, et al. Infiltration of tumor-associated macrophages is involved in tumor programmed death-ligand 1 expression in early lung adenocarcinoma. Cancer Sci. 2020; 111: 727-738. doi: 10.1111/cas.14272.

Yang Z, Peng Y, Guo W, et al. PD-L1 and CD47 co-expression predicts survival and enlightens future dual-targeting immunotherapy in non-small cell lung cancer. Thorac Cancer. 2021; 12: 1743-1751. doi: 10.1111/1759-7714.13989.

Zhou Q, Liang J , Yang T, et al. Carfilzomib modulates tumor microenvironment to potentiate immune checkpoint therapy for cancer. EMBO Mol Med. 2022; 14:e14502. doi: 10.15252/emmm.202114502.

Liu M, Tong Z, Ding C, et al. Transcription factor c-Maf is a checkpoint that programs

macrophages in lung cancer. J Clin Invest. 2020; 130:2081-2096. doi: 10.1172/JCI131335.

Koto S, Chihara N, Akatani R, et al. Transcription Factor c-Maf Promotes Immunoregulation of Programmed Cell Death 1-Expressed $CD8^+$ T Cells in Multiple Sclerosis. Neurol Neuroimmunol Neuroinflamm. 2022; 9(4):e1166. doi: 10.1212/NXI.0000000000001166.

Gusak A, Fedorova L, Lepik K, et al. Immunosuppressive Microenvironment and Efficacy of PD-1 Inhibitors in Relapsed/Refractory Classic Hodgkin Lymphoma: Checkpoint Molecules Landscape and Macrophage Populations. Cancers (Basel). 2021; 13(22):5676. doi: 10.3390/cancers13225676.

Nakanishi Y, Masuda T, Yamaguchi K, et al. Albumin–globulin ratio is a predictive biomarker of antitumor effect of anti-PD-1 antibody in patients with non-small cell lung cancer. Int. J. Clin. Oncol. 2020; 25: 74–81. doi: 10.1007/s10147-019-01539-2.

Mariathasan S, Turley SJ, Nickles D, et al. TGF-β attenuates tumour response to PD-L1 blockade by contributing to exclusion of T cells. Nature. 2018, 554: 544-548. doi: 10.1038/nature25501.

Li L, Wei JR, Dong J, et al. Laminin γ2–mediating T cell exclusion attenuates response to anti–PD-1 therapy. Sci. Adv. 2021; 7 : eabc8346. doi: 10.1126/sciadv.abc8346.

Reuben A, Zhang J, Chiou SH, et al. Comprehensive T cell repertoire characterization of non-small cell lung cancer. Nat Commun. 2020; 11: 603. doi: 10.1038/s41467-019-14273-0.

Kamphorst AO, Pillai RN, Yang S. Proliferation of $PD\text{-}1^+$ CD8 T cells in peripheral blood after PD-1-targeted therapy in lung cancer patients. PNAS 2017; 114: 4993-4998. https://doi.org/10.1073/pnas.1705327114.

Zheng Y, Han L, Chen Z, et al. PD-L1^{+}CD8^{+} T cells enrichment in lung cancer exerted regulatory function and tumor-promoting tolerance. iScinece. 2022; 25: 103785. https://doi.org/10.1016/j.isci.2022.103785.

Bailly C, Thuru X and Quesnel B. Soluble Programmed Death Ligand-1 (sPD-L1): A Pool of Circulating Proteins Implicated in Health and Diseases. Cancers 2021; 13(12), 3034. https://doi.org/10.3390/cancers13123034.

Sagawa R, Sakata S, Gong B, et al. Soluble PD-L1 works as a decoy in lung cancer immunotherapy via alternative polyadenylation. JCI Insight. 2022; 7: e153323. doi: 10.1172/jci.insight.153323.

Lu F, Dong Y, Li Q and Wang M. The Change of Soluble Programmed Death Ligand 1 (sPD-L1) in Plasma of Small Cell Lung Cancer and Its Clinical Significance. Comput Math Methods Med. 2022; 2022: 8375349. doi:10.1155/2022/8375349.

Yuan Y, He Y, Wang X, et al. Investigation on the effects of soluble programmed death-1 (sPD-1) enhancing anti-tumor immune response. J Huazhong Univ Sci Technolog Med Sci. 2004; 24(6):531–4. doi: 10.1007/bf02911345.

He L, Zhang G, He Y, et al. Blockade of B7-H1 With sPD-1 Improves Immunity Against Murine Hepatocarcinoma. Anticancer Res. 2005; 25(5):3309–13.

Meyo MT, Jouinot A, Giroux-Leprieur E, et al. Predictive Value of Soluble PD-1, PD-L1, VEGFA, CD40 Ligand and CD44 for Nivolumab Therapy in Advanced Non-Small Cell Lung Cancer: A Case-Control Study. Cancers 2020; 12, 473; doi:10.3390/cancers12020473.

Ohkuma R, Ieguchi K, Watanabe M, et al. Increased Plasma Soluble PD-1 Concentration Correlates with Disease Progression in Patients with Cancer Treated with Anti-PD-1

Antibodies. Biomedicines. 2021; 9(12): 1929. doi: 10.3390/biomedicines9121929.

Yang Q, Chen M, Gu J, et al. Novel Biomarkers of Dynamic Blood PD-L1 Expression for Immune Checkpoint Inhibitors in Advanced Non-Small-Cell Lung Cancer Patients. Front Immunol. 2021; 12:665133. doi: 10.3389/fimmu.2021.665133.

Ferrarini M., Pupa S. M., Zocchi M. R., et al. Distinct pattern of HSP72 and monomeric laminin receptor expression in human lung cancers infiltrated by gamma/delta T lymphocytes. Int J Cancer. 1994; 57(4):486-90. doi: 10.1002/ijc.2910570408.

Ferrarini M., Heltal S., Chiesa G., et al. Vδ1^{+} Gamma/Delta T Lymphocytes Infiltrating Human Lung Cancer Express the CD8α/α Homodimer. Scand J Immunol. 1994; 40(3):363-7. https://doi.org/10.1111/j.1365-3083.1994.tb03475.x.

Zocchi M.R., Ferrarini M., Rugarli C. Selective lysis of the autologous tumor by delta TCS1^{+} gamma/delta^{+} tumor-infiltrating lymphocytes from human lung carcinomas. Eur J Immunol. 1990; 20(12):2685-9. doi: 10.1002/eji.1830201224.

Wu Y, Biswas D, Usaite I, et al. A local human Vδ1 T cell population is associated with survival in nonsmall-cell lung cancer. Nat Cancer. 2022; 3(6):696-709. doi: 10.1038/s43018-022-00376-z.

Tosolini M., Pont F., Poupot M., et al. Assessment of tumor-infiltrating TCRV γ 9V δ 2 γδ lymphocyte abundance by deconvolution of human cancers microarrays. Oncoimmunology. 2017; 6(3):e1284723. doi: 10.1080/2162402X.2017.1284723.

Cazzetta V., Bruni E., Terzoli S., et al. NKG2A expression identifies a subset of human Vδ2 T cells exerting the highest antitumor effector functions. Cell Rep. 2021; 37(3):109871. doi: 10.1016/j.celrep.2021.109871.

Sun S, Schiller JH, Gazdar AF. Lung cancer in never smokers-a different disease. Nat Rev Cancer. 2007; 7: 778-90. doi: 10.1038/nrc2190.

Lamberti G, Sisi M, Andrini E, et al. The Mechanisms of PD-L1 Regulation in Non-Small-Cell Lung Cancer (NSCLC): Which Are the Involved Players? Cancers 2020; 12: 3129. doi:10.3390/cancers12113129.

Re MD, Cucchiara F, Rofi E, et al. A multiparametric approach to improve the prediction of response to immunotherapy in patients with metastatic NSCLC. Cancer Immunol Immunother. 2021;70(6):1667-1678. doi: 10.1007/s00262-020-02810-6.

Dhakar R, Dakal TC, Sharma A. Genetic determinants of lung cancer: Understanding the oncogenic potential of somatic missense mutations. Genomics. 2022;114(4):110401. doi: 10.1016/j.ygeno.2022.110401.

Shinohara T, Taniwaki M, Ishida Y, et al. Structure and chromosomal localization of the human PD-1 gene (PDCD1). Genomics. 1994; 23: 704–6. doi: 10.1006/geno.1994.1562.

Jiang X, Wang J, Deng X, et al. Role of the tumor microenvironment in PD-L1/PD-1-mediated tumor immune escape. Mol Cancer. 2019; 18: 10. doi: 10.1186/s12943-018-0928-4.

Wartewig T, Kurgyis Z, Keppler S, et al. PD-1 is a haploinsufficient suppressor of T cell lymphomagenesis. Nature. 2017; 552: 121–5. doi: 10.1038/nature24649.

Patsoukis N, Brown J, Petkova V, et al. Selective Effects of PD-1 on Akt and Ras Pathways Regulate Molecular Components of the Cell Cycle and Inhibit T Cell Proliferation. Sci Signal. 2012; 5: ra46. doi: 10.1126/scisignal.2002796.

Gulati P, Rühl J, Kannan A, et al. Aberrant Lck Signal via CD28 Costimulation Augments

Antigen-Specific Functionality and Tumor Control by Redirected T Cells with PD-1 Blockade in Humanized Mice. Clinical Trial Clin Cancer Res. 2018; 24: 3981-3993. doi: 10.1158/1078-0432.CCR-17-1788.

Wang X, Yang X, Zhang C, et al. Tumor cell-intrinsic PD-1 receptor is a tumor suppressor and mediates resistance to PD-1 blockade therapy. Proc Natl Acad Sci U S A. 2020; 117:6640-6650.https://doi.org/10.1073/pnas.192144511.

Horn L, Spigel DR, Vokes EE, et al. Nivolumab versus docetaxel in previously treated patients with advanced non-small-cell lung cancer: two-year outcomes from two randomized, open-label, phase III trials (CheckMate 017 and CheckMate 057). J. Clin. Oncol 2017; 35: 3924-3933. doi: 10.1200/JCO.2017.74.3062.

Lu S, Wang J, Cheng Y, et al. Nivolumab versus docetaxel in a predominantly Chinese patient population with previously treated advanced non-small cell lung cancer: 2-year follow-up from a randomized, open-label, phase 3 study (CheckMate 078). Lung Cancer 2021;152:7-14. doi: 10.1016/j.lungcan.2020.11.013.

Hellmann MD, Callahan MK, Awad MM, et al. Tumor mutation burden and efficacy of nivolumab monotherapy and in combination with ipilimumab in small cell lung cancer. Cancer Cell 2018; 33: 853–861.e4. doi: 10.1016/j.ccell.2018.04.001.

Alexandrov LB, Nik-Zainal S, Wedge DC, et al. Signatures of mutational processes in human cancer. Nature 2013; 500: 415-421. doi: 10.1038/nature12477.

Byers LA, Rudin CM. Small cell lung cancer: where do we go from here? Cancer 2015; 121: 664-672. doi: 10.1002/cncr.29098.

Friedman CF, Proverbs-Singh TA, Postow MA. Treatment of the Immune-Related Adverse

Effects of Immune Checkpoint Inhibitors: A Review. JAMA Oncol 2016; 2:1346-53. doi: 10.1001/jamaoncol.2016.1051.

Edinger M, Cao Y, Verneris MR, et al. Revealing lymphoma growth and the efficacy of immune cell therapies using in vivo bioluminescence imaging. Blood. 2003; 101: 640-8. doi: 10.1182/blood-2002-06-1751.

Pievani A, Borleri G, Pende D, et al. Dual-functional capability of $CD3^+CD56^+$ CIK cells, a T-cell subset that acquires NK function and retains TCR-mediated specific cytotoxicity. Blood. 2011; 118: 3301-10. doi: 10.1182/blood-2011-02-336321.

Wu X, Sharma A, Oldenburg J, et al. NKG2D Engagement Alone Is Sufficient to Activate Cytokine-Induced Killer Cells While 2B4 Only Provides Limited Coactivation. Front Immunol. 2021; 12: 731767. Published online 2021 Oct 7. doi: 10.3389/fimmu.2021.731767.

Verneis MR, Kornacker M, Mailänder V, Negrin RS. Resistance of ex vivo expanded $CD3^+CD56^+$ T cells to Fas-mediated apoptosis. Cancer Immunol Immunother. 2000; 49(6):335-45. doi: 10.1007/s002620000111.

Cappuzzelloa E, Tosia A, Zanovelloa P, et al. Retargeting cytokine-induced killer cell activity by CD16 engagement with clinical-grade antibodies. Oncoimmunology. 2016, 5, e1199311. http://dx.doi.org/10.1080/2162402X.2016.1199311.

Zhang Y, Schmidt-Wolf IGH. Ten-year update of the international registry on cytokine-induced killer cells in cancer immunotherapy. J Cell Physiol. 2020; 235: 9291–303. https://doi.org/10.1002/jcp.29827.

Zhang L, Wang J, Wei F, et al. Profiling the dynamic expression of checkpoint molecules on cytokine-induced killer cells from non-small-cell lung cancer patients. Oncotarget. 2016; 7:

43604-43615. doi: 10.18632/oncotarget.9871.

Han Y, Mu D, Liu T, et al. Autologous cytokine-induced killer (CIK) cells enhance the clinical response to PD-1 blocking antibodies in patients with advanced non-small cell lung cancer: A preliminary study. Thorac Cancer 2021; 12: 145-152. doi: 10.1111/1759-7714.13731.

Chen CL, Pan QZ, Weng DS, et al. Safety and activity of PD-1 blockade-activated DC-CIK cells in patients with advanced solid tumors. Oncoimmunology. 2018; 7: e1417721. doi: 10.1080/2162402X.2017.1417721.

Zhou L, Xiong Y, Wang Y, et al. A Phase IB Trial of Autologous Cytokine-Induced Killer Cells in Combination with Sintilimab, Monoclonal Antibody Against Programmed Cell Death-1, plus Chemotherapy in Patients with Advanced Non-Small-Cell Lung Cancer. Clin Lung Cancer. 2022; 23(8):709-719. doi: 10.1016/j.cllc.2022.07.009.

Mankor JM, Disselhorst MJ, Poncin M, et al. Efficacy of nivolumab and ipilimumab in patients with malignant pleural mesothelioma is related to a subtype of effector memory cytotoxic T cells: Translational evidence from two clinical trials. EBioMedicine. 2020; 62:103040. doi: 10.1016/j.ebiom.2020.103040.

Spigel DR, Reynolds C, Waterhouse D, Garon EB, Chandler J, Babu S, et al. Phase 1/2 Study of the Safety and Tolerability of Nivolumab Plus Crizotinib for the First-Line Treatment of Anaplastic Lymphoma Kinase Translocation -Positive Advanced Non-Small Cell Lung Cancer (CheckMate 370). Clin Trial J Thorac Oncol 2018; 13(5):682–8. doi: 10.1016/j.jtho.2018.02.022.

Yamaguchi O, Kaira K, Kawasaki T, Mouri A, Hashimoto K, Shiono A, et al. Severe Hepatotoxicity Due to Osimertinib After Nivolumab Therapy in Patients With Non-Small Cell Lung Cancer Harboring EGFR Mutation. Thorac Cancer 2020; 11(4):1045–51. doi:

10.1111/1759-7714.13363.

Du P, Hu T, An Z, Li P, Liu L. In Vitro and In Vivo Synergistic Efficacy of Ceritinib Combined With Programmed Cell Death Ligand-1 Inhibitor in Anaplastic Lymphoma Kinase-Rearranged non-Small Cell Lung Cancer. Cancer Sci 2020; 111(6):1887–98. doi: 10.1111/cas.14397.

Felip E, de Braud FG, Maur M, Loong HH, Shaw AT, Vansteenkiste JF, et al. Ceritinib Plus Nivolumab in Patients With Advanced ALK-Rearranged Non-Small Cell Lung Cancer: Results of an Open-Label, Multi-Center, Phase 1b Study. J Thorac Oncol 2020; 15(3):392–403. doi: 10.1016/j.jtho.2019.10.006.

Stankovic B, Bjørhovde HAK, Skarshaug R, Aamodt H, Frafjord A, Müller E, et al. Immune Cell Composition in Human Non-Small Cell Lung Cancer. Front Immunol 2019; 9:3101. doi: 10.3389/fimmu.2018.03101.

Sheng SY, Gu Y, Lu CG, Zou JY, Hong H, Wang YF. The Distribution and Function of Human Memory T Cell Subsets in Lung Cancer. Immunol Res 2017; 65:639–50. doi: 10.1007/s12026-016-8882-y.

Zhang Y, Schmidt-Wolf IGH. Ten-Year Update of the International Registry on Cytokine-Induced Killer Cells in Cancer Immunotherapy. J Cell Physiol 2020; 235(12):9291–303. doi: 10.1002/jcp.29827.

Li Y, Sharma A, Bloemendal M, Schmidt-Wolf R, Kornek M, Schmidt-Wolf IGH. PD-1 Blockade Enhances Cytokine-Induced Killer Cell-Mediated Cytotoxicity in B-Cell non-Hodgkin Lymphoma Cell Lines. Oncol Lett 2021; 22(2):613. doi: 10.3892/ol.2021.12874.

Wu X, Sharma A, Oldenburg J, Weiher H, Essler M, Skowasch D. And Schmidt-Wolf I.G.H. NKG2D Engagement Alone Is Sufficient to Activate Cytokine-Induced Killer Cells While 2b4

Only Provides Limited Coactivation. Front Immunol 2021; 12:731767. doi: 10.3389/fimmu.2021.731767.

Zhang Y, Sharma A, Weiher H, Schmid M, Kristiansen G. And Schmidt-Wolf I.G.H. Clinical Studies on Cytokine-Induced Killer Cells: Lessons From Lymphoma Trials. Cancers 2021; 13(23):6007. doi: 10.3390/cancers13236007.

Li DP, Li W, Feng J, Chen K, Tao M. Adjuvant Chemotherapy With Sequential Cytokine-Induced Killer (CIK) Cells in Stage IB Non-Small Cell Lung Cancer. Oncol Res 2015; 22(2):67–74. doi: 10.3727/096504014X14024160459168.

Luo H, Gong L, Zhu B, Huang Y, Tang C, Yu S, et al. Therapeutic Outcomes of Autologous CIK Cells as a Maintenance Therapy in the Treatment of Lung Cancer Patients: A Retrospective Study. BioMed Pharmacother 2016; 84:987–93. doi: 10.1016/j.biopha.2016.10.022.

Wu C, Jiang J, Shi L, Xu N. Prospective Study of Chemotherapy in Combination With Cytokine-Induced Killer Cells in Patients Suffering From Advanced Non-Small Cell Lung Cancer. Random Controlled Trial Anticancer Res 2008; 28(6B):3997–4002.

Li R, Wang C, Liu L, Du C, Cao S, Yu J, et al. Autologous Cytokine-Induced Killer Cell Immunotherapy in Lung Cancer: A Phase II Clinical Study. Clin Trial Cancer Immunol Immunother 2012; 61(11):2125–33. doi: 10.1007/s00262-012-1260-2.

Gu Y, Lv H, Zhao J, Li Q, Mu G, Li J, et al. Influence of the Number and Interval of Treatment Cycles on Cytokine-Induced Killer Cells and Their Adjuvant Therapeutic Effects in Advanced Non-Small-Cell Lung Cancer (NSCLC). Int Immunopharmacol 2017; 50:263–9. doi: 10.1016/j.intimp.2017.07.006.

Mohsenzadegan M, Peng RW, Roudi R. Dendritic Cell/Cytokine-Induced Killer Cell-Based Immunotherapy in Lung Cancer: What We Know and Future Landscape. J Cell Physiol. 2020; 235(1):74–86. doi: 10.1002/jcp.28977.

Chen J, Chen Y, Feng F, Chen C, Zeng H, Wen S, et al. Programmed Cell Death Protein-1/Programmed Death-Ligand 1 Blockade Enhances the Antitumor Efficacy of Adoptive Cell Therapy Against Non-Small Cell Lung Cancer. J Thorac Dis 2018; 10(12):6711–21. doi: 10.21037/jtd.2018.10.111.

Han Y, Mu D, Liu T, Zhang H, Zhang J, Li S, et al. Autologous Cytokine-Induced Killer (CIK) Cells Enhance the Clinical Response to PD-1 Blocking Antibodies in Patients With Advanced Non-Small Cell Lung Cancer: A Preliminary Study. Thorac Cancer 2021; 12(2):145–52. doi: 10.1111/1759-7714.13731.

Wang P, Fang X, Yin T, Tian H, Yu J, Teng F. Efficacy and Safety of Anti-PD-1 Plus Anlotinib in Patients With Advanced Non-Small-Cell Lung Cancer After Previous Systemic Treatment Failure-A Retrospective Study. Front Oncol 2021; 11:628124. doi: 10.3389/fonc.2021.628124.

Schmidt-Wolf IG, Negrin RS, Kiem HP, Blume KG, Weissman IL. Use of a SCID Mouse/Human Lymphoma Model to Evaluate Cytokine-Induced Killer Cells With Potent Antitumor Cell Activity. J Exp Med 1991; 174(1):139–49. doi: 10.1084/jem.174.1.139.

Wu X, Zhang Y, Li Y, Schmidt-Wolf IGH. Increase of Antitumoral Effects of Cytokine-Induced Killer Cells by Anti-Body-Mediated Inhibition of MICA Shedding. Cancers (Basel) 2020; 12(7):1818. doi: 10.3390/cancers12071818.

Mariotti FR, Petrini S, Ingegnere T, Tumino N, Besi F, Scordamaglia F, et al. PD-1 in Human NK Cells: Evidence of Cytoplasmic mRNA and Protein Expression. Oncoimmunology 2019;

8(3):1557030. doi: 10.1080/2162402X.2018.1557030.

Chen Y, Meng L, Shang H, Dou Q, Lu Z, Liu L, et al. b2 Spectrin-Mediated Differentiation Repressed the Properties of Liver Cancer Stem Cells Through b-Catenin. Cell Death Dis 2018; 9(4):424. doi: 10.1038/s41419-018-0456-6.

Dehno MN, Li Y, Weiher H, Schmidt-Wolf IGH. Increase in Efficacy of Checkpoint Inhibition by Cytokine-Induced-Killer Cells as a Combination Immunotherapy for Renal Cancer. Int J Mol Sci 2020; 21(9):3078. doi: 10.3390/ijms21093078.

Zhang L, Xie D, Lei Y, Na A, Zhu L. Preclinical Activity of Cobimetinib Alone or in Combination With Chemotherapy and Targeted Therapies in Renal Cell Carcinoma. Future Oncol 2021; 17(23):3051–60. doi: 10.2217/fon-2021-0256.

Sanchez JN, Subramanian C, Chanda M, Shanguan G, Zhang N, Wang T, et al. A Novel C-Terminal Hsp90 Inhibitor KU758 Synergizes Efficacy in Combination With BRAF or MEK Inhibitors and Targets Drug-Resistant Pathways in BRAF-Mutant Melanomas. Melanoma Res 2021; 31(3):197–207. doi: 10.1097/CMR.0000000000000734.

Pezeshki PS, Eskian M, Hamblin MR, Rezaei N. Immune Checkpoint Inhibition in Classical Hodgkin Lymphoma. Expert Rev Anticancer Ther 2021; 21(9):1003–16. doi: 10.1080/14737140.2021.1918548.

Ma H, Li Q, Wang J, Pan J, Su Z, Liu S. Dual Inhibition of Ornithine Decarboxylase and A(1) Adenosine Receptor Efficiently Suppresses Breast Tumor Cells. Front Oncol 2021; 11:636373. doi: 10.3389/fonc.2021.636373.

Wu X, Wang L, Ye Y, Aakre JA, Pu X, Chang GC, et al. Genome-Wide Association Study of Genetic Predictors of Overall Survival for non-Small Cell Lung Cancer in Never Smokers.

Cancer Res 2013; 73(13):4028–38. doi: 10.1158/0008-5472.

Arauz RF, Byun JS, Tandon M, Sinha S, Kuhn S, Taylor S, et al. Whole-Exome Profiling of NSCLC Among African Americans. J Thorac Oncol 2020; 15 (12):1880–92. doi: 10.1016/j.jtho.2020.08.029.

Aye PS, McKeage MJ, Tin ST, Khwaounjoo P, Elwood JM. Population-Based Incidence Rates and Increased Risk of EGFR Mutated non-Small Cell Lung Cancer in Māori and Pacifica in New Zealand. PloS One 2021; 16(5):e0251357. doi: 10.1371/journal.pone.0251357.

Sundar R, Cho BC, Brahmer JR, Soo RA. Nivolumab in NSCLC: Latest Evidence and Clinical Potential. Ther Adv Med Oncol 2015; 7(2):85–96. doi: 10.1177/1758834014567470.

Osa A, Uenami T, Koyama S, Fujimoto K, Okuzaki D, Takimoto T, et al. Clinical Implications of Monitoring Nivolumab Immunokinetics in non-Small Cell Lung Cancer Patients. Observat Stud JCI Insight (2018) 3(19):e59125. doi: 10.1172/jci.insight.59125.

Xiong Y, Neskey DM, Horton JD, Paulos CM, Knochelmann HM, Armeson KE, et al. Immunological Effects of Nivolumab Immunotherapy in Patients With Oral Cavity Squamous Cell Carcinoma. BMC Cancer 2020; 20(1):229. doi: 10.1186/s12885-020-06726-3.

He Y, Liu S, Mattei J, Bunn PA Jr, Zhou C, Chan D. The Combination of Anti-KIR Monoclonal Antibodies With an-Ti-PD-1/PD-L1 Monoclonal Antibodies Could be a Critical Breakthrough in Overcoming Tumor Immune Escape in NSCLC. Drug Design Dev Ther 2018; 12:981–6. doi: 10.2147/DDDT.S163304.

Niu C, Jin H, Li M, Xu J, Xu D, Hu J, et al. In Vitro Analysis of the Proliferative Capacity and Cytotoxic Effects of Ex Vivo Induced Natural Killer Cells, Cytokine-Induced Killer Cells, and

Gamma-Delta T Cells. BMC Immunol 2015; 16:61. doi: 10.1186/s12865-015-0124-x.

Zhang W, Song Z, Xiao J, Liu X, Luo Y, Yang Z, et al. Blocking the PD-1/PDL1 Axis in Dendritic Cell-Stimulated Cytokine-Induced Killer Cells With Pembrolizumab Enhances Their Therapeutic Effects Against Hepatocellular Carcinoma. J Cancer. 2019; 10(11):2578–87. doi: 10.7150/jca.26961.

Verneris MR, Kornacker M, Mailänder V, Negrin RS. Resistance of Ex Vivo Expanded $CD3^{+}CD56^{+}$ T Cells to Fas-Mediated Apoptosis. Cancer Immunol Immunother 2000; 49(6):335–45. doi: 10.1007/s002620000111.

Sharma A, Reutter H, Ellinger J. DNA Methylation and Bladder Cancer: Where Genotype Does Not Predict Phenotype. Curr Genomics 2020; 21(1):34–6. doi: 10.2174/1389202921666200102163422.

Byers LA, Diao L, Wang J, Saintigny P, Girard L, Peyton M, et al. An Epitheli-Al-Mesenchymal Transition Gene Signature Predicts Resistance to EGFR and PI3K Inhibitors and Identifies Axl as a Therapeutic Target for Overcoming EGFR Inhibitor Resistance. Clin Cancer Res 2013; 19(1):279–90. doi: 10.1158/1078-0432.CCR-12-1558.

Wang X, Yang X, Zhang C, Wang Y, Cheng T, Duan L, et al. Tumor Cell-Intrinsic PD-1 Receptor Is a Tumor Suppressor and Mediates Resistance to PD-1 Blockade Therapy. Proc Natl Acad Sci USA 2020; 117(12):6640–50. doi: 10.1073/pnas.1921445117.

Testa U, Castelli G, Pelosi E. Lung Cancers: Molecular Characterization, Clonal Heterogeneity and Evolution, and Cancer Stem Cells. Cancers (Basel) 2018; 10(8):248. doi: 10.3390/cancers10080248.

Kubo T, Takigawa N, Osawa M, Harada D, Ninomiya T, Ochi N, et al. Subpopulation of Small-

Cell Lung Cancer Cells Expressing CD133 and CD87 Show Resistance to Chemotherapy. Cancer Sci 2013; 104(1):78–84. doi: 10.1111/cas.12045.

Raniszewska A, Vroman H, Dumoulin D, Cornelissen R, Aerts JGIV, Domagała-Kulawik J. PD-L1^{+} Lung Cancer Stem Cells Modify the Metastatic Lymph-Node Immunomicroenvironment in Nsclc Patients. Cancer Immunol Immunother 2021; 70(2):453–61. doi: 10.1007/s00262-020-02648-y.

Sharma A, Schmidt-Wolf IGH. 30 Years of CIK Cell Therapy: Recapitulating the Key Breakthroughs and Future Perspective. J Exp Clin Cancer Res 2021; 40(1):388. doi: 10.1186/s13046-021-02184-2.

Hill H, Robinson M, Lu L, Slaughter D, Amin A, Mileham K, et al. Venous Thromboembolism Incidence and Risk Factors in non-Small Cell Lung Cancer Patients Receiving First-Line Systemic Therapy. Thromb Res 2021; 208:71–8. doi: 10.1016/j.thromres.2021.10.014.

Ried JM, Barth DM, Brueckl WM, Zeitler G, Foris V, Mollnar S, et al. C Reactive Protein (CRP) Levels in Immune Checkpoint Inhibitor Response and Progression in Advanced Non-Small Cell Lung Cancer: A Bi-Center Study. Cancers (Basel) 2020; 12(8):2319. doi: 10.3390/cancers12082319.

Liu H, Li H, Luo K, Sharma A, Sun X. Prognostic Gene Expression Signature Revealed the Involvement of Mutational Pathways in Cancer Genome. J Cancer 2020; 11(15):4510–20. doi: 10.7150/jca.40237.

STUDY II

Discovering single cannabidiol or synergistic antitumor effects of cannabidiol and cytokine-induced killer cells on non-small cell lung cancer cells

Published as: Li Y, Sharma A, Hoffmann MJ, Skowasch D, Essler M, Weiher H and Schmidt-Wolf IGH (2024) Discovering single cannabidiol or synergistic antitumor effects of cannabidiol and cytokine-induced killer cells on non-small cell lung cancer cells. Front. Immunol. 15:1268652. doi: 10.3389/fimmu.2024.1268652

2.1. Introduction

2.1.1 CBD treatment in cancer

Undoubtedly, cannabidiol (CBD) can relieve cancer pain and even mitigate the side effects of chemotherapy, yet there has been a paucity of knowledge concerning its anti-cancer effect. It's has been discussed for decades that the activation of cannabinoid receptors (CB1 and CB2) may exert anti-inflammatory, proapoptotic and anti-proliferative effects that could help fight cancer (Velasco G., et al., 2016; Mangal N., et al., 2021). Besides, the receptors (G-protein receptors; transient receptor potential vanilloid ion channels (TRPV1 and 2); peroxisome proliferatoractivated receptors) that CBD interacts with, are also believed to be involved in several key biological processes (Mangal N., et al., 2021; O'Brien K., 2022). Cannabinoid receptors (CB1 and CB2 receptors) are not the ligands of CBD. CBD has low affinity for CB1 and CB2 receptors (Pumroy R.A., et al., 2019). A previous study on nanomolar-range high affinity binding demonstrated a negative effect of CBD on cannabinoid receptor activation through an allosteric site (Laprairie R. B., et al., 2015). However, CBD

acts as a selective TRPV2 agonist. CBD preferentially binds to TRPV2 rather than TRPV1 based on computational and structural data (Landucci E., et al., 2022). Therefore, we focus on the TRPV2 channel in this study. In preclinical models, like other cancer types, CBD-related research on lung cancer (LC) has also been conducted. LC is known to involve an accumulation of genetic and epigenetic events and, with its two main subtypes (small cell lung cancer/SCLC and non-small cell lung cancer/NSCLC), is responsible for numerous cancer-related deaths (Dhakar R., et al., 2022; Peng Y., et al., 2022; Zhang G., et al., 2022). Recently, it was shown that CBD decreased viability and induced cell death in lung cancer stem cells and adherent lung cancer cells (Hamad H., et al., 2021). The authors also revealed that CBD activated the effector caspases 3/7, increased the expression of pro-apoptotic proteins and levels of reactive oxygen species. An independent study showed CBD as a novel therapeutic agent targeting TRPV2 to inhibit the growth and metastasis of aggressive cisplatin-resistant NSCLC (Misri S., et al., 2022). CBDs have been shown to increase the lysis of lung cancer cells by lymphokine-activated killer cells via upregulation of Intercellular Adhesion Molecule 1 (ICAM-1) (Haustein M., et al., 2014). Additionally, it has been demonstrated that CBD can inhibit cancerassociated fibroblasts (Milián L., et al., 2022) and suppress proliferation and reduce in vitro migration of lung cancer cell lines (Milian L., et al., 2020). Mechanically, a combination of THC (Tetrahydrocannabinol) and CBD leads to the signalling activation of mitogen-activated protein kinase pathway (ERK1/2 phosphorylation) in HEK 293 cells (Raïch L., et al., 2021).

2.1.2. TRPV2 channel

The TRPV2 channel is implicated in signalling pathways that mediate cell survival,

proliferation, and metastasis. TRPV2 is a homotetrameric N-glycosylated protein that is largely located in the endoplasmic reticulum compartment under unstimulated conditions. When TRPV2 is stimulated by CBD, the activity of phosphatidylinositol 3-kinase (PI3K) triggers the translocation of TRPV2 to the plasma membrane, where it acts as an ion channel. Subsequently, the increase in TRPV2-mediated Ca^{2+} entry leads to the activation of signalling pathways involved in cell survival, apoptosis, proliferation, differentiation, and metastasis (Siveen K.S., et al., 2020). Previous studies demonstrated that TRPV1 was functionally expressed in $CD4^{+}$ T cells, contributed to T cell antigen receptor (TCR)-induced Ca^{2+} influx, TCR signalling and T cell activation (Bertin S., et al., 2014). However, there are no investigations indicating that TRPV2 impacts T cell activation.

2.1.3. KRAS mutation in lung cancer

KRAS genes are the most commonly mutated oncogenes in non-small cell lung cancer, but effective therapeutic strategies to target RAS-mutant cancers have proved elusive since direct inhibition of RAS proteins has proved difficult (Cully M., et al., 2016). In a previous study, CBD induced cancer cell apoptosis via activation of p53-dependent apoptotic pathways in cancer cells with wild-type p53 (De Petrocellis L., et al., 2013; Vladimir N., et al., 2017). A549 cells (KRAS-G12D mutation, P53 wide-type), NCI-H2228 (EML4-ALK variant 3, P53 Q331* mutation) and HCC-827 (EGFR exon19 deletion mutant, inactivation P53 mutation) used in the current study contain rearrangements of chromosomes and substantial changes in the genomic landscape. Besides, in our previous study, it was shown that NSCLC cells harbouring an EML4-ALK rearrangement have higher responses to CIK therapy (Li Y., et al., 2022). In addition, Long Interspersed Nuclear Element-1 (LINE-1) promotes

tumorigenicity and exacerbates tumor progression in NSCLC cell lines and mice model (Sun Z., et al., 2022). A recent study reported that LINE-1 regulates T cell quiescence and exhaustion (Marasca F., et al., 2022).

2.1.4. The propose of this study

Owing to these findings, herein, we questioned, 1) whether CBD has any particular effects on LC cell lines with diverse genetic backgrounds; 2) whether CBD can exert any influence on CIK cells aiming to enhance their therapeutic potential or function targeting NSCLC cells. Of importance, we, for the first time in the literature, investigated if CBD or CBD in the presence of a lower amount of CIK cells can affect the expression and methylation of LINE-1 repetitive sequences in NSCLC cells.

2.2. Materials and methods

2.2.1. Regents and Antibodies

CBD (purity ≥ 98% (HPLC) (Bio-Techne, Wiesbaden-Nordenstadt, Germany) and tranilast (Cayman Chemical Company, Hamburg, Germany) were dissolved in dimethyl sulfoxide (DMSO). All antibodies used in the study such as fluorochrome-conjugated FITC anti-human CD3 antibody (clone OKT3), APC antihuman CD3 antibody (clone OKT3), PerCP/cyanine5. 5 anti-human CD3 antibody (clone OKT3), Brilliant Violet 421 anti-human CD8 antibody (clone RPA-T8), APC/cyanine7 anti-human CD4 antibody (clone RPAT4), PE anti-human CD56 antibody (clone 5. 1 H11), APC anti-human CD56 antibody (clone 5. 1 H11), PE/Cyanine7 anti-human CD69 antibody (clone FN50), PE anti-human CD25 antibody (clone BC96), PE anti-human CD45RA antibody (clone HI100), FITC anti-human CD62L antibody (clone DREG-56) were purchased from Biolegend (San Diego, CA, U.S.A.).

2.2.2. Cell Culture

Cytokine induce killer (CIK) cells were generated, as previously described (Schmidt-Wolf I.G., et al., 1999; Wu X., et al., 2020). PBMCs required for the experiments were isolated from the blood of healthy donors registered at the blood bank of University Hospital Bonn. Three human non-small cell lung cancer cell lines with distinct genotypes were used in this study: A549 cells (KRAS mutation, P53 wide-type), NCI-H2228 (EML4-ALK variant 3, P53 Q331* mutation) and HCC-827 (EGFR exon19 deletion mutant, inactivation P53 mutation). A549 and HCC-827 were purchased from Leibniz Institute DSMZ-German Collection of Microorganisms and Cell Cultures GmbH (DSMZ, Braunschweig, Leibniz, Germany) and NCI-H2228 was purchased from the American Type Culture Collection (ATCC, Manassas, VA, U.S.A.). All cell lines were tested for mycoplasma negative and cultured in RPMI 1640 medium supplemented with 10% heat-inactivated FBS (Gibco, Munich, Germany) and 1% penicillin/streptomycin (P/S) (Gibco, Munich, Germany) at 37°C (5% CO_2).

2.2.3. Phenotypes of CB2 Expression by Flow Cytometry

CellTrace™ Violet (Thermo Fisher Scientific, Waltham, U.S.A.)-labeled 5 x 10^5 tumor cells were incubated with CIK cells at various E:T ratio for 24 h. Following 24 h co-culture, the tumor cells were digested by Accutase Cell Detachment Solution (PAN Biotech, Aidenbach, Germany) for 5 minutes. In order to detect surface expression of CB2 receptor, after washing with cold DPBS, the cells were stained with CB2 receptor polyclonal FITC antibody for 30 minutes on ice (Cayman Chemical Company, Hamburg, Germany). Rabbit IgG Isotype Control Antibody (FITC) LS-C149376 (LifeSpan Biosciences, Seattle, U.S.A.) was used as a control. Cells were stained with 7-AAD to exclude dead cells and CB2 receptor expression

was quantified using BD FACS Canto II. To detect intracellular CB2 receptor expression, after 24 h co-culture with CIK cells, the tumor cells were stained with intracellular viability dye Zombie Aqua™ (Zombie Aqua™ Fixable Viability Kit, Biolegend, San Diego, CA, U.S.A.). Afterwards, the cells were fixed, permeabilized using fixation buffer and intracellular staining permeabilization wash buffer (Biolegend, San Diego, CA, U.S.A.) before CB2 receptor labelling. Following washing, the percentage of CB2 positive live cells was analyzed by FlowJo V10 software (Tree Star, Ashland, Oregon).

2.2.4. RNA Extraction, Reverse Transcription (RT)-PCR and Global LINE-1 Methylation

RNA was isolated from the cells using the miRNeasy Micro kit (Qiagen, Hilden, Germany) and subsequently cDNA synthesis was performed using the SuperScriptTM III First -Strand Synthesis Super Mix kit (Invitrogen, CA, U.S.A.), following the manufacturer's instructions. QuantStadio 3 Real-Time PCR System (Applied Biosystems, CA, U.S.A.) using PowerTrack™ SYBR Green Master Mix (Applied Biosystems, CA, U.S.A.) was used for MMP-9 mRNA detection. QuantiTect SYBR® Green PCR Kits (QIAGEN, Hilden, Germany) was used for LINE-1 mRNA measurement. The relative amount of target genes was normalized by the amount of HPRT for MMP-9. The primer sequences were: MMP-9-PF/MMP-9-PR (5`-CGC AGA CAT CGT CAT CCA GT-3`/ 5`-AAC CGA GTT GGA ACC ACG AC-3`) and HPRT-PF/HPRT-PR (5´-TCA GGC AGT ATA ATC CAA AGA TGG T-3´/ 5´-AGT CTG GCT TAT ATC CAA CAC TTC G-3´), as previously described (Staiano R.I., et al., 2016). TATA binding protein (TBP) was used as the reference gene for LINE-1. The primer pairs for the amplification of LINE-1 and TBP were LINE-1-PF/LINE-1-PR (5′-GTA CCG GGT TCA TCT CAC TAG G-3′/5′-TGT GGG ATA TAG TCT CGT GGT G-3′), TBP-PF/TBP-PR (5′-ACA

ACA GCC TGC CAC CTT A-3′/5′-GAA TAG GCT GTG GGG TCA GT-3′), as previously described (Whongsiri P., et al., 2020). The experiments were repeated three times, and each sample was analyzed in triplicate by ΔΔCt method. For investigating global LINE-1 methylation, first genomic DNA was extracted using the Qiagen genomic DNA purification kit (Qiagen, Hilden, Germany), according to the manufacturer's recommendations. Subsequently, the Global DNA Methylation LINE-1 kit (Active Motif, Carlsbad, CA, U.S.A.) was used to quantify global LINE-1 methylation levels. For synergistic experiments with a combination of CBD and CIK targeting NSCLC cells, mixture cells were washed with cold DPBS three times to exclude CIK cells, then only adherent NSCLC cells were on the six-well plate. NSCLC cells were trypsinized and washed twice with 2 mL ice-cold DPBS and cell pellets were finally harvested.

2.2.5. Cell Viability Assessment by CCK-8 Assay and the Cytotoxicity of CIK cells Analysis by Flow Cytometry

CCK-8 cell viability assay was performed, as described by the manufacturer (Dojindo Laboratories, Kumamoto, Japan). Briefly, NSCLC cells were seeded into 96-well plates ($1x10^4$ cells/well) and treated with various concentrations of CBD or DMSO control for 24 h. Similarly, the flow cytometry-based cytotoxicity was performed, as described protocol. Briefly, the target cells were labelled with CFSE (1×10^6 cells in 1 ml PBS with 0.5 µM CFSE, 20 min, 37˚C in the dark) and washed twice with warm culture medium. CFSE labelled 5×10^4 tumor cells were incubated at various concentrations of CBD for 24 h with CIK cells to perform redirected cytolysis assay at an E:T ratio of 10:1. Following 24 h of culturing, the cells were stained with Hoechst 33258 (Cayman Chemical, Hamburg, Germany) and were quantified

using BD FACS Canto II. Then the percentage of cytotoxicity of CIK cells was analyzed by FlowJo V10 software (Tree Star, Ashland, Oregon) and calculated by the following formula as previously described (Wu X., et al., 2020):

Specific lysis (%) = ((CT − TE)/CT) × 100

CT: cell count of live $CFSE^+$ tumor cells in control tubes (tumor cells alone or tumor + CBD);

TE: cell count of live $CFSE^+$ tumor cells in test tubes (tumor + effector).

To dissect the underlying mechanisms of the synergistic effects of the combination treatment, we have investigated whether combination-induced cytotoxicity was related to inhibition of ERK signaling pathways. CIK cells were incubated with 10 µM ERK-selective inhibitor FR180204 (Cayman Chemical, Hamburg, Germany) for 2 h before being cocultured with CFSE-labeled tumor cells at various concentrations of CBD for 24 h, as previously described (Ohori M., et al.,2005; Niba ET., et al.,2013).

2.2.6. Enzyme-Linked Immunosorbent Assay (ELISA)

The ELISA assay was performed using the standard protocol. Briefly, 5 x 10^5 CIK cells were co-cultured with 5 x 10^4 tumor cells in the presence of various concentrations of CBD or DMSO control for 24 h at E:T 10:1. Thereafter, the cell-free supernatant was collected to perform sandwich ELISA assay (IFN Gamma Kit, Invitrogen, Camarillo, CA, U.S.A.), according to the manufacturer's instructions.

2.2.7. Intracellular Calcium Response of CIK cells and Intracellular Expression of P-ERK and TRPV2 by Flow Cytometry

1x10^6 CIK cells were stained with 1 µM Fluo-4 AM (Thermo Fisher Scientific, Waltham, U.S.A.) in DPBS (with calcium and magnesium) for 20 minutes at 37˚C. Cells were pelleted and

resuspended in DPBS (with calcium and magnesium) and were subsequently exposed to CBD/ TRPV2 antagonist tranilast (TLS) at 37 °C for 1 minute. Dead cells were gated and excluded by Hoechst 33258 for Fluo-4 AM expression. Cells were acquired for 30 seconds and analyzed on an BD FACS Canto II on the FITC channel. To determine the intracellular p-ERK expression, a Fixable Viability Zombie Aqua™ Dye was used to exclude dead cells from the analysis. Mainly, CIK cells were incubated with Brefeldin A, which is a protein transport inhibitor commonly used to enhance intracellular staining signals. After gently mixing, the cells were then incubated with CBD for 15 minutes and then were fixed with 100 µL fixation buffer for 30 min at room temperature in the dark. Cells were then washed and resuspended in 100 µL 1x True-Phos™ Perm Buffer at -20°C for 1 h and then stained with FITC anti-ERK1/2 Phospho (Thr202/Tyr204) antibody for 30 min at room temperature. Subsequently, the cells were washed twice with 2 mL DPBS, centrifuged at 1000 x g at room temperature for 5 minutes, and recorded with a BD Canto II cytometer. All reagents were purchased from Biolegend (San Diego, CA, U.S.A.). Since not all cell surface markers are compatible with BioLegend's True-Phos™ Perm Buffer, the subpopulations of CIK cells were not further identified in this experiment.

CIK cells or NSCLC cells were stained with a Fixable Viability Zombie Aqua™ Dye exclude dead cells. After that, CIK cells were stained by APC anti-human CD3 antibody (clone OKT3), Brilliant Violet 421 anti-human CD8 antibody (clone RPA-T8), APC/cyanine7 anti-human CD4 antibody (clone RPA-T4), PE anti-human CD56 antibody (clone 5. 1 H11) at 4°C for 20 min. Afterwards, the cells were fixed and permeabilized using fixation buffer and intracellular staining permeabilization wash buffer (Biolegend, San Diego, CA, U.S.A.). The blocking step

was carried out in permeabilization wash buffer with 2% normal goat serum for 15 min. Cells were incubated with anti-TRPV2 antibody (1:100 dilution, EpigenTek, Farmingdale, NY, U.S.A) at 4 °C for 30 min. Subsequently, cells were washed and incubated with Alexa Fluor™ 488-labeled goat anti-rabbit IgG (H+L) (1:250 dilution, A-11008, Invitrogen, CA, U.S.A.) for 30 min. After staining, cells were washed and suspended in DPBS for flow cytometric analysis, as previously described (Zhang W., et al., 2022).

2.2.8. Immunocytochemistry (ICC) for Detection of Phospho-γH2AX/TRPV2

NSCLC cells were seeded on the sterile round coverslips Ø13mm (Carl Roth GmbH + Co. KG, Karlsruhe, Germany) with 0.1% gelatin coating on a 24-well plate at a density of 5×10^3 cells/well in complete culture medium. After 48 h, cells were incubated with 10 µM CBD or 10 µM CBD with 10 µM TLS for 3 h in fresh culture medium. The cells were fixed in 4% paraformaldehyde (PFA) and permeabilized with 0.1% Triton in PBS for 10 min. Alternatively, 1×10^6 cells/well CIK cells were incubated with 10 µM CBD or DMSO for 3 h in fresh CIK culture medium. Fix the cells with 4% PFA for 20 min by adding an equal volume of 4% PFA to the culture medium. After that, the cells were resuspended in 200 µL deionized H_2O. Add 5 uL cell suspension to 0.1% gelatin-coated slide (3 spots per slide) and smear with the side of a pipette tip. Air dry to evaporate for 2 min. The subsequent steps are the same as for NSCLC cells. Cells were then washed three times in PBS with 0.1% BSA. The blocking step was carried out in PBS with 10% normal goat serum and 0.3% Triton for 45 min. Thereafter, the anti-phospho-Histone H2AX (Ser139) antibody (clone JBW301) (Merck Millipore, Darmstadt, Germany) was diluted 1:500, and secondary antibody Alexa Fluor 488 In review 9 (Thermo Fisher Scientific, San Diego, CA, U.S.A.) was diluted 1:2000 in dilution buffer (1%

BSA, 0.3% Triton in PBS). Finally, diluted DAPI solution was added to each slice. Morphological analysis was performed by Visitron VisiScope Spinning Disk Confocal Microscopy (Visitron Systems GmbH, Puchheim, Germany). Confocal images were acquired using VisiVIEW® Image software. The image analyses were facilitated by FiJi ImageJ software (Shihan M.H., et al., 2021). In order to detect TRPV2 expression, NSCLC cells or CIK cells were treated as mentioned before. The anti-TRPV2 polyclonal rabbit antibody (EpigenTek, Farmingdale, NY, U.S.A) was diluted 1:200, and the secondary antibody Donkey Anti-Rabbit IgG NorthernLights™ NL557-conjugated antibody (R&D Systems, Inc., Minneapolis, Minnesota, U.S.A.) was diluted 1:500 in dilution buffer (1% BSA, 0.3% Triton in PBS).The slide was finally stained with a diluted DAPI solution.

2.2.9. Cell Migration, Invasion and Wound Healing Measurements

The migration assay was conducted using a Cell Culture Insert with a pore size of 8 µm (BD Biosciences, Bedford, MA, U.S.A.) as previously described (Kim S.Y., et al., 2021). Matrigel LDEV-Free Reduced Growth Factor Basement Membrane Matrix (Thermo Fisher Scientific, San Diego, CA, U.S.A.) was used to evaluate cell invasion potential. 200 uL of a 1:50 dilution of Geltrex matrix was added to each insert well and kept in a 37 °C incubator for 1 h initially. 1×10^5 tumor cells per well were seeded in the upper chamber in 200 µL serum free RPMI 1640 medium with either of 10 µM CBD, DMSO control or 10 µM CBD with 10 µM TRPV2 antagonist tranilast for 72 h. The lower chamber contained RPMI 1640 medium with 20% FBS to form a chemoattractant gradient to favour migration directionality. The chambers were incubated at 37 °C for 96 h in 5% CO_2, and non-migrating or non-invading cells were then removed from the upper side of the membrane. The migrating or invading cells in the lower

chamber were washed with DPBS and fixed with 4% formaldehyde for 10 minutes. After 100% methanol permeabilizing for 15 minutes, the cells were stained with crystal violet 0.1% diluted in water (Sigma-Aldrich Chemie GmbH, Taufkirchen, Germany). Each assay was performed in triplicate. The migratory cells or invasive cells were observed and counted manually under light microscopy in six different fields. The wound healing assay was performed as previously described (Cormier N., et al., 2015; Grada A., et al., 2017; Trepat X., et al., 2012), with slight modifications. Mainly, we utilized a sterile marker pen and a sterile ruler to draw four horizontal lines on the outside bottom of a 6-well plate. For preparing confluent monolayers, 2 x 10^5 tumor cells were seeded and cultured to confluence 90% in six-well culture plates. Then, tumor cells in the culture medium were scratched to produce two ‘wound’ vertical lines using a sterile 20 µL pipette tip and a sterile ruler. Cell debris was removed from the culture by gently washing with sterile warm DPBS twice. The cells were then cultured in RPMI 1640 medium with 5% FBS in the presence of either 10 µM CBD or DMSO or 10 µM CBD combined with 10 µM tranilast for 24-72 h. The cell migration images in 15 different fields divided by horizontal and vertical lines were observed and acquired under 10X magnification by a Zeiss Primovert inverted cell culture microscope equipped with an Axio digital camera (Carl Zeiss, Oberkochen, Germany). Wound closure was monitored at 24-72 h, until the borders of the wound could no longer be identified. Images were compared with the same field at different timepoints and quantified using Fiji Image J software and the migration rate was calculated as the percentage of area reduction or wound closure as previously described (Grada A., et al., 2017).

Wound Closure % = $\left[\frac{At=0h - At=\Delta h}{At=0h}\right]$

At=0h is the area of the wound measured immediately after scratching (t = 0 h)

At=Δh is the area of the wound measured h hours after the scratch is performed.

2.2.10. Genomic DNA Extraction and Global DNA Methylation

LINE-1 Detection Genomic DNA was extracted using the Qiagen genomic DNA purification kit (Qiagen, Hilden, Germany), according to the manufacturer's recommendations. $1x10^6$ cells were lysed in lysis solution, after that QIAGEN protease was added, and the mixture was incubated at 50 °C for 60 min. The samples were proceeded with Genomic-tip 20/G, washed and eluted. The genomic DNA was precipitated with isopropanol and washed with cold 70% ethanol. The DNA was dissolved in 10 mM Tris.HCL, PH 8.5) at 55°C overnight and quantified using a NanoDrop ND-1000 spectrophotometer (Thermo Fisher Scientific, San Diego, CA, U.S.A.). In the Global DNA Methylation LINE-1 kit, genomic DNA of interest is fragmented by enzymatic digestion and quantified using a NanoDrop ND-1000 again. After that, 320 ug fragmented DNA is hybridized with a biotinylated human LINE-1 consensus probe. Hybridized DNA is immobilized onto a streptavidin-coated plate, while unbounded DNA fragments are washed away. A 5-Methylcytosine antibody and a secondary antibody conjugated to horseradish peroxidase (HRP) are used for detection of methylated fragments. The colorimetric readout is easily quantified by spectrophotometry using a microplate reader at 450 nm and 655 nm. For quantitative analysis, the % 5-Methylcytosine associated with each sample can be calculated based on the CpG content: The 290 bp LINE-1 Msel fragments that hybridize to the LINE-1 probe contain 10 detectable CpG residues. The

provided DNA standards are either 100% methylated or 0% methylated for all 10 CpGs. Therefore, the standard curve generated by mixing the DNA standards together quantitates methylation in the range of 0% to 100% 5- Methylcytosine for the CpG content of the samples. MasterPlex ReaderFit curve fitting software is available for data analysis. Statistical Analysis All data were presented as the mean ± SD from at least three independent experiments. FACS data sets were analyzed using FlowJo V10.6 software (FlowJo, LLC, Ashland, Oregon).

2.2.11. Statistical analysis

All data were presented as the mean ± SD from at least three independent experiments. FACS data sets were analyzed using FlowJo V10.6 software (FlowJo, LLC, Ashland, Oregon). A statistical analysis was performed using a paired t-test for CIK cells on day 14 in comparison to relative PBL cells. For multiple group comparisons one-way or two-way analysis of variance with the Dunnett post hoc test or Tukey post hoc test was performed via GraphPad Prism 9.0.0 software. P-values < 0.05 were considered significant differences and are marked: * < 0.05; ** < 0.01; *** < 0.001, ****p < 0.0001.

2.3. Results

2.3.1. CBD inhibits proliferation of A549 cells and induces p-γH2AX expression, apparently by involving TRPV2 channel regulation

It is generally believed that the ATM/ATR signalling pathway mediates G0–G1 arrest by regulating the expression of p53. Some investigations have reported that CBD-induced G1 arrest may be due to DNA damage via activation of ATM and downregulation of the P53 expression in response to CBD (Zhang X., et al., 2019; Go Y.Y., et al., 2020). Therefore, we chose A549 cells (KRAS mutation, P53 wide-type), NCI-H2228 (EML4-ALK variant 3, P53

Q331* mutation) and HCC-827 (EGFR exon19 deletion mutant, inactivation P53 mutation) with different genetic backgrounds. We investigated the dose dependence of CBD in NSCLC cell lines and found that A549 appeared to be more sensitive compared to NCI-H2228 and HCC-827. A CBD dose-response curve for A549 is shown in Figure 11A (The cell viability at 15 µM CBD vs. DMSO 24.6 ± 5.6% vs. 95.37 ± 3.3%, P=0.0186; 20 µM CBD vs. DMSO 21.5 ± 2.5% vs. 95.37 ± 3.3%, P=0.0004). Since, it cannot be excluded that certain CBD concentrations may cause DNA-related damage, so we checked the early cellular response to the induction of DNA double-strand breaks by assaying phospho-γH2AX in NSCLC cells. We found that after 3 hours of CBD exposure, both foci and mean fluorescence intensity (MFI) of p-γH2AX were significantly increased compared with DMSO control in A549 cells (foci/total DAPI nuclear area: 183.6 ± 30.5 vs. 65.8 ± 15.4, P= 0.0483; MFI/total DAPI nuclear area: 11.3 ± 0.8 vs. 2.9 ± 0.6, P= 0.0130 (Fig. 11B, C, D, E, F). Of interest, the enhancement of p-γH2AX expression was completely abolished when the TRPV2 channel antagonist tranilast (TLS) was co-administered with CBD at a dose of 10 µM (CBD vs. CBD+TLS, Foci/total DAPI nuclear area: 183.6 ± 30.5 vs. 25.6 ± 0.2, P= 0.0220; 11.3 ± 0.8 vs. 5.1 ± 1.2, P= 0.0300, respectively). However, no such changes were observed in NCI-H2228 and HCC-827 (Figure 12A, B). The expression of p-γH2AX was not detectable in CIK cells after 3 h incubation, neither with 10 µM CBD nor with DMSO control (Figure 12C). Thus, it is suggested that CBD may actively increase the expression of p-γH2AX in NSCLC cell lines, particularly A549 (P53 wide-type genotype).

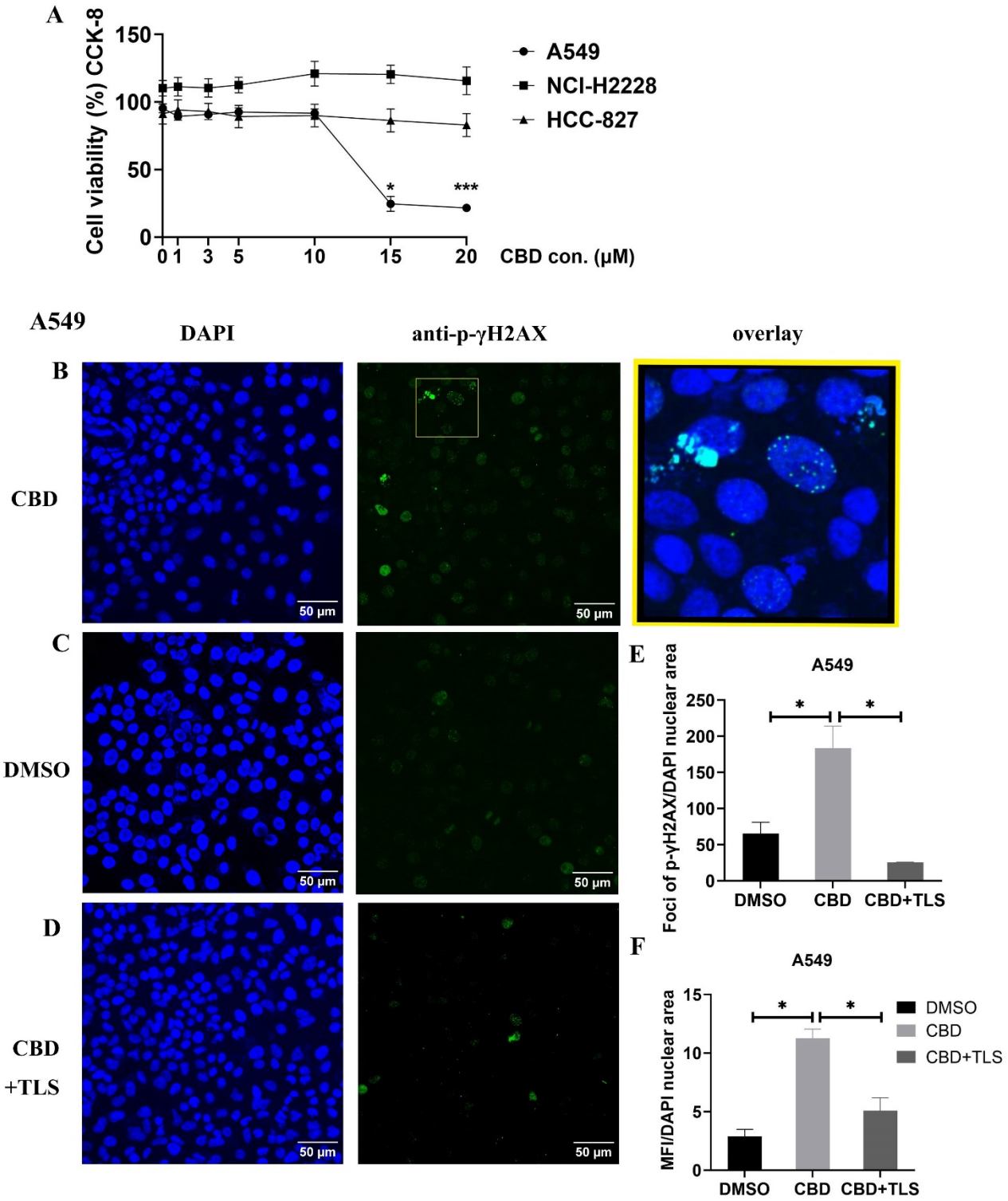
A
Cell viability (%) CCK-8
150
100
50
0
0 1 3 5 10 15 20
CBD con. (μM)
A549
NCI-H2228
HCC-827
*
***
A549
DAPI
anti-p-γH2AX
overlay
B
CBD
C
DMSO
D
CBD
+TLS
50 μm
E
A549
Foci of p-γH2AX/DAPI nuclear area
250
200
150
100
50
0
DMSO
CBD
CBD+TLS
F
A549
MFI/DAPI nuclear area
15
10
5
0
DMSO
CBD
CBD+TLS

Figure 11. The cell viability of NSCLC cell lines and p-γH2AX expression after incubation with CBD. (A) The cell viability of NSCLC cell lines after incubation with CBD for 24 h was detected by CCK-8 assay. *p < 0.05, ***p < 0.001 vs. DMSO (0 μM) control. Data are shown as the mean ± SD, representative of five independent experiments. (B) Subcellular localization of p-γH2AX in A549 cells. A549 cells were incubated with CBD for 3 h with either DMSO, CBD or CBD and TLS, then fixed and immunolabeled. Nuclear fluorescent signals were captured by Visitron VisiScope Spinning Disk Confocal Microscopy and VisiVIEW® Image software. The image analyses were facilitated by the FiJi ImageJ software. Left panel A, B, C, D, Nuclei of A549 cells were stained with blue signals for DAPI. Middle panel, A549 cells were immunolabeled of the anti-phospho-Histone H2AX (Ser139) antibody (clone JBW301) with green signals for Alexa Fluor 488. Upper right panel: a merged image of the DAPI and p-γH2AX signals in an enlarged yellow figure is presented. Scale bar = 50 μm. (E, F) Statistical analyses of Foci and MFI of p-γH2AX were carried out, respectively. *p < 0.05, CBD vs. DMSO control or CBD vs. CBD+TLS. All data are shown as the mean ± SD, representative of three independent experiments. Statistical analysis was performed using one-way ANOVA followed by Tukey’s multiple comparison test by GraphPad Prism software version 9.0.0.

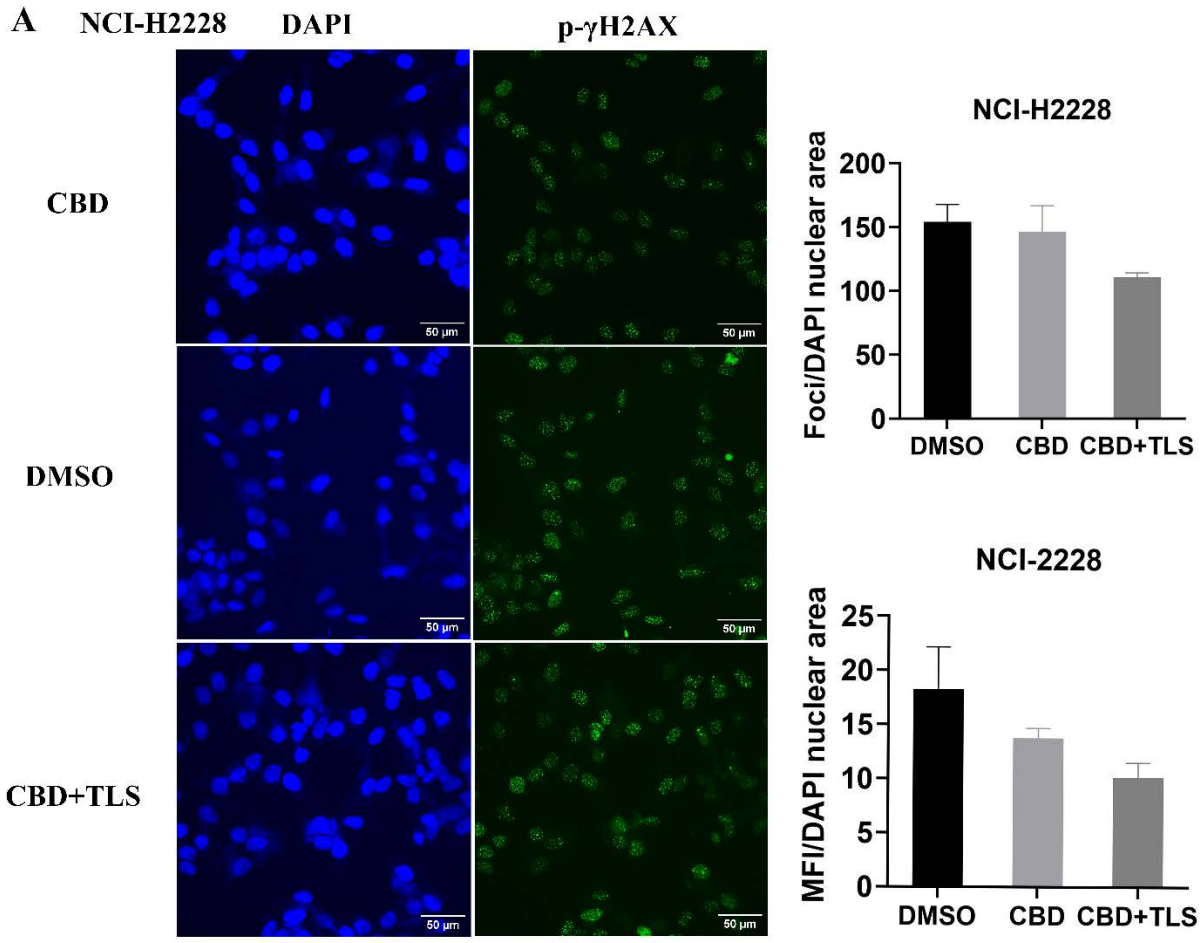
A
NCI-H2228
DAPI
p-γH2AX
CBD
DMSO
CBD+TLS
50 μm
NCI-H2228
Foci/DAPI nuclear area
200
150
100
50
0
DMSO
CBD
CBD+TLS
NCI-2228
MFI/DAPI nuclear area
25
20
15
10
5
0
DMSO
CBD
CBD+TLS

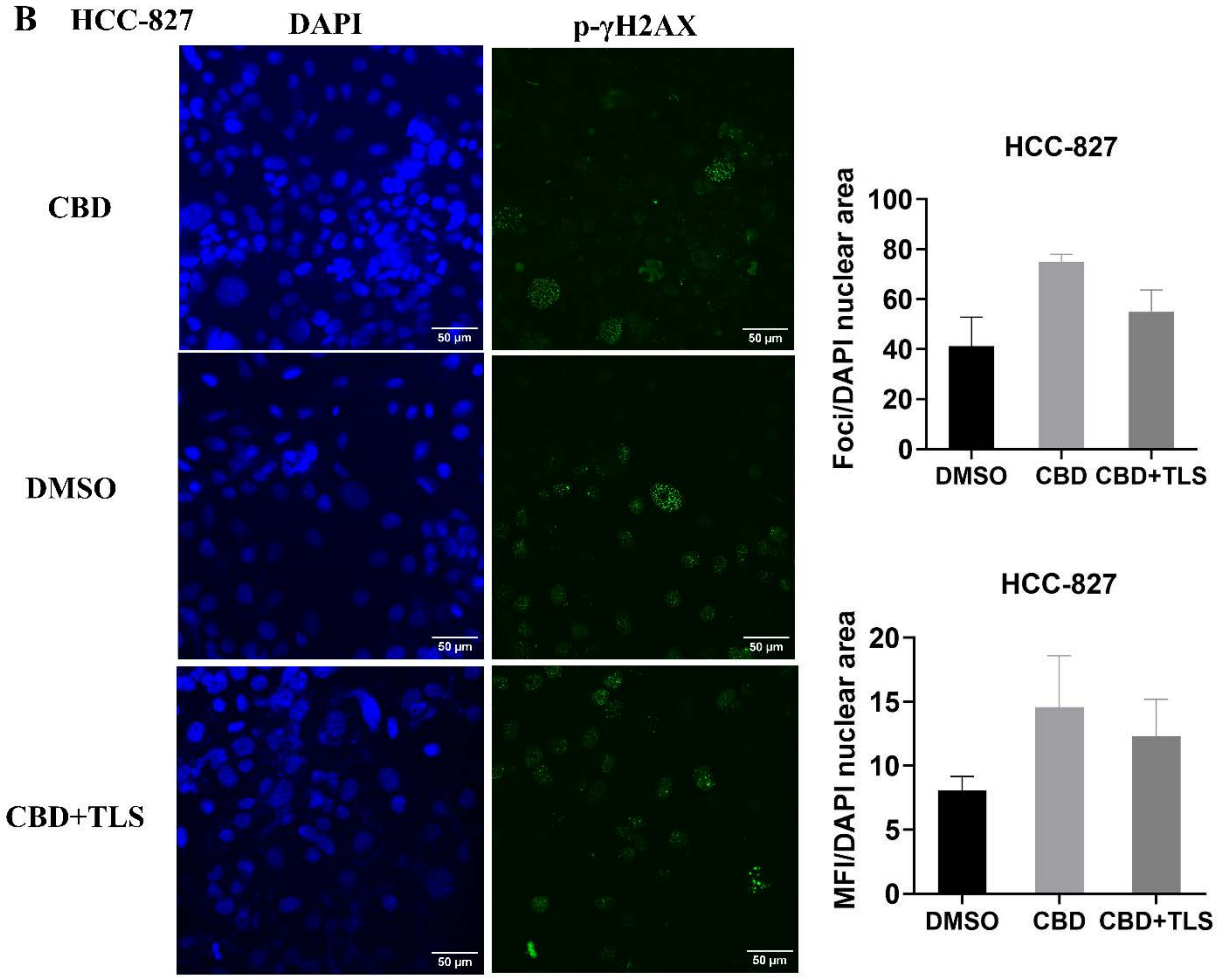
B
HCC-827
DAPI
p-γH2AX
CBD
DMSO
CBD+TLS
50 μm
HCC-827
Foci/DAPI nuclear area
100
80
60
40
20
0
DMSO
CBD
CBD+TLS
HCC-827
MFI/DAPI nuclear area
20
15
10
5
0
DMSO
CBD
CBD+TLS

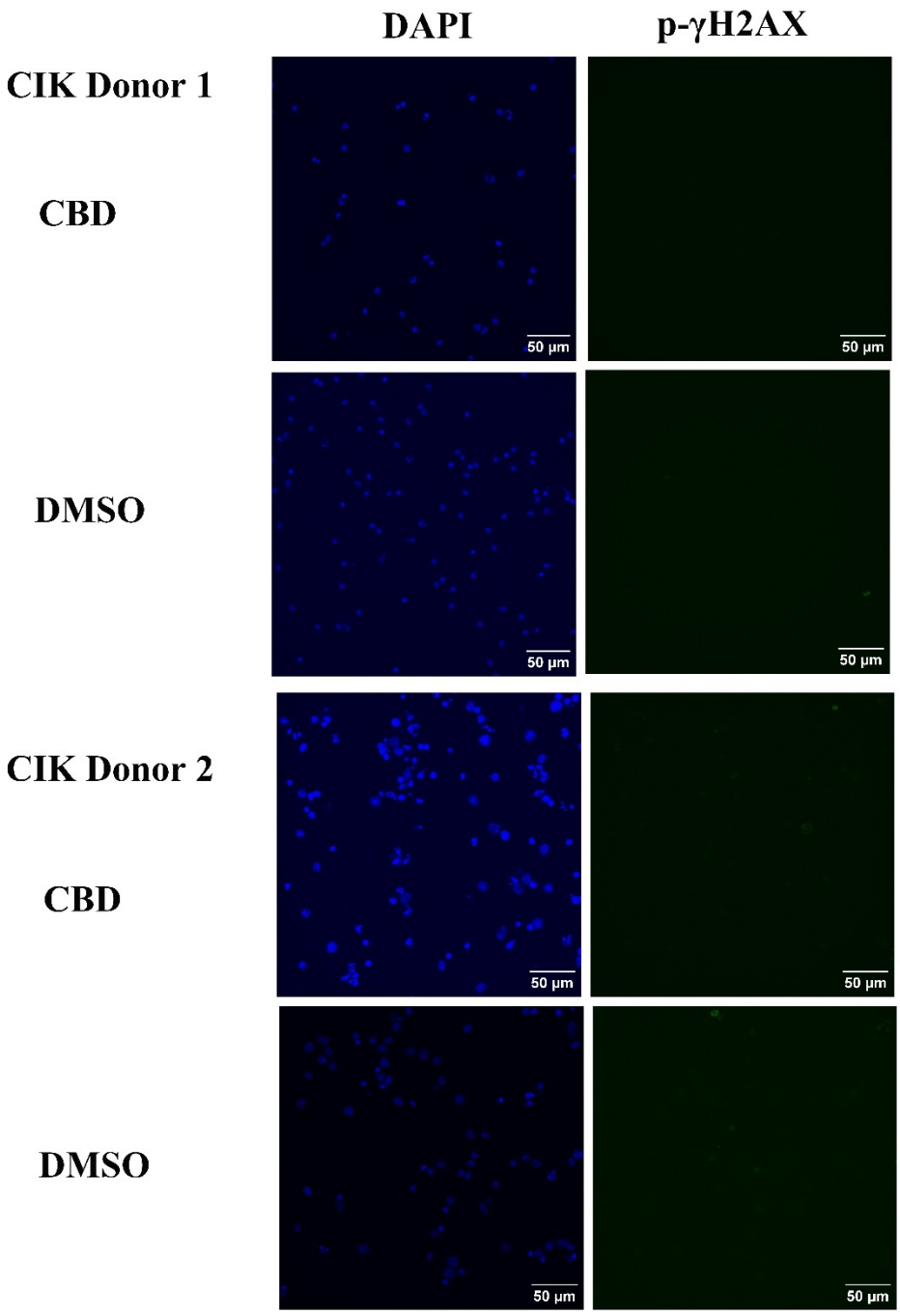

Figure 12. The effect of CBD on foci and MFI of p-γH2AX in NCI-H2228, HCC-827 and CIK cells. (A) NCI-H2228 cells or (B) HCC-827 cells or (C) CIK cells were incubated with CBD for 3 h with either

DMSO, CBD, then fixed and immunolabelled. Nuclear fluorescent signals were captured by Visitron VisiScope Spinning Disk Confocal Microscopy and VisiVIEW® Image software. The image analyses were facilitated by the FiJi ImageJ software. Nuclei of cancer cells were stained with blue signals for DAPI and phospho-Histone H2AX (Ser139) antibody (clone JBW301) with green signals for Alexa Fluor 488. Scale bar = 50 µm. All data are shown as the mean ± SD, representative of three independent experiments. Statistical analyses of Foci and MFI of p-γH2AX were carried out using one-way ANOVA followed by Tukey's multiple comparison test by GraphPad Prism software version 9.0.0.

2.3.2. CBD significantly suppressed the migration and invasion ability of NSCLC cells

Like p-γH2AX expression, we subsequently investigated whether CBD may also influence the migration and invasion potential of NSCLC cell lines. The results revealed that CBD significantly suppressed the migration and invasion ability of A549 cells, and this inhibition was abolished by the TRPV2 antagonist tranilast (Figure 13A), (Migratory cells per field: CBD + A549 vs. DMSO control, P= 0.0177; CBD + A549 vs. CBD + TLS + A549, P= 0.0096. Invasive cells per field: CBD + A549 vs. DMSO control, P= 0.0002; CBD + A549 vs. CBD + TLS + A549, P= 0.0007, respectively). In contrast, we found that NCI-H2228 and HCC-827 cells were not capable of invading neither the membranes nor the Matrigel-coating membranes and they migrated fast and collectively. Considering that some cell types can migrate horizontally faster without invading a pore membrane (Cormier N., et al., 2015), we therefore performed wound healing assays and observed significant migration ability for NCI-H2228 and HCC-827 (Figure 13B, C. CBD + NCI-H2228 vs. DMSO control, P= 0.0002; CBD + NCI-H2228 vs. CBD + TLS + NCI-H2228, P= 0.0009; CBD + HCC-827 vs. DMSO control, P= 0.0184; CBD + HCC-827 vs. CBD + TLS + HCC-827, P= 0.4017, respectively). In addition,

we assessed the messenger RNA (mRNA) expression of matrix metalloproteinase-9 (MMP-9), which has been shown to represent the invasiveness of NSCLC (Hiratsuka S., et al., 2002). The level of mRNA of MMP-9 significantly was reduced after incubation with 10 μM CBD for 24 h in NSCLC cells (Figure. 13D. CBD + A549 vs. DMSO control, $P< 0.0001$; CBD + A549 vs. CBD + TLS + A549, $P< 0.0001$; CBD+NCI-H2228 vs. DMSO control, $P< 0.0001$; CBD + NCI-H2228 vs. CBD + TLS + NCI-H2228, $P< 0.0001$; CBD+HCC-827 vs. DMSO control, $P= 0.0002$; CBD + HCC-827 vs. CBD + TLS + HCC-827, $P= 0.0007$, respectively). Collectively, CBD effectively inhibited the migration and invasion of NSCLC cell lines, presumably via the TRPV2 channel.

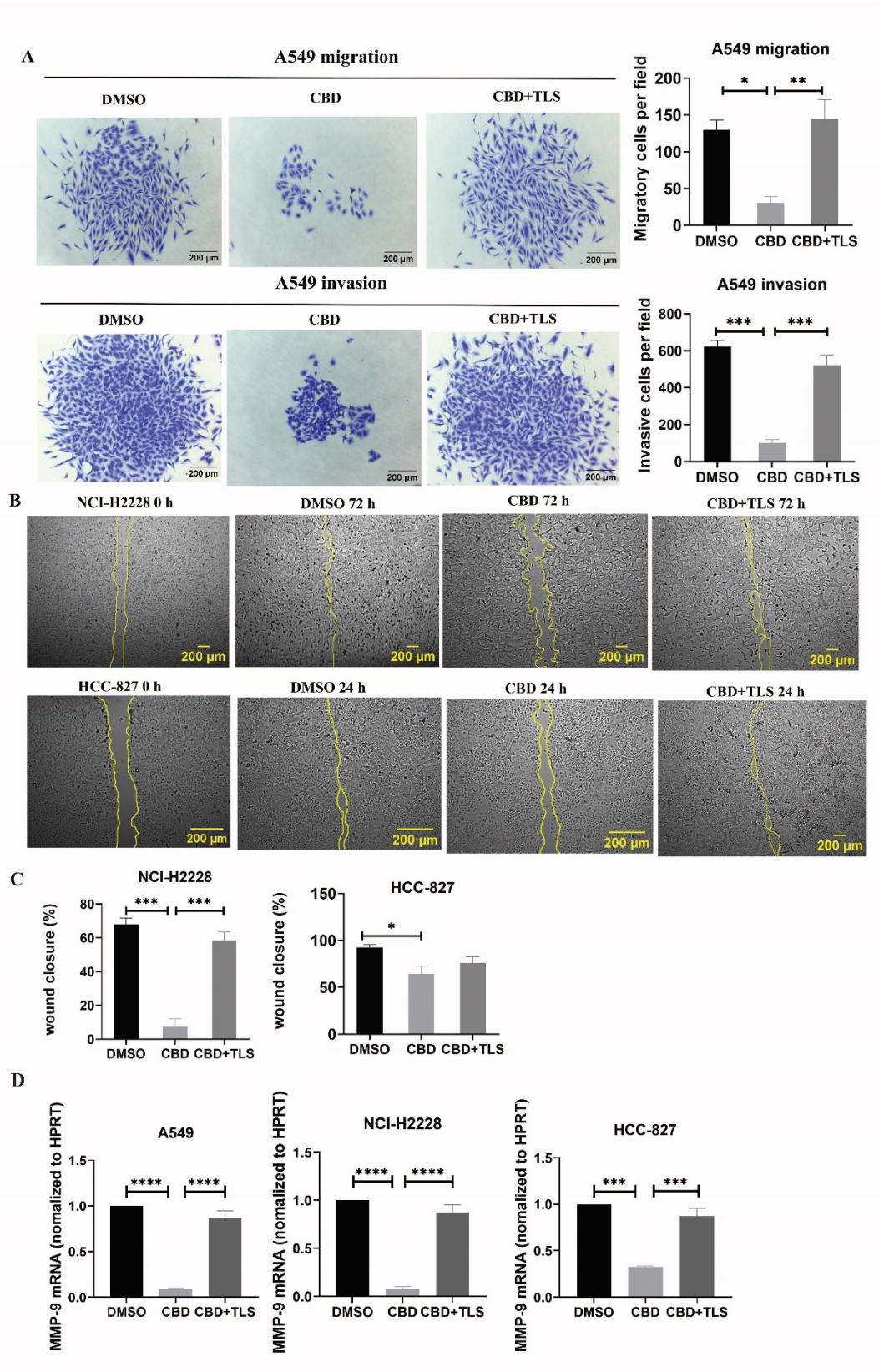
A
A549 migration
DMSO
CBD
CBD+TLS
200 μm
A549 migration
Migratory cells per field
DMSO CBD CBD+TLS
A549 invasion
Invasive cells per field
B
NCI-H2228 0 h
DMSO 72 h
CBD 72 h
CBD+TLS 72 h
HCC-827 0 h
DMSO 24 h
CBD 24 h
CBD+TLS 24 h
C
NCI-H2228
HCC-827
wound closure (%)
D
A549
NCI-H2228
HCC-827
MMP-9 mRNA (nomalized to HPRT)

Figure 13. The migration and invasion of non-small cell line cancer cells after incubation with CBD. (A) A549 trans-well migration and invasion assays showed that A549 cells incubated with 10 µM CBD had lower migratory and invasive potentials than the control (DMSO control and 10 µM CBD with 10 µM TLS) for 72 h. (B) Effect of 10 µM CBD on NCI-H2228 or HCC-827 cell migration for 24-72 h in a scratch wound healing assay. The wound healing area was measured by the FiJi ImageJ software and the percentage of wound closure was calculated. (C) shows the statistical results. (D) Quantitative analysis of mRNA levels of MMP-9 in tumor cells after incubation with CBD for 24h in free-serum RPMI 1640 medium. Phosphoribosyltransferase (HPRT) served as an internal standard. Data represented the mean ± SD of four independent experiments. *$p < 0.05$, **$p < 0.01$, ***$p < 0.001$. Scale bar = 200 µm. All data are shown as the mean ± SD, representative of three independent experiments. Statistical analysis was performed using a one-way ANOVA followed by Tukey's multiple comparison test by GraphPad Prism software version 9.0.0.

2.3.3. CIK cells significantly enhanced the surface and intracellular expression of CB2 receptors in NCI-H2228

As a combination therapy for lung cancer, we next investigated whether CBD could influence the expression level of CB1/CB2 on the surface of CIK cells. Of interest, a high expression of CB2 compared to CB1 was observed in both human PBLs (P=0.0168) and CIK cells (P=0.0193) (Figure 14A). We also examined the percentage of CB2 receptor surface expression in all cell lines and found a significant increase following incubation with CIK cells, especially in NCI-H2228 at an effector to target cell ratio (E:T) ratio of 10:1 (Fig. 14B, C, 14.8±1.0% vs 81.6±11.5%, P= 0.0003). In contrast, no significant change was observed in A549 and HCC-827 (P= 0.9858 and P=0.0646, respectively. Similar results were also observed for intracellular expression of CB2, i.e. a significant increase after incubation with CIK cells at E:T 10:1 solely in NCI-H2228 (Figure 14B, 55.0 ± 2.8% vs 99.5 ± 0.5%, P= 0.0223). These results indicate that CIK cells can enhance both surface and intracellular

expression of CB2 receptors NCI-H2228, a cell line with in particular genetic rearrangement of EML4-ALK variant 3, P53 Q331* mutation.

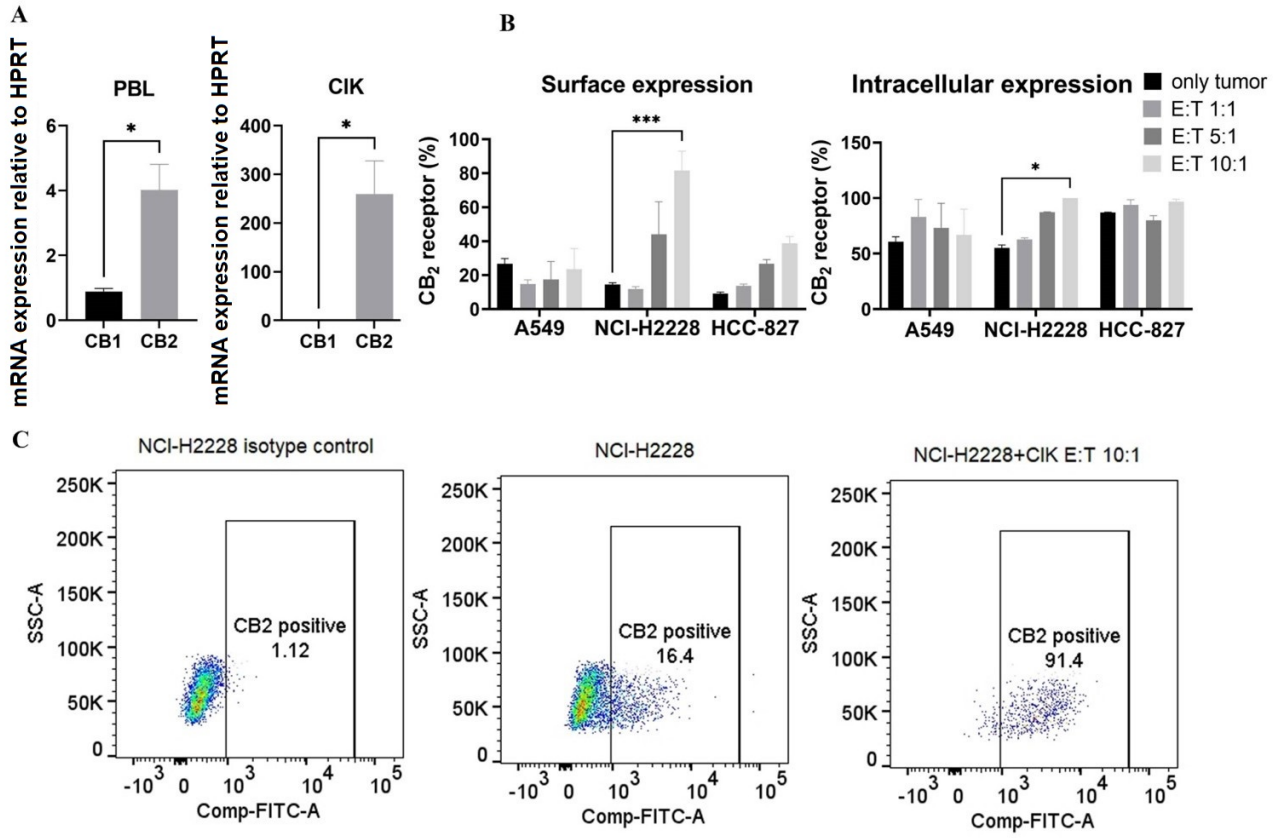

Figure 14. The expression of cannabinoid type 2 (CB2) receptors in CIK cells and the CB2 expression of NSCLC cell lines after coculture with CIK cells. (A) Quantitative analysis of mRNA levels of CB1 and CB2 receptors in CIK cells at day 0 and day 14. Hypoxanthine-guanine phosphoribosyltransferase (HPRT) served as internal standard. (B) Summary of the percentage of FITC-CB2 surface and intracellular expression on NSCLC cell lines are shown after 24 h co-culture with CIK cells at different effector to target cell ratio (E:T) ratios. Tumor cells were pre-stained by CellTrace™ Violet dye before being incubated with CIK cells. Dead cells were gated and excluded by 7-AAD for surface expression or Zombie Aqua™ dye for intracellular expression. The rabbit IgG isotype controls is indicated. All data are shown as the mean ± SD, representative of three independent experiments. The E:T ratio represents effector-target ratio. (C) Representative flow cytometry dot-plots display CB2 surface expression results from a single experiment for NCI-H2228

by flow cytometry. Each experiment was repeated 3 times. All data are shown as the mean ± SD. *P < 0.05, vs. CB1 in 14A or *P < 0.05, vs. only tumor cells in 14B, ***P < 0.001, vs. only tumor cells in 14B, calculated by two-way ANOVA with Dunnett for multiple comparison tests in GraphPad Prism 9.0.0 software. CIK cells are derived from three healthy donors.

2.3.4. TRPV2 highly expressed both in CIK cells and NSCLC cell lines

Immunocytochemistry revealed that most TRPV2 resides in an intracellular compartment. There is no TRPV2 present at the cell surface, both in CIK cells and NSCLC cell lines (Figure 15). Similarly, the intracellular percentage of FITC-TRPV2 was 98.92 ± 0.44% in $CD3^+CD56^+$ CIK cells, 99.95 ± 0.05% in $CD3^+CD4^+$ CIK cells, 99.82 ± 0.07% in $CD3^+CD8^+$ CIK cells detected by flow cytometric method. Moreover, the percentage of FITC-TRPV2 in A549 was 99.76 ± 0.23%, 99.9 ± 0.03% in NCI-H2228, and 91.95 ± 0.55 % in HCC-827 (Figure 16).

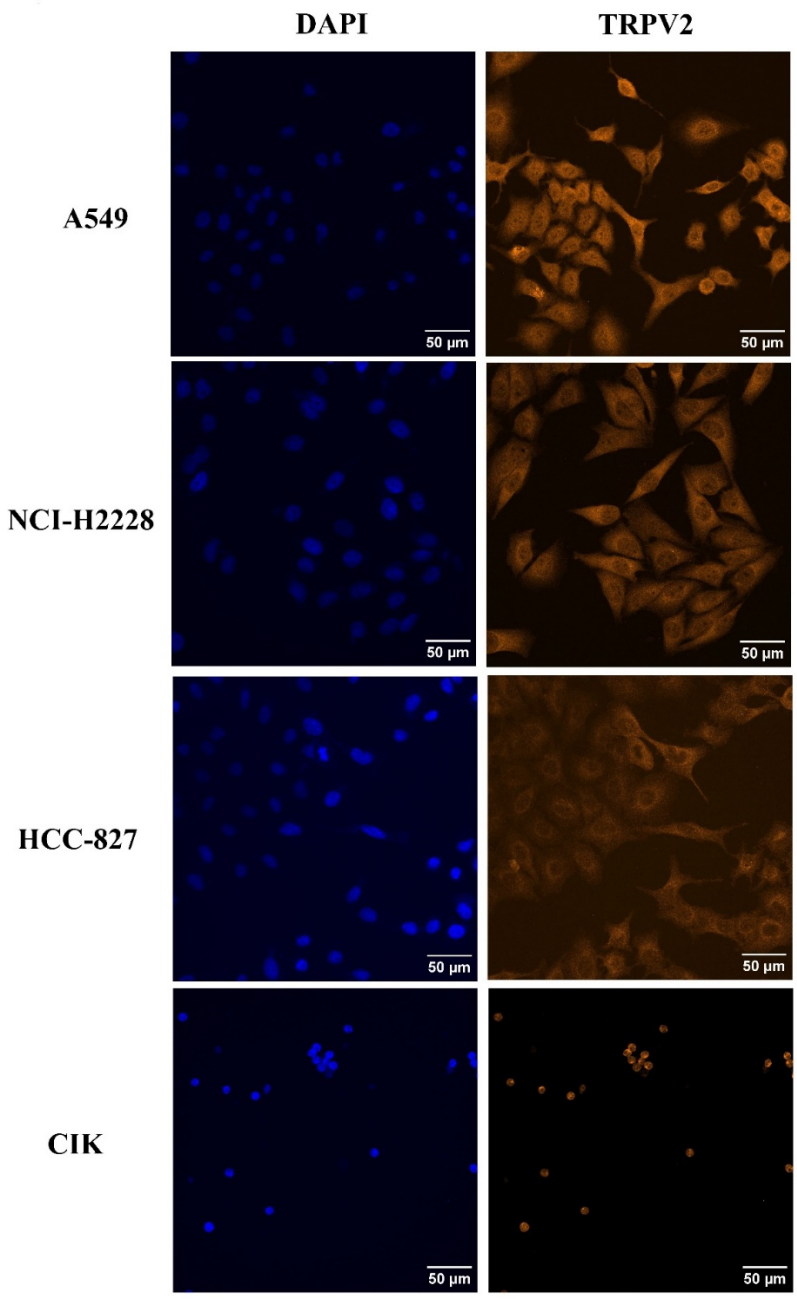

Figure 15. Subcellular localization of TRPV2 in NSCLC cell lines and CIK cells detected by Fluorescent IHC. Cells were fixed and stained with NorthernLights™ NL557 with orange signals for TRPV2 and blue signals for nuclear DAPI. Fluorescent signals were captured by Visitron VisiScope Spinning Disk Confocal Microscopy and VisiVIEW® Image software. Scale bar = 50 µm.

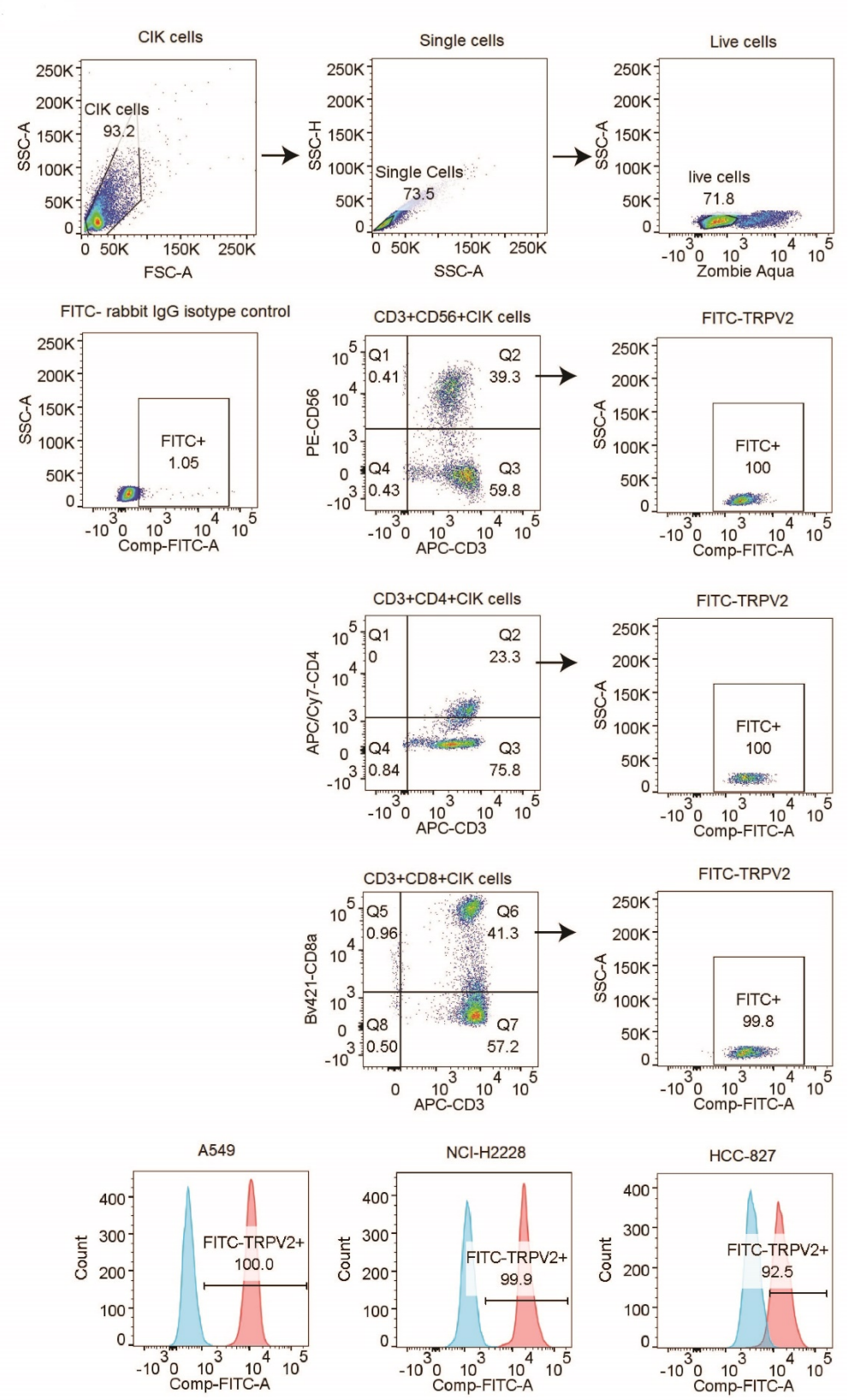
CIK cells
CIK cells
93.2
SSC-A
FSC-A
Single cells
Single Cells
73.5
SSC-H
SSC-A
Live cells
live cells
71.8
SSC-A
Zombie Aqua
FITC- rabbit IgG isotype control
FITC+
1.05
SSC-A
Comp-FITC-A
CD3+CD56+CIK cells
Q1
0.41
Q2
39.3
Q4
0.43
Q3
59.8
PE-CD56
APC-CD3
FITC-TRPV2
FITC+
100
SSC-A
Comp-FITC-A
CD3+CD4+CIK cells
Q1
0
Q2
23.3
Q4
0.84
Q3
75.8
APC/Cy7-CD4
APC-CD3
FITC-TRPV2
FITC+
100
SSC-A
Comp-FITC-A
CD3+CD8+CIK cells
Q5
0.96
Q6
41.3
Q8
0.50
Q7
57.2
Bv421-CD8a
APC-CD3
FITC-TRPV2
FITC+
99.8
SSC-A
Comp-FITC-A
A549
FITC-TRPV2+
100.0
Count
Comp-FITC-A
NCI-H2228
FITC-TRPV2+
99.9
Count
Comp-FITC-A
HCC-827
FITC-TRPV2+
92.5
Count
Comp-FITC-A

Figure 16. Intracellular TRPV2 expression in NSCLC cell lines and CIK cells detected by flow cytometry. CIK cells or NSCLC cells were stained with a Fixable Viability Zombie Aqua™ Dye exclude dead cells. After that, CIK cells were stained by APC anti-human CD3 antibody (clone OKT3), Brilliant Violet 421 anti-human CD8 antibody (clone RPA-T8), APC/cyanine7 anti-human CD4 antibody (clone RPA-T4), PE anti-human CD56 antibody (clone 5. 1 H11) at 4°C for 20 min. Afterwards, the cells were fixed and permeabilized using fixation buffer and intracellular staining permeabilization wash buffer. The blocking step was carried out in permeabilization wash buffer with 2% normal goat serum for 15 min. Cells were incubated with anti-TRPV2 antibody (1:100 dilution) at 4 °C for 30 min. Subsequently, cells were washed and incubated with Alexa Fluor™ 488-labeled goat anti-rabbit IgG (H+L) (1:250 dilution) for 30 min.

2.3.5. CBD promotes the cytotoxic activity of CIK cells in NSCLC cell lines, with NCI-H2228 being the most sensitive concerning IFN-γ secretion.

To evaluate the effect of CBD on the cytotoxic activity of CIK cells, we prelabeled NSCLC cells with carboxyfluorescein diacetate succinimidyl ester (CFSE) and co-cultured them with CIK cells at an ET ratio of 10:1. It was found that the percentage of cytotoxicity of CIK cells against A549 was significantly increased after the combination of 3 μM CBD/5 μM CBD compared with DMSO control (51.8 ± 2.1% vs. 34.7 ± 3.6%, P< 0.05; 52.7 ± 4.4% vs. 34.7 ± 3.6%, P< 0.05, respectively. In the case of NCI-H2228, a significant increase was observed at 5 μM, 10 μM, 15 μM, and 20 μM CBD compared with the DMSO control after 24 hours of incubation (84.0 % ± 2.1 % vs. 74. 3 ± 0.9%, P= 0.0037; 85.7% ± 1.4% vs. 74.3 ± 0.9%, P= 0.0009; 90.0% ± 0.2% vs. 74.3 ± 0.9%, P < 0.0001; 90.0% ± 0.8% vs. 74.3 ± 0.9%, P <0.0001, respectively. Whereas 20 μM CBD appeared to be sufficient in case of HCC-827 (64.9 ± 3.5 % vs. 47.6 ± 4.5 %, P < 0.05) (Figure 17A). Representative flow cytometry plots illustrated the typical gating strategy used to identify the viable tumor cells after treatment with a

combination of CIK cells and CBD (Figure 17B). Next, we examined the potential variations in IFN-γ cytokine release (due to cytotoxicity of CIK cells) and found that NCI-H2228 responded strongly for IFN-γ secretion when exposed to 5 μM, 10 μM, 15 μM, and 20 μM CBD concentrations (106. 7 ± 9.8 vs. 69.9 ± 1.7 pg/mL, P= 0.0251; 116.3 ± 10.3 vs. 69.9 ± 1.7 pg/mL, P= 0.0045; 176.3 ± 14.9 vs. 69.9 ± 1.7 pg/mL, P < 0.0001; 159.4 ± 7.6 vs. 69.9 ± 1.7 pg/mL, P < 0.0001). A549 and HCC-827 showed a significant increase in IFN-γ at a concentration of 15 μM/20 μM (Figure 17C). Thus, it can be concluded that CBD promotes the cytotoxic activity of CIK cells in all NSCLC cell lines, with NCI-H2228 being the most sensitive concerning IFN-γ secretion.

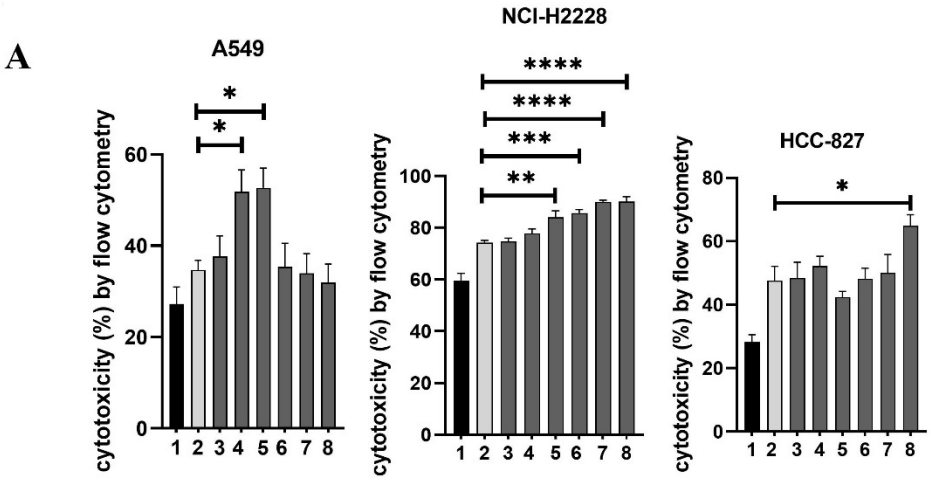

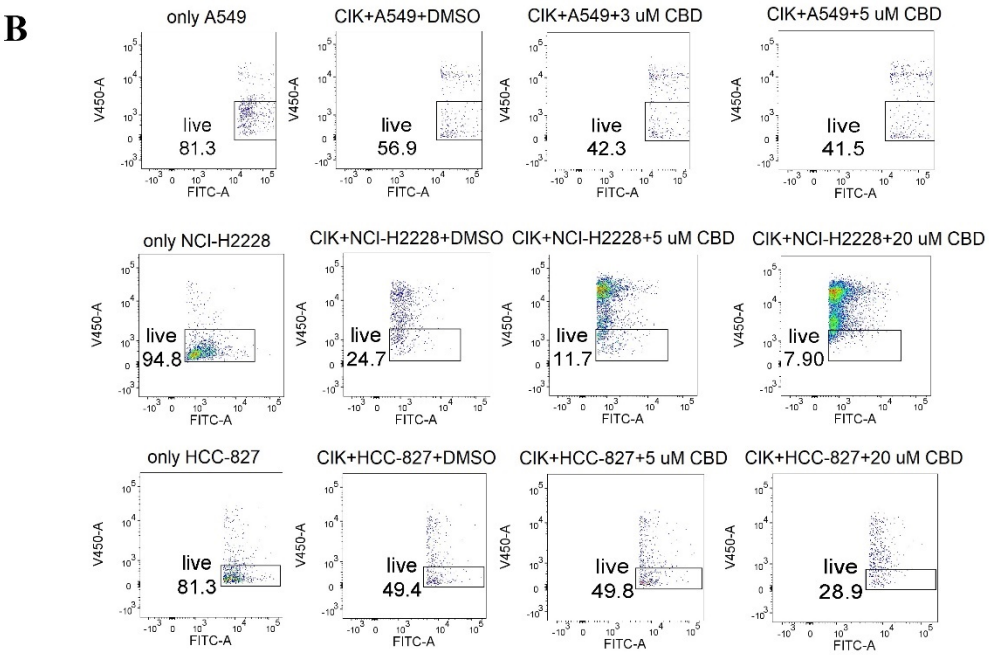

1	CIK+tumor
2	CIK+tumor+DMSO
3	CIK+tumor+1 μM CBD
4	CIK+tumor+3 μM CBD
5	CIK+tumor+5 μM CBD
6	CIK+tumor+10 μM CBD
7	CIK+tumor+15 μM CBD
8	CIK+tumor+20 μM CBD

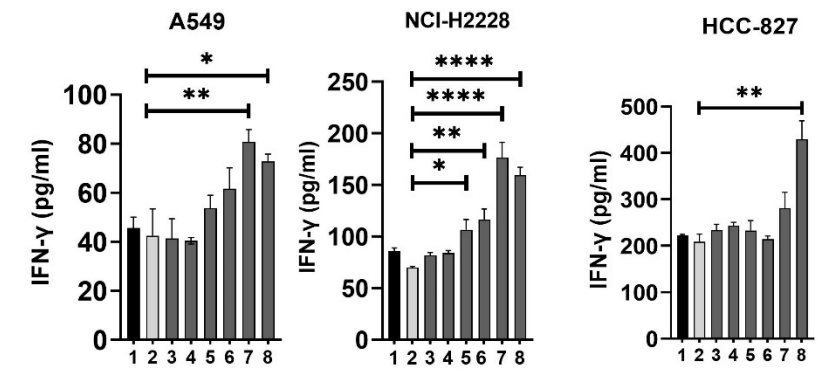

Figure 17. The cytotoxicity of CIK cells was measured using flow cytometry and IFN-γ secreted from CIK cells was detected by ELISA. (A) The cytotoxicity of CIK cells against A549, NCI-H2228 or HCC-827 with CBD treatment was detected by flow cytometry assessment after 24 h at different concentrations of CBD. (B) Representative flow cytometry plots illustrated the typical gating strategy used to identify viable tumor cells after treatment with a combination of CIK cells and CBD. (C) IFN-γ levels from CIK cells after treatment with a combination of CBD on NSCLC target cells detected by ELISA. E:T (effector-target) ratio =10:1. *p < 0.05, **p < 0.01, ***p < 0.001, ****p < 0.0001 vs. CIK combines DMSO targeting NSCLC cell control. Statistical analysis was performed using two-way ANOVA followed by Dunnett's multiple comparison test by GraphPad Prism software version 9.0.0. Data are shown as the mean ± SD, representative of three independent experiments. CIK cells were derived from 3 donors.

2.3.6. CBD in combination with CIK cells significantly alters the LINE-1 expression and methylation in NSCLC cell lines

Limited evidence suggests that CBD may modulate epigenetic-related changes (Domingos L.B., et al., 2022; Griffiths C., et al., 2021; Wanner N.M., et al., 2021). While the main focus of studies remains in genomic DNA methylation, any alterations in the repetitive genome (e.g. LINE-1) have never been investigated. We therefore focused on the effect of CBD on the CIK cells alone and in combination with NSCLC cell lines, especially for global LINE-1 expression and methylation. We found that the level of mRNA of LINE-1 was significantly reduced on CIK day 14 compared to PBL control (P= 0.0122) (Figure 18A). We also found that CBD alone has no effect on the expression of LINE-1 in CIK cells (Figure 18B), however in combination it can significantly reduce the LINE-1 expression in A549 cells at an E:T ratio of 0.1:1 (Figure 18C, 5 μM CBD + A549 vs. DMSO, P= 0.0436; 5 μM CBD + A549 + CIK vs. DMSO, P= 0.0436, respectively). Similarly, 10 μM CBD with CIK cells significantly decreased

the level of global LINE-1 methylation in A549 (Figure 18D, %5-mC associated with detectable CpG residues: 10 µM CBD + A549 + CIK vs DMSO + A549, 45.5 ± 1.1% vs. 32.6 ± 3.5%, P= 0.0388). Significant alterations were also observed in NCI-H2228 compared to DMSO control (5 µM CBD + NCI-2228 vs DMSO, 56.1 ± 8.6% vs 29.7 ± 7.2%, P= 0.0002; 10 µM CBD + NCI-H2228 + CIK vs DMSO, 51.6 ± 7.2% vs 29.7 ± 7.2%, P= 0.0026, respectively). However, no change was noticed in HCC-827 cells.

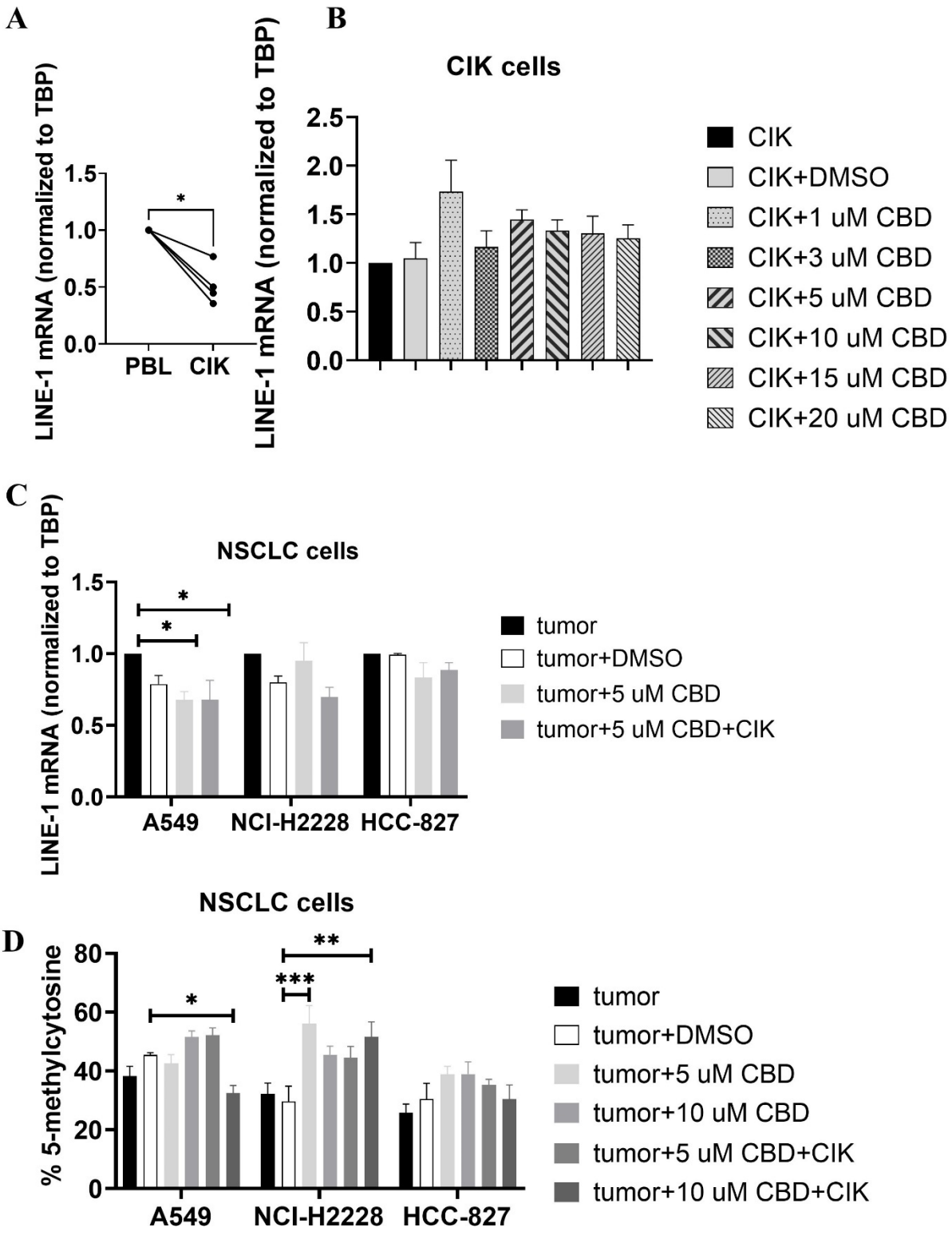
A
LINE-1 mRNA (normalized to TBP)
1.5
1.0
0.5
0.0
*
PBL
CIK
B
CIK cells
LINE-1 mRNA (normalized to TBP)
2.5
2.0
1.5
1.0
0.5
0.0
CIK
CIK+DMSO
CIK+1 uM CBD
CIK+3 uM CBD
CIK+5 uM CBD
CIK+10 uM CBD
CIK+15 uM CBD
CIK+20 uM CBD
C
NSCLC cells
LINE-1 mRNA (normalized to TBP)
1.5
1.0
0.5
0.0
*
*
A549
NCI-H2228
HCC-827
tumor
tumor+DMSO
tumor+5 uM CBD
tumor+5 uM CBD+CIK
D
NSCLC cells
% 5-methylcytosine
80
60
40
20
0
*
**
***
A549
NCI-H2228
HCC-827
tumor
tumor+DMSO
tumor+5 uM CBD
tumor+10 uM CBD
tumor+5 uM CBD+CIK
tumor+10 uM CBD+CIK

Figure 18. DNA genomic changes on CIK cells and NSCLC cells after incubation with CBD for 24 h. (A) LINE-1 mRNA expression in CIK cells on day 14 compared to PBL (B) LINE-1 mRNA expression in CIK cells after incubation with CBD for 24 h (C) LINE-1 mRNA expression in NSCLC cells after incubation with CBD or CBD with CIK cells. E:T ratio =0.1:1 (D) %5-mC associated with the detectable CpG residues in NSCLC cells after incubation with CBD or CBD with CIK cells. E:T ratio =0.1:1. All data are shown as the mean ± SD, representative of four independent experiments. Statistical analysis was performed using a paired t test for CIK cells on day 14 in comparison to relative PBL cells. A Two-way ANOVA followed by Dunnett's multiple comparisons test was performed on another data using GraphPad Prism software version 9.0.0. *p < 0.05, **p < 0.01, ***p < 0.001.CIK cells were derived from 4 donors.

2.3.7. Mechanistically, CBD affects NKT subpopulations of CIK cells and may modulate TRPV2 channel and the p-ERK1/2 pathway.

Given that CIK cells are a heterogeneous cell population, among which NKT cells constitute a significant proportion. We therefore investigated the effect of CBD on the CIK cell populations, particularly the receptors associated with NKT activation (CD25 and CD69 (Clausena J., et al., 2003) present on the surface of CIK cells. To mention, CD69 is a useful marker for the cytotoxic activity of NK cells, whereas CD25 expression serves as an indicative of the proliferative potential. We found that the expression of $CD25^{+}CD69^{+}$ on the $CD3^{+}CD56^{+}$ CIK cells increased significantly when CIK cells were incubated with 1 µM, 5 µM, and 10 µM CBD for 24 hours (Figure 19A). In addition, the percentage of $CD25^{+}CD69^{+}$ NKT cells increased after 24-hour activation by 1 µM CBD compared with the DMSO control (15.2 ± 3.2% vs. 6.9 ± 1.0%, P<0.0001). The isotype PE-Cy7 IgG1k was a PE-Cy7-CD69 control and the isotype PE-IgG1k was a PE-CD25 control (Figure. 20). Also, CD45RA and CD62L expression patterns were used to identify naïve T cells ($CD45RA^{+}CD62L^{+}$), central memory

T cells (TCM; $CD45RA^{-}CD62L^{+}$), effector memory T cells (TEM; $CD45RA^{-}CD62L^{-}$), and terminal effector memory T cells (TEMRA; $CD45RA^{+}CD62L^{-}$). We found significantly high percentage of $CD45RA^{+}CD62L^{-}$ TEMRA terminal effector memory NKT subset of CIK cells at 20 µM CBD for 24 h compared with DMSO control (52.7 ± 16.5% vs. 23.1 ± 9.1%, P= 0.0473, Figure 19B). In other subsets of CIK cells, no significant differences were seen (Figure 20). Thus, suggesting that CBD may contribute to the cytotoxic activation phase of $CD3^{+}CD56^{+}$CIK cells.

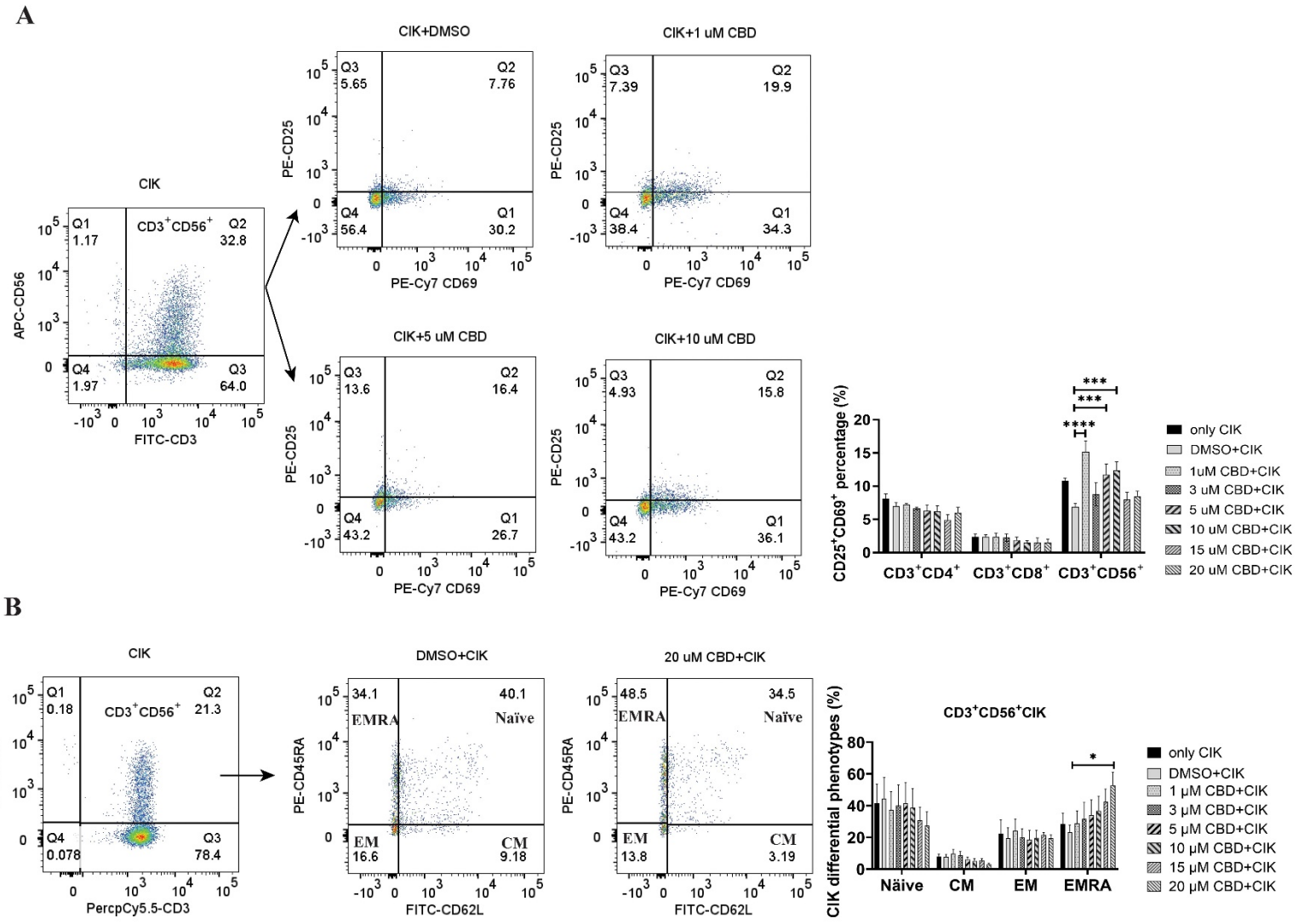

Figure 19. The phenotypes of CIK cells were measured using flow cytometry after incubation with CBD for 24 h. (A) The surface expression of CD25 and CD69 on CIK cells after 24 h CBD treatment was detected by flow cytometry assessment at different concentrations of CBD. (B) The surface expression of CD45RA and CD62L on CIK cells after 24 h CBD treatment was detected by flow cytometry assessment at different concentrations of CBD. Naïve: $CD45RA^{+}CD62L^{+}$ T cells, CM: central memory T cells ($CD45RA^{-}CD62L^{+}$), EM: effector memory T cells ($CD45RA^{-}CD62L^{-}$), EMRA: terminal effector memory T cells ($CD45RA^{+}CD62L^{-}$). *p < 0.05, ***p < 0.001, ****p < 0.0001 vs. CIK

combined with DMSO control. Statistical analysis was performed using two-way ANOVA followed by Dunnett's multiple comparison test by GraphPad Prism software version 9.0.0. CIK cells were derived from 4 donors.

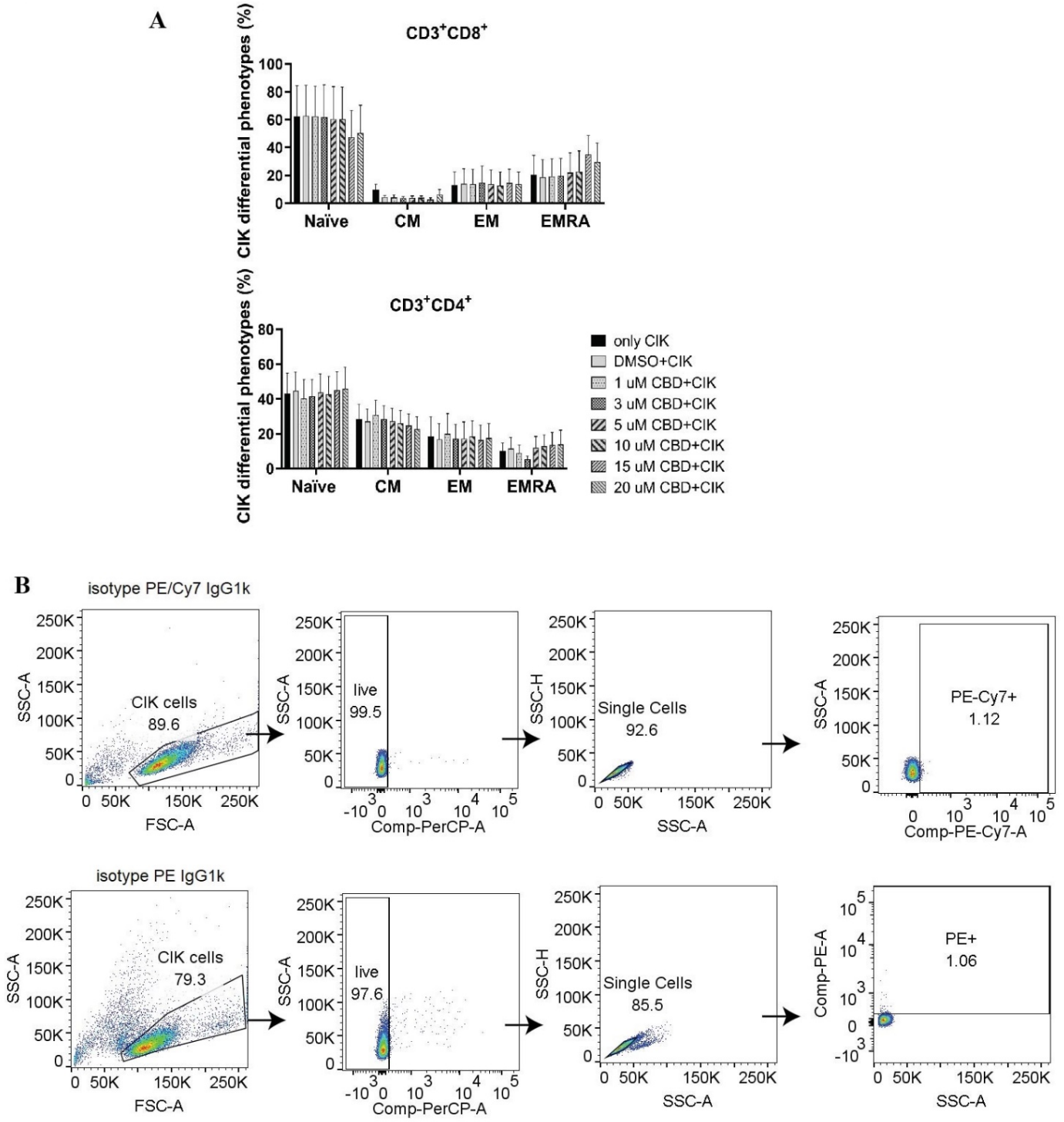

Figure 20. (A) The surface expression of CD45RA and CD62L on $CD3^+CD8^+$CIK or $CD3^+CD4^+$ CIK

cells after 24 h CBD treatment was detected by flow cytometry assessment. Naïve: $CD45RA^{+}CD62L^{+}$ T cells, CM: central memory T cells ($CD45RA^{-}CD62L^{+}$), EM: effector memory T cells ($CD45RA^{-}CD62L^{-}$), EMRA: terminal effector memory T cells ($CD45RA^{+}CD62L^{-}$). Statistical analysis was performed using a two-way ANOVA followed by Dunnett's multiple comparison test by GraphPad Prism software version 9.0.0. CIK cells were derived from 4 donors. (B) PE-CD25 and PE-Cy7-CD69 gate strategies. The isotype PE-Cy7 IgG1k was a PE-Cy7-CD69 control and the isotype PE-IgG1k was a PE-CD25 control.

Considering that CBD can also act via transient receptor potential vanilloid-2 (TRPV2) manner, we therefore evaluated the intracellular calcium level in CIK cells by treating them using variable concentrations of CBD and the specific TRPV2 channel antagonist tranilast (TLS). Interestingly, we observed that CBD as a TRPV2 agonist significantly increased intracellular Ca^{2+} levels in CIK cells at 3 µM, 5 µM, 10 µM, 15 µM, and 20 µM CBD after 1 minute (mean fluorescence intensity MFI 10943.63 ± 921.61 vs. 6966.25 ± 739. 06, P= 0.0373; 11545.75 ± 650.99 vs. 6966.25 ± 739.06, P= 0.0126; 14021 ± 1309.35 vs. 6966.25 ± 739.06, P <0.0001; 15022.88 ± 1547.10 vs. 6966.25 ± 739.06, P <0.0001; 15035.88 ± 1604.35 vs. 6966.25 ± 739.06, P <0.0001, respectively). On the contrary, 10 µM tranilast significantly affected the intracellular Ca^{2+} levels with mean of 9.96% (5 µM CBD+10 µM TLS vs. 5 µM CBD, P= 0.0298), 18.35% (10 µM CBD+10 µM TLS vs. 10 µM CBD, P= 0.0342), 14.07% (15 µM CBD+15 µM TLS vs. 15 µM CBD, P= 0.0110), and 15.54% (15 µM CBD+15 µM TLS vs. 10 µM CBD, P= 0.0342), 14.07% (15 µM CBD+15 µM TLS vs. 15 µM CBD, P= 0.0110), and 15.54% (20 µM CBD+20 µM TLS vs. 20 µM CBD, P= 0.0095) (Figure 21A). This outcome suggests that CBD may promote intracellular calcium through the TRPV2 channel. Continuing the analysis, we also found a significant increase in the percentage of intracellular

expression of FITC anti-ERK1/2 phospho (Thr202/Tyr204) in CIK cells after incubation with CBD at concentrations of 3, 5, 10, 15, 20 μM for 15 min compared with DMSO control (Figure 21B). Meanwhile, we investigated the effect of FR180204 (a selective inhibitor of ERK) on the cytotoxicity of CBD-treated CIK cells against NSCLC cells. FR180204 abolished CBD-induced cytotoxicity of CIK cells against A549 (CBD group: 3 μM CBD vs. DMSO, P= 0.0002, 5 μM CBD vs. DMSO, P< 0.0001; FR18028+CBD group: 10 μM FR18028+ 3 μM CBD vs. DMSO, P= 0.9811, 10 μM FR18028+5 μM CBD vs. DMSO, P= 0.9825, respectively). Similarly, Pretreated-FR180204 in CIK cells reduced CBD-induced cytotoxicity of CIK cells against NCI-H2228 (CBD group: 5 μM CBD vs. DMSO, P= 0.0002; 10 μM CBD vs. DMSO, P= 0.0002; 15 μM CBD vs. DMSO, P= 0.0002; 20 μM CBD vs. DMSO, P< 0.0001; FR18028+CBD group: 10 μM FR18024+5 μM CBD vs. DMSO, P= 0.4064; 10 μM FR18024+10 μM CBD vs. DMSO, P= 0.5480; 10 μM FR18024+15 μM CBD vs. DMSO, P= 0.4192; 10 μM FR18024+20 μM CBD vs. DMSO, P= 0.1627, respectively) and HCC-827 (CBD group: 20 μM CBD vs. DMSO, P< 0.0001; FR18028+CBD group: 10 μM FR18028+ 20 μM CBD vs. DMSO control, P= 0.2535, respectively) (Figure 22). Overall, these results suggest that CIK cells are activated by CBD through the TRPV2 channel and CBD-induced cytotoxicity is regulated the p-ERK1/2 pathway.

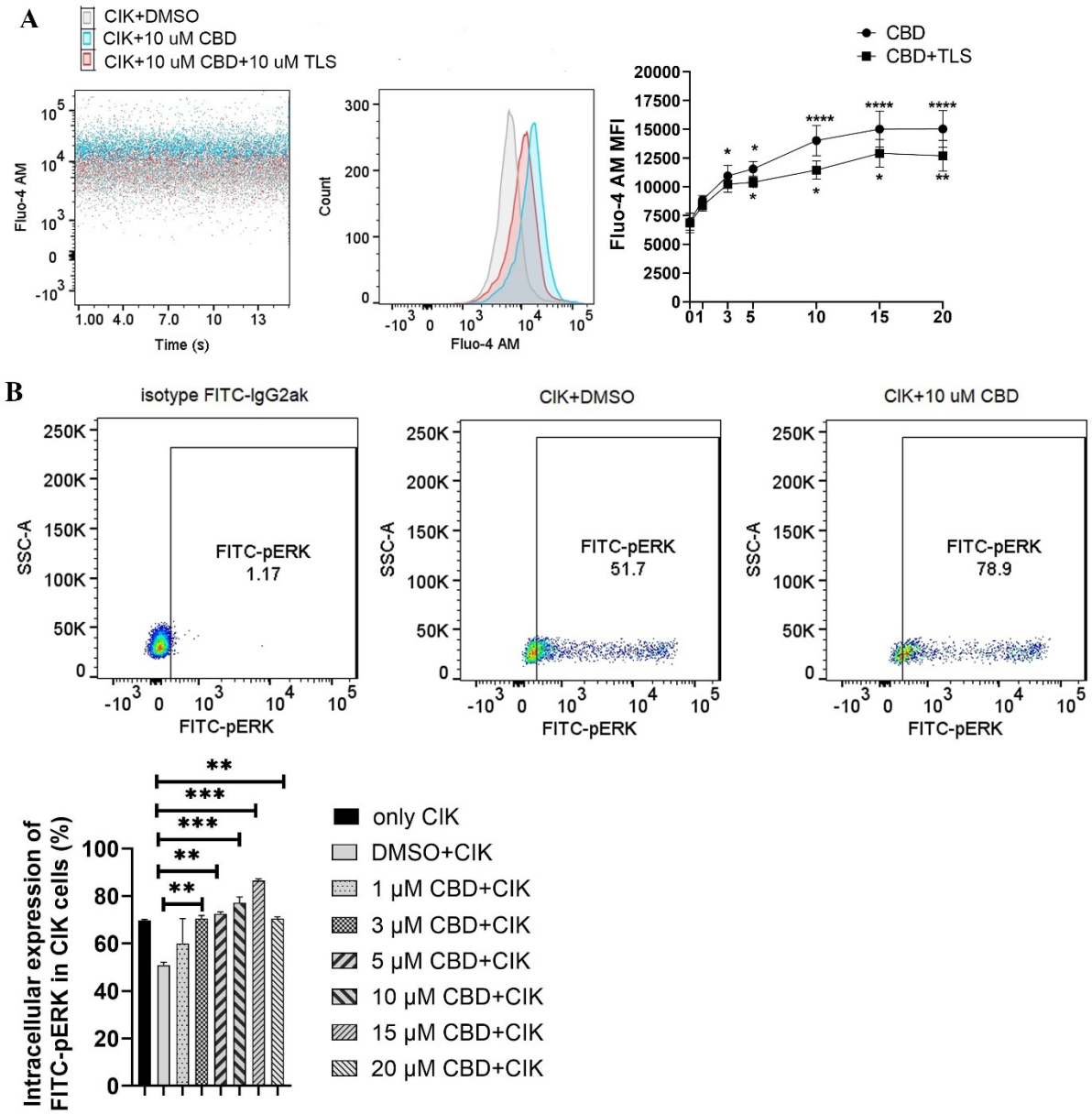

Figure 21. Characterization of intrinsic alternation in the CIK cells in the CBD-inducing culture by flow cytometric analysis. A) CIK cells were exposed to either CBD or CBD combined with TRPV2 channel antagonist tranilast at 37 °C for 1 minute. Dead cells were gated and excluded by Hoechst 33258 for Fluo-4 AM expression. B) The phosphorylation levels of Erk1/2 in CIK cells were determined by flow cytometry. Dead cells were gated and excluded by Zombie Aqua™ dye for intracellular expression. The rabbit of isotype controls is indicated. The percentage of FITC anti-ERK1/2 Phospho

(Thr202/Tyr204) was analyzed using the Flowjo V10 software. *p < 0.05, **p < 0.01, ***p < 0.001, ****p < 0.0001 vs. CIK combined with DMSO control. All data are shown as the mean ± SD, representative of four independent experiments. Statistical analysis was performed using two-way ANOVA followed by Dunnett's multiple comparisons test by GraphPad Prism software version 9.0.0. CIK cells were derived from 4 donors.

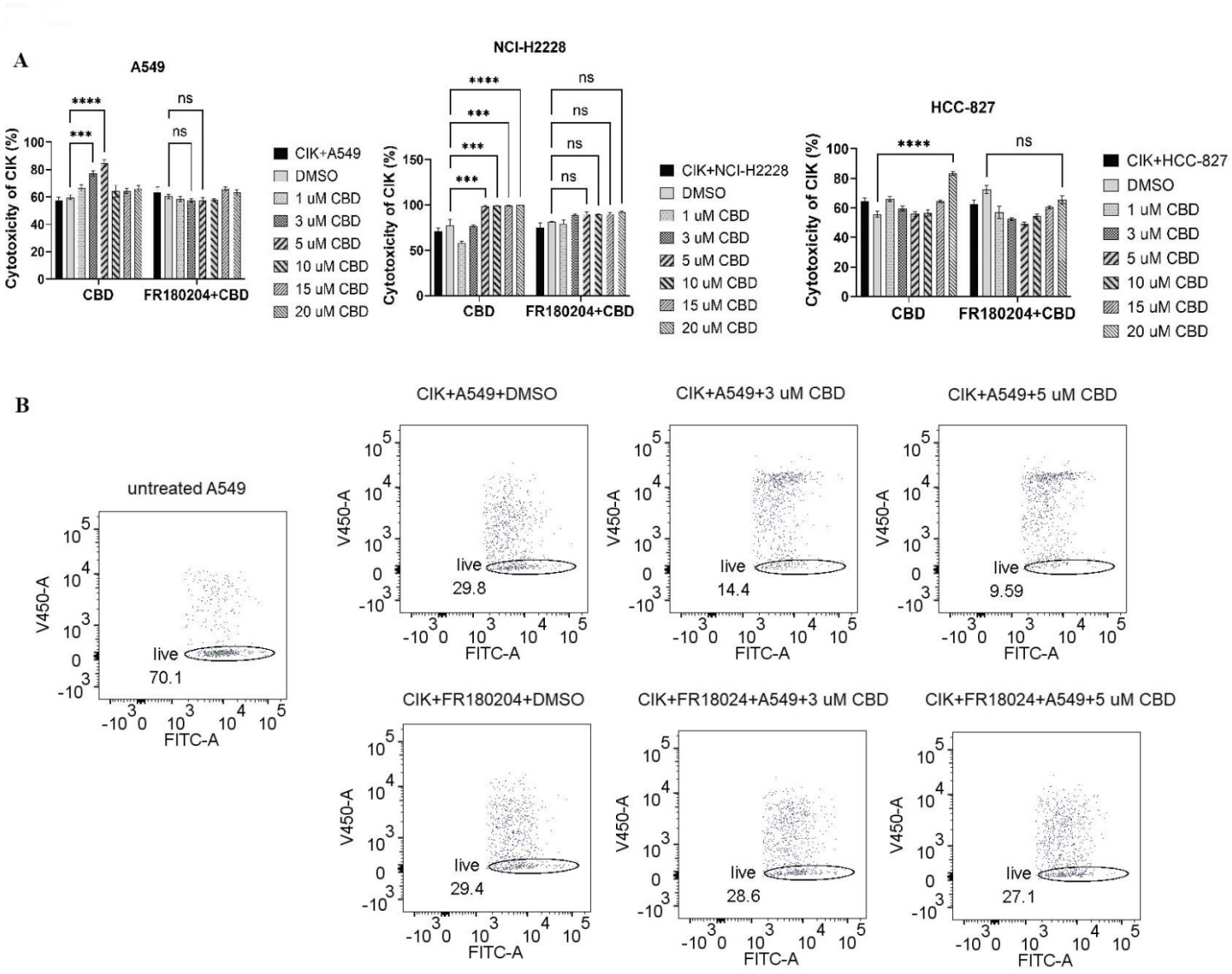

Figure 22. The effects of ERK inhibitor FR180204 on the cytotoxicity of CBD-treated CIK cells against NSCLC cells. CIK cells were pretreated with 10 μM FR18024 for 2 h then cocultured with CFSE-labeled A549 (A), NCI-H2228 (B) and HCC-827(C) at different CBD concentrations. E:T (effector-

target) ratio =10:1. *p < 0.05, **p < 0.01, ***p < 0.001, ****p < 0.0001 vs. CIK combined DMSO targeting NSCLC cells was designed as a control. Statistical analysis was performed using a two-way ANOVA followed by Dunnett's multiple comparison test by GraphPad Prism software version 9.0.0. Data are shown as the mean ± SD, representative of three independent experiments. CIK cells were derived from 3 donors.

2.4. Discussion

There have been several ongoing efforts to understand the molecular function of cannabidiol (CBD) in cancer (Śledziński P., et al., 2018), primarily as a potential anti-cancer agent with relevance to multiple clinical therapies. Herein, we sought to understand the functional aspect of CBD in the preclinical lung cancer model and its compatibility with cytokine-induced killer (CIK) cell immunotherapy (Sharma A., et al., 2021), which is now approved in several countries, including Germany. We primarily addressed, 1) whether CBD has any particular effects on NSCLC cell lines with diverse genetic backgrounds, 2) whether CBD can exert any influence on CIK cells aiming to enhance their therapeutic potential/function in NSCLC cells, 3). If CBD combined with CIK cells can affect the expression and methylation of LINE-1 repetitive sequences in NSCLC cells.

To determine this, we first investigated whether CBD has any particular effects on NSCLC cell lines with diverse genetic backgrounds such as A549 cells (KRAS mutation, P53 wide-type), NCI-H2228 (EML4-ALK variant 3, P53 Q331* mutation) and HCC-827 (EGFR exon19 deletion mutant, inactivation P53 mutation). A study concluded that CBD treatment regulates several types of cell death via upregulating apoptosis-related proteins, such as p53 in A549 (Park Y.J., et al., 2022). Similarly, our analysis revealed that A549 cells were more sensitive

to CBD treatment compared to other cell types, presumably attributable to their p53 wild-type state. These findings are consistent with the notion that marijuana smoke condensates (MSCs) induce DNA/chromosome damage and apoptosis in human lung cancer cells, and the apoptotic responses induced by MSCs appeared to be higher in p53-WT H460 cells than in p53-null H1299 cells (Kim H.R., et al., 2012). The expression of p-γH2AX increased significantly in A549 in the presence of CBD, suggesting that CBD may promote DNA DSBs, p53 may also partially contribute here. Similar to p-γH2AX expression, we subsequently investigated whether CBD may also influence the migration and invasion potential of NSCLC cell lines. We found that CBD significantly suppressed the migration and invasion ability and this inhibition was restrained by the TRPV2 antagonist tranilast. However, this effect was again limited to A549 and other two cell lines (NCI-H2228 and HCC-827) were unable to invade either the membranes or the Matrigel coating membranes. In fact, similar results were observed in NCI-H2228 and HCC-827 when wound healing rates were assessed to evaluate the efficacy of CBD on collective migration of cells. Using Matrigel invasion assays and wound healing assays we found cannabidiol-driven impaired migration in NSCLC cells that was reversed by antagonists to transient receptor potential vanilloid 2 (TRPV2). The decrease in invasion by cannabidiol appeared concomitantly with the downregulation of matrix metalloproteinases-9 (MMP-9). Interestingly, there is several evidence supporting the role of CBD in TRPV1-elicited p42/44 MAPK activation and downstream TIMP-1-dependent inhibition of invasion (Ramer, R., et al., 2010; Harpe A., et al., 2022). TIMP-1, as a strong inhibitor of MMP-9 activation and activity, keeps the intracellular and nuclear MMP-9 activation status under surveillance in a healthy retina (Lee EJ., et al., 2021). Higher

expression of MMP-9 in cancerous tissue in NSCLC patients compared to non-cancerous tissue, and unchanged expression of TIMP-1, suggest imbalanced regulation of MMP-9/TIMP-1 (Pietrzak J., et al., 2023). In our study, TRPV2-dependent MMP-9 reduction also exhibits a pivotal role in the anti-invasive action of CBD. Collectively, CBD might modulate the TIMP1/MMP9 gene expression axis to impair the metastasis of NSCLC cells.

Next, we asked, whether CBD can exert any influence on CIK cells aiming to enhance their therapeutic potential function in NSCLC cells. We confirmed that CBD promotes the cytotoxic activity of CIK cells in NSCLC cell lines, with NCI-H2228 being the most sensitive concerning IFN-γ secretion. To subvert the exact cell population within CIK cells as a target of CBD, we performed phenotype analysis and found that the expression of $CD25^{+}CD69^{+}$ NKT on $CD3^{+}CD56^{+}$ CIK cells increased significantly when CIK cells were incubated with CBD. To mention, our findings underscore the impact of CBD on the differentiation of terminal effector memory (EMRA) ($CD45RA^{+}CD62L^{-}$) NKT CIK cells rather than $CD4^{+}$ or $CD8^{+}$ CIK cells, revealing that the desired terminal effector memory NKT response might contribute to the cytotoxicity of CIK cells in the presence of CBD. Since it has been suggested that CBD interacts with TRPV2 through a hydrophobic pocket (Pumroy R.A., et al., 2019), we therefore examined intracellular calcium levels in CIK cells by treating them with CBD and the TRPV2 channel antagonist tranilast (TLS). Interestingly, we found that CBD as a TRPV2 agonist significantly increased intracellular Ca^{2+} levels in CIK cells and the p-ERK1/2 pathway. To our knowledge, this is the first study to provide evidence of activation of CIK cells by CBD that is related to Ca^{2+} influx and modulated by TRPV2 channel activation.

It is worth mentioning that the therapeutic potential of CBD in combination with epigenetic

and classical chemotherapy drugs is of importance (Griffiths C., et al., 2021), but the biological (unfavorable) effects of CBD itself on the epigenetic system cannot be excluded. There have been studies focusing on CBD-induced abnormal changes in DNA methylation (Domingos L.B., et al., 2022; Pucci M., et al., 2013; Bartolomeo M.D., et al., 2021), however, to our knowledge, the effect of CBD on long interspersed element 1 (LINE-1 or L1) remains elusive. In cancer cells, long interspersed element-1 (LINE-1 or L1) is a repetitive DNA retrotransposon that duplicates via a copy-and-paste genetic mechanism. With LINE-1 comprising a substantial portion (approximately 17%) of the human genome, its methylation often correlates with the global genomic methylation (Sharma A., et al., 2019). As we mentioned before, LINE-1 promotes tumorigenicity and exacerbates tumor progression in NSCLC cell lines and mice model (Sun Z., et al., 2022). A recent study revealed that LINE1 elements were specifically expressed in the nuclei of näive $CD4^+$ T cells (RNA-FISH and RT–qPCR). LINE-1 expression in Th1 cells was rapidly downregulated upon activation and remained at low levels during differentiation (Marasca F., et al., 2022). Our results in Figure 18A are consistent with this study. When CIK cells were activated and matured at day 14, LINE-1 mRNA significantly decreased. It seems like higher LINE-1 expression demonstrates the resting stage of T cells. In the current study, we observed that the combination of CIK cells and CBD suppressed LINE-1 mRNA and also decreased LINE-1 DNA methylation levels in A549 cells. Redi E, et al. discovered aberrant DNA methylation patterns in ALK^+ tumor cells, overlapping with regulatory regions, plus a high degree of epigenetic heterogeneity between individual tumours. This discrepancy might be associated with an increasing of DNA methylation of LINE-1 in NCI-H2228 in the presence of CBD (Redl E., et al., 2021).

Importantly, CBD alone had no effect on mRNA LINE-1 expression or p-rH2AX expression in CIK cells, suggesting CBD does not lead to genome instability or DNA damage in CIK cells. This study has limitations. Firstly, we did not investigate the effects of CBD distinctly in squamous cell carcinomas (SCC) subgroup and cancer stem cells. Hamad H. et al. found that CBD decreased viability and induced cell death in NSCLC (A549, H1299), SCLC (H69) and decreased the cancer stem cell spheres of both NSCLC and SCLC (Hamad H., et al., 2021). Ramer R. et al. reported that treatment with 5 mg/kg CBD inhibits lung cancer cell invasion and metastasis via intercellular adhesion molecule-1 in athymic nude mice xenografted with A549 cells (Ramer R., et al., 2011) while there was no evidence for in vivo investigations of the antimetastatic effect of CBD in SCLC. However, there is evidence that prognostic value of MMP-9 may be of more importance in adenocarcinoma than in SCC. In addition, MMP-9 was significantly associated with both disease-free survival and OS in the adenocarcinoma group (Lee CY., et al., 2015). Secondly, the suppressive effect of combinations of CBD with THC or tyrosine kinase inhibitors or immune checkpoint inhibitors on lung cancer cells might also be examined in the future (Heider CG., et al., 2022).

2.5. Conclusions

In conclusion, CBD holds a great potential for treating NSCLC with CIK cell immunotherapy and its complete success requires careful consideration of the patients' genetic backgrounds. Cell lines with KRAS mutation (A549 cells) and EML4-ALK rearrangement (NCI-H2228) appear to be highly responsive in this combinatorial setup. Beyond that, CBD affects NKT subpopulations of CIK cells and may modulate the TRPV2 channel and the p-ERK1/2 pathway. However, the biosafety of a combination of CIK cells and CBD requires further

validation in animal models.

2.6. Abstract

A multitude of findings from cell cultures and animal studies are available to support the anti-cancer properties of cannabidiol (CBD). Since CBD acts on multiple molecular targets, its clinical adaptation, especially in combination with cancer immunotherapy regimen remains a serious concern. Considering this, we extensively studied the effect of CBD on the cytokine-induced killer (CIK) cell immunotherapy approach using multiple non-small cell lung cancer (NSCLC) cells harboring diverse genotypes. Our analysis showed that, a) The Transient Receptor Potential Cation Channel Subfamily V Member 2 (TRPV2) channel was intracellularly expressed both in NSCLC cells and CIK cells. b) A synergistic effect of CIK combined with CBD, resulted in a significant increase in tumor lysis and Interferon gamma (IFN-γ) production. c) CBD had a preference to elevate the $CD25^{+}CD69^{+}$ population and the $CD62L^{-}CD45RA^{+}$ terminal effector memory (EMRA) population in NKT-CIK cells, suggesting early-stage activation and effector memory differentiation in $CD3^{+}CD56^{+}$ CIK cells. Of interest, we observed that CBD enhanced the calcium influx, which was mediated by the TRPV2 channel and elevated phosphor-Extracellular signal-Regulated Kinase (p-ERK) expression directly in CIK cells, whereas ERK selective inhibitor FR180204 inhibited the increasing cytotoxic CIK ability induced by CBD. Further examinations revealed that CBD induced DNA double-strand breaks via upregulation of histone H2AX phosphorylation in NSCLC cells and the migration and invasion ability of NSCLC cells suppressed by CBD were rescued using the TRPV2 antagonist (Tranilast) in the absence of CIK cells. We further investigated the epigenetic effects of this synergy and found that adding CBD to CIK cells decreased the Long

Interspersed Nuclear Element-1 (LINE-1) mRNA expression and the global DNA methylation level in NSCLC cells carrying KRAS mutation. Taken together, CBD holds a great potential for treating NSCLC with CIK cell immunotherapy. In addition, we utilized NSCLC with different driver mutations to investigate the efficacy of CBD. Our findings might provide evidence for CBD-personized treatment with NSCLC patients (Published in *Frontiers in immunology*, 2024, 15: 1268652).

2.7. List of figures

2.8. References

Velasco G., Sánchez C., Guzmán M. Anticancer mechanisms of cannabinoids. Curr Oncol. 2016; 23: S23-32. doi: 10.3747/co.23.3080.

Mangal N., Erridge S., Habib N., Sadanandam A., Reebye V., Sodergren MH. J Cancer Res Clin Oncol. 2021;147:2507-2534. doi: 10.1007/s00432-021-03710-7.

Kylie O'Brien. Cannabidiol (CBD) in Cancer Management. Cancers (Basel). 2022;14:885. doi: 10.3390/cance

Pumroy RA, Samanta A, Liu Y, Hughes TE, Zhao S, Yudin Y, Rohacs T, Han S, Moiseenkova-Bell VY. Molecular mechanism of TRPV2 channel modulation by cannabidiol. Elife. 2019;8:e48792. Doi: 10.7554/eLife.48792.

Laprairie R B, Bagher A M, Kelly M E M, Denovan-Wright EM. Cannabidiol is a negative allosteric modulator of the cannabinoid CB1 receptor. Br J Pharmacol. 2015; 172: 4790–4805. https://doi.org/10.1111/bph.13250.

Landucci E, Pellegrini-Giampietro D.E, Gianoncelli A, and Ribaudo G. Cannabidiol preferentially binds TRPV2: a novel mechanism of action. Neural Regen Res. 2022; 17(12): 2693–2694. doi: 10.4103/1673-5374.335821.

Dhakar R, Dakal TC, Sharma A. Genetic determinants of lung cancer: Understanding the oncogenic potential of somatic missense mutations. Genomics. 2022;114:110401. doi: 10.1016/j.ygeno.2022.110401.

Peng Y, Qi W, Luo Z, Zeng Q, Huang Y, Wang Y, et al. Role of 18F-FDG PET/CT in patients affected by pulmonary primary lymphoma. Front Oncol. 2022;12:973109. doi: 10.3389/fonc.2022.973109.

Zhang G, Wang Z, Song P, Zhan X. DNA and histone modifications as potent diagnostic and therapeutic targets to advance non-small cell lung cancer management from the perspective of 3P medicine. EPMA J. 2022;13:649-669. doi: 10.1007/s13167-022-00300-6.

Hamad H, Olsen BB. Cannabidiol Induces Cell Death in Human Lung Cancer Cells and Cancer Stem Cells. Pharmaceuticals (Basel) 2021;14:1169. doi: 10.3390/ph14111169.

Misri S, Kaul K, Mishra S, Charan M, Verma AK, Barr MP, et al. Cannabidiol Inhibits Tumorigenesis in Cisplatin-Resistant Non-Small Cell Lung Cancer via TRPV2. Cancers (Basel). 2022;14:1181. doi: 10.3390/cancers14051181.

Haustein M, Ramer R, Linnebacher M, Manda K, Hinz B. Cannabinoids increase lung cancer cell lysis by lymphokine-activated killer cells via upregulation of ICAM-1. Biochem Pharmacol 2014;92:312-25. doi: 10.1016/j.bcp.2014.07.014.

Milián L, Monleón-Guinot I, Sancho-Tello M, Galbis JM, Cremades A, Almenar-Ordaz M, et al. In Vitro Effect of Δ9-Tetrahydrocannabinol and Cannabidiol on Cancer-Associated Fibroblasts Isolated from Lung Cancer. Int J Mol Sci 2022;23:6766. doi: 10.3390/ijms23126766.

Milian L, Mata M, Alcacer J, Oliver M, Sancho-Tello M, Martín de Llano JJ, et al. Cannabinoid receptor expression in non-small cell lung cancer. Effectiveness of tetrahydrocannabinol and cannabidiol inhibiting cell proliferation and epithelial-mesenchymal transition in vitro. PLoS One 2020;15:e0228909. doi: 10.1371/journal.pone.0228909.

Raïch L, Rivas-Santisteban R, Lillo A, Lillo J, Reyes-Resina I, Nadal X, et al. Similarities and differences upon binding of naturally occurring Δ9-tetrahydrocannabinol-derivatives to cannabinoid CB1 and CB2 receptors. Pharmacol Res. 2021;174:105970. doi: 10.1016/j.phrs.2021.105970.

Siveen KS, Nizamuddin PB, Uddin S, Al-Thani M, Frenneaux MP, Janahi IA, et al. TRPV2: A Cancer Biomarker and Potential Therapeutic Target. Dis Markers. 2020;2020:8892312. doi: 10.1155/2020/8892312.

Bertin S, Aoki-Nonaka Y, de Jong PR, Nohara LL, Xu H, Stanwood SR, et al. The ion channel TRPV1 regulates the activation and proinflammatory properties of $CD4^+$ T cells. Nat Immunol. 2014;15:1055-1063. doi: 10.1038/ni.3009.

Megan Cully. Closing the door on KRAS-mutant lung cancer. Nature Reviews Drug Discovery 2016; 15:747. doi:10.1038/nrd.2016.216.

De Petrocellis L, Ligresti A, Schiano Moriello A, Iappelli M, Verde R, Stott CG, Cristino L, Orlando P, Di Marzo V. Non-THC cannabinoids inhibit prostate carcinoma growth in vitro and in vivo: pro-apoptotic effects and underlying mechanisms. Br J Pharmacol. 2013;168:79–102. doi: 10.1111/j.1476-5381.2012.02027.x.

Vladimir N. Ivanov, Jinhua Wu, and Tom K. Hei. Regulation of human glioblastoma cell death by combined treatment of cannabidiol, γ-radiation and small molecule inhibitors of cell signaling pathways. Oncotarget. 2017;8: 74068–74095. doi: 10.18632/oncotarget.18240.

Li Y, Sharma A, Wu X, Weiher H, Skowasch D, Essler M, et al. A Combination of Cytokine-Induced Killer Cells With PD-1 Blockade and ALK Inhibitor Showed Substantial Intrinsic Variability Across Non-Small Cell Lung Cancer Cell Lines. Front Oncol. 2022;12:713476. doi: 10.3389/fonc.2022.713476.

Sun Z, Zhang R, Zhang X, Sun Y, Liu P, Francoeur N, et al. LINE-1 promotes tumorigenicity and exacerbates tumor progression via stimulating metabolism reprogramming in non-small cell lung cancer. Molecular Cancer. 2022;21:147. doi: 10.1186/s12943-022-01618-5.

Marasca F, Sinha S, Vadalà R, Polimeni B, Ranzani V, Paraboschi EM, et al. LINE1 are spliced in non-canonical transcript variants to regulate T cell quiescence and exhaustion. Nature Genetics 2022, 54, 180–193. doi: 10.1038/s41588-021-00989-7.

Schmidt-Wolf IG, Negrin RS, Kiem HP, Blume KG, Weissman IL. Use of a SCID mouse/human lymphoma model to evaluate cytokine-induced killer cells with potent antitumor cell activity. J Exp Med 1991;174:139-149. doi: 10.1084/jem.174.1.139.

Wu X, Zhang Y, Li Y, Schmidt-Wolf IGH. Increase of Antitumoral Effects of Cytokine-Induced Killer Cells by Anti-Body-Mediated Inhibition of MICA Shedding. Cancers (Basel) 2020;12:1818. doi: 10.3390/cancers12071818.

Yang F, Xu J, Li H, Tan M, Xiong X, Sun Y. FBXW2 suppresses migration and invasion of

lung cancer cells via promoting β-catenin ubiquitylation and degradation. Nat Commun 2019;10:1382. Doi: 10.1038/s41467-019-09289-5.

Staiano RI, Loffredo S, Borriello F, Iannotti FA, Piscitelli F, Orlando P, et al. Human lung-resident macrophages express CB1 and CB2 receptors whose activation inhibits the release of angiogenic and lymphangiogenic factors. J Leukoc Biol, 2016;99:531–540. doi: 10.1189/jlb.3HI1214-584R.

Whongsiri P, Goering W, Lautwein T, Hader C, Niegisch G, Köhrer K, et al. Many Different LINE-1 Retroelements Are Activated in Bladder Cancer. Int J Mol Sci 2020;21:9433. doi: 10.3390/ijms21249433.

Ohori M, Kinoshita T, Okubo M, Sato K, Yamazaki A, Arakawa H, et al. Identification of a selective ERK inhibitor and structural determination of the inhibitor-ERK2 complex. Biochem Biophys Res Commun. 2005;336:357-63. Doi: 10.1016/j.bbrc.2005.08.082.

Niba ET, Nagaya H, Kanno T, Tsuchiya A, Gotoh A, Tabata C, et al. Crosstalk between PI3 Kinase/PDK1/Akt/Rac1 and Ras/Raf/MEK/ERK Pathways Downstream PDGF Receptor. Cellular Physiology and Biochemistry. 2013; 31: 905–913. https://doi.org/10.1159/000350108

Zhang W, He X, Yin H, Cao W, Lin T, Chen W, et al. Allosteric activation of the metabolic enzyme GPD1 inhibits bladder cancer growth via the lysoPC-PAFR-TRPV2 axis. J Hematol Oncol. 2022;15:93. Doi: 10.1186/s13045-022-01312-5.

Shihan MH, Novo SG, Le Marchand SJ, Wang Y, Duncan MK. A simple method for quantitating confocal fluorescent images. Biochem Biophys Rep 2021;25:100916. https://doi.org/10.1016/j.bbrep.2021.100916.

Kim SY, Shin MS, Kim GJ, Kwon H, Lee MJ, Han AR, et al. Inhibition of A549 Lung Cancer Cell Migration and Invasion by Ent-Caprolactin C via the Suppression of Transforming Growth Factor-β-Induced Epithelial—Mesenchymal Transition. Mar Drugs 2021;19:465. doi: 10.3390/md19080465.

Cormier N, Yeo A, Fiorentino E, and Paxson J. Optimization of the Wound Scratch Assay to Detect Changes in Murine Mesenchymal Stromal Cell Migration After Damage by Soluble Cigarette Smoke Extract. J Vis Exp 2015;106: e53414. doi: 10.3791/53414.

Grada A, Otero-Vinas M, Prieto-Castrillo F, Obagi Z, Falanga V. Research Techniques Made Simple: Analysis of Collective Cell Migration Using the Wound Healing Assay. J Invest Dermatol 2017;137: e11-e16. https://doi.org/10.1016/j.jid.2016.11.020 pmid:28110712.

Trepat X, Chen Z, and Jacobson K. Cell migration. Compr. Physiol 2012;2:2369–2392. doi: 10.1002/cphy.c110012.

Zhang X., Qin Y., Pan Z., Li M., Liu X., Chen X., et al. Cannabidiol induces cell cycle arrest and cell apoptosis in human gastric cancer SGC-7901 cells. Biomolecules. 2019;9:302. Doi: 10.3390/biom9080302.

Go Y.Y., Kim S.R., Kim D.Y., Chae S.W., Song J.J. Cannabidiol enhances cytotoxicity of anti-cancer drugs in human head and neck squamous cell carcinoma. Sci. Rep. 2020;10:20622. doi: 10.1038/s41598-020-77674-y.

Hiratsuka S, Nakamura K, Iwai S, Murakami M, Itoh T, Kijima H, et al. MMP9 induction by vascular endothelial growth factor receptor-1 is involved in lung-specific metastasis. Cancer Cell. 2002;2:289-300. Doi: 10.1016/s1535-6108(02)00153-8.

Domingos LB, Silva NR, Filho AJMC, Sales AJ, Starnawska A, Joca S. Regulation of DNA Methylation by Cannabidiol and Its Implications for Psychiatry: New Insights from In Vivo and In Silico Models. Genes (Basel). 2022;13:2165. doi: 10.3390/genes13112165.

Griffiths C, Aikins J, Warshal D, Ostrovsky O. Can Cannabidiol Affect the Efficacy of Chemotherapy and Epigenetic Treatments in Cancer? Biomolecules. 2021;11:766. doi: 10.3390/biom11050766.

Wanner NM, Colwell M, Drown C, Faulk C. Developmental cannabidiol exposure increases anxiety and modifies genome-wide brain DNA methylation in adult female mice. Clin Epigenetics. 2021;13:4. doi: 10.1186/s13148-020-00993-4.

Clausena J, Vergeiner B, Enk M, Petzer AL, Gast G, Gunsilius E. Functional significance of the activation-associated receptors CD25 and CD69 on human NK-cells and NK-like T-cells. Immunobiology 2003;207:85-93. https://doi.org/10.1078/0171-2985-00219.

Śledziński P, Zeyland J, Słomski R, Nowak A. The current state and future perspectives of cannabinoids in cancer biology. Cancer Med. 2018;7:765-775. doi: 10.1002/cam4.1312.

Sharma A, Schmidt-Wolf I G.H. 30 years of CIK cell therapy: recapitulating the key breakthroughs and future perspective. J Exp Clin Cancer Res 2021;40:388. doi: 10.1186/s13046-021-02184-2.

Park YJ, Na HH, Kwon IS, Hwang YN, Park HJ, Kwon TH, et al. Cannabidiol Regulates Pear-Dependent Vesicle Formation as well as Cell Death in A549 Human Lung Cancer Cells. Pharmaceuticals (Basel) 2022;15:836. doi: 10.3390/ph15070836.

Kim HR, Son BH, Lee SY, Chung KH, and Oh SM. The Role of p53 in Marijuana Smoke Condensates-induced Genotoxicity and Apoptosis. Environ Health Toxicol 2012;27:e2012017. doi: 10.5620/eht.2012.27.e2012017.

Ramer, R., Merkord, J., Rohde, H., and Hinz, B. Cannabidiol inhibits cancer cell invasion via upregulation of tissue inhibitor of matrix metalloproteinases-1. Biochem. Pharmacol. 2010;79, 955-966. doi: 10.1096/fj.11-198184.

Harpe A, Beukes N, Frost CL. CBD activation of TRPV1 induces oxidative signaling and subsequent ER stress in breast cancer cell lines. Biotechnol Appl Biochem. 2022;69:420-430. Doi: 10.1002/bab.2119.

Lee EJ, Zheng M, Craft CM, Jeong S. Matrix metalloproteinase-9 (MMP-9) and tissue inhibitor of metalloproteinases 1 (TIMP-1) are localized in the nucleus of retinal Müller glial cells and modulated by cytokines and oxidative stress. PloS One. 2021;16: e0253915. Doi: 10.1371/journal.pone.0253915

Pietrzak J, Wosiak A, Szmajda-Krygier D, Świechowski R, Łochowski M, Pązik M, et al. Correlation of TIMP1-MMP2/MMP9 Gene Expression Axis Changes with Treatment Efficacy

and Survival of NSCLC Patients. Biomedicines 2023;11,1777. https://doi.org/10.3390/biomedicines11071777

Pumroy RA, Samanta A, Liu Y, Hughes TE, Zhao S, Yudin Y, et al. Molecular mechanism of TRPV2 channel modulation by cannabidiol. Elife. 2019;8:e48792. doi: 10.7554/eLife.48792.

Pucci M, Rapino C, Di Francesco A, Dainese E, D'Addario C, Maccarrone M. Epigenetic control of skin differentiation genes by phytocannabinoids. Br J Pharmacol. 2013;170:581-91. doi: 10.1111/bph.12309.

Bartolomeo MD, Stark T, Maurel OM, Iannotti FA, Kuchar M, Ruda-Kucerova J. Crosstalk between the transcriptional regulation of dopamine D2 and cannabinoid CB1 receptors in schizophrenia: Analyses in patients and in perinatal Δ9-tetrahydrocannabinol-exposed rats. Pharmacol Res. 2021;164:105357. doi: 10.1016/j.phrs.2020.105357.

Sharma A, Jamil MA, Nuesgen N, Dauksa A, Gulbinas A, Schulz WA. Detailed methylation map of LINE-1 5'-promoter region reveals hypomethylated CpG hotspots associated with tumor tissue specificity. Mol Genet Genomic Med. 2019;7:e601. doi: 10.1002/mgg3.601.

Redl E., Sheibani-Tezerji R., de Jesus Cardona C., Hamminger, P., Timelthaler, G., et al. Requirement of DNMT1 to orchestrate epigenomic reprogramming for NPM-ALK–driven lymphomagenesis. Life Sci Alliance. 2021;4: e202000794. doi: 10.26508/lsa.202000794.

Ramer R, Bublitz K, Freimuth N, Merkord J, Rohde H, Haustein M, et al. Cannabidiol inhibits lung cancer cell invasion and metastasis via intercellular adhesion molecule-1. FASEB J. 2011;26:1535–1548. https://doi.org/10.1096/fj.11-198184

Lee CY, Shim HS, Lee S, Lee JG, Kim DJ, Chung KY. Prognostic effect of matrix metalloproteinase-9 in patients with resected Non small cell lung cancer. J Cardiothorac Surg. 2015;10:44. doi: 10.1186/s13019-015-0248-3.

Heider CG, Itenberg SA, Rao J, Ma H, and Wu X. Mechanisms of Cannabidiol (CBD) in Cancer Treatment: A Review. Biology 2022;11:817. https://doi.org/10.3390/biology11060817

2.9. List of my publications

MD/Ph.D. publications (2018-2023) in Bonn University, Germany

1. **Yutao Li**, Amit Sharma, Michèle J. Hoffmann, Dirk Skowasch, Markus Essler, Ingo G. H. Schmidt-Wolf. Discovering single cannabidiol or synergistic antitumor effects of cannabidiol and cytokine-induced killer cells on non-small cell lung cancer cells Frontiers in Immunology. Front. Immunol. 2024, 15:1268652. doi: 10.3389/fimmu.2024.1268652.
2. **Yutao Li**, Amit Sharma, Ingo G. H. Schmidt-Wolf. Evolving insights into the improvement of adoptive T-cell immunotherapy through PD-1/PD-L1 blockade in the clinical spectrum of lung cancer. It has been accepted by Molecular Cancer.
3. Chunmei Hu, Min Liu, **Yutao Li**, Yi Zhao, Amit Sharma, Haotian Liu and Ingo Schmidt-Wolf. Recent Advances and Future Perspectives of CAR-T Cell Therapy in Head and Neck Cancer. Front. Immunol. 2023, 14, 716. DOI: 10.3389/fimmu.2023.1213716.
4. Rohulla Vaseq, Amit Sharma, **Yutao Li**, Ingo G H Schmidt-Wolf. Revising the Landscape of Cytokine-Induced Killer Cell Therapy in Lung Cancer: Focus on Immune Checkpoint Inhibitors. Int J Mol Sci. 2023 Mar 15;24(6):5626. doi: 10.3390/ijms24065626.
5. **Yutao Li**, Amit Sharma, Xiaolong Wu, Hans Weiher, Dirk Skowasch, Markus Essler, Ingo G. H. Schmidt-Wolf. A Combination of Cytokine-Induced Killer Cells With PD-1 Blockade and ALK Inhibitor Showed Substantial Intrinsic Variability Across Non-Small Cell Lung Cancer Cell Lines. Front Oncol. 2022; 12: 713476. doi:10.3389/fonc.2022.713476.
6. **Yutao Li**, Amit Sharma, Maurits W.J.R. Bloemendal, Roland Schmidt-Wolf, Miroslaw Kornek, Ingo G.H. Schmidt-Wolf. PD-1 blockade enhances cytokine-induced killer cell-mediated cytotoxicity in B-cell non-Hodgkin lymphoma cell lines. Oncol Lett. 2021 Aug; 22(2): 613. doi: 10.3892/ol.2021.12874.
7. **Yutao Li**, Amit Sharma, Jarek Maciaczyk, Ingo G. H. Schmidt-Wolf. Recent Development in NKT-Based Immunotherapy of Glioblastoma: From Bench to Bedside.

Int J Mol Sci. 2022; 23(3): 1311. doi: 10.3390/ijms23031311.

8. Mojgan Naghizadeh Dehno, **Yutao Li**, Hans Weiher, Ingo G.H. Schmidt-Wolf. Increase in Efficacy of Checkpoint Inhibition by Cytokine-Induced-Killer Cells as a Combination Immunotherapy for Renal Cancer. Int J Mol Sci. 2020; 21(9): 3078. doi: 10.3390/ijms21093078.
9. Xiaolong Wu, Ying Zhang, **Yutao Li**, Ingo G.H. Schmidt-Wolf. Increase of Antitumoral Effects of Cytokine-Induced Killer Cells by Antibody-Mediated Inhibition of MICA Shedding. Cancers (Basel) 2020; 12(7): 1818. doi: 10.3390/cancers12071818.
10. Xiaolong Wu, Ying Zhang, **Yutao Li**, Schmidt-Wolf IGH. Improvements in Flow Cytometry-Based Cytotoxicity Assay. Cytometry A. 2021;99(7): 680-688. doi: 10.1002/cyto.a.24242.

Master publications (2004-2008) in Peking University, China

11. **Yu-Tao Li**, Bei He, Yu-Zhu Wang & Jing Wang. Effects of intratracheal administration of nuclear factor-kappaB decoy oligodeoxynucleotides on long-term cigarette smoke-induced lung inflammation and pathology in mice. Respiratory Research. 2009-08-25. DOI: 10.1186/1465-9921-10-79.
12. **Yu-Tao Li**, Bei He &Yu-Zhu Wang. Exposure to cigarette smoke upregulates AP-1 activity and induces TNF-alpha overexpression in mouse lungs. Inhalation Toxicology. 2009-06-01. DOI: 10.1080/08958370802322596.

2.10. Acknowledgments

I would like to thank my supervisor Prof. Dr. med. Ingo Schmidt-Wolf for giving me the chance to work in his lab as a Ph.D. student and for guiding me on how to be a scientist. I am grateful for his enormous support with valuable discussions and suggestions. In addition, thank him for giving me the chance to get to know German culture. It was a fantastic experience for me.

I would also like to thank my second supervisor Prof. Dr. Hans Weiher, for his helpful discussions and suggestions in every lab meeting and for his support and review of my thesis. I want to thank Prof. Dr. med. Dirk Skowasch and Prof. Dr. med. Markus Essler for being part of my dissertation committee. They always gave me helpful advice in every annual committee report.

Furthermore, I would like to thank my colleagues, Maria Fitria Setiawan and Oliver Rudan for their great organizing and coordinating work in the lab. I am very thankful to Amit Sharma for improving my English writing ability and to other colleagues (Xiaolong Wu, Ying Zhang, Yulu Wang, FangFang Ge, Jingjing Pu, Peng Chen and Rohulla Vaseq) for their support in my work. I also thank Mrs.Tanja Schuster who is the secretary of Prof. Ingo Schmidt-Wolf giving me some help in life and work.

I am also very thankful for my family’s support and volunteers blood donations for research work.